ELECTROMAGNETIC RESPONSE OF THIN WIRES OVER AN HOMOGENEOUS EARTH

by

Jeffrey Lee Young

A Dissertation Submitted to the Faculty of the

DEPARTMENT OF ELECTRICAL AND COMPUTER ENGINEERING

In Partial Fulfillment of the Requirements
For the Degree of

DOCTOR OF PHILOSOPHY

WITH A MAJOR IN ELECTRICAL ENGINEERING

In the Graduate College

THE UNIVERSITY OF ARIZONA

1 9 8 9

Order Number 9013164

Electromagnetic response of thin wires over an homogeneous earth

Young, Jeffrey Lee, Ph.D.

The University of Arizona, 1989

U·M·I
300 N. Zeeb Rd.
Ann Arbor, MI 48106

ELECTROMAGNETIC RESPONSE OF THIN WIRES OVER AN HOMOGENEOUS EARTH

by

Jeffrey Lee Young

A Dissertation Submitted to the Faculty of the

DEPARTMENT OF ELECTRICAL AND COMPUTER ENGINEERING

In Partial Fulfillment of the Requirements
For the Degree of

DOCTOR OF PHILOSOPHY

WITH A MAJOR IN ELECTRICAL ENGINEERING

In the Graduate College

THE UNIVERSITY OF ARIZONA

1 9 8 9

THE UNIVERSITY OF ARIZONA
GRADUATE COLLEGE

As members of the Final Examination Committee, we certify that we have read the dissertation prepared by Jeffrey L. Young

entitled Electromagnetic Response of Thin Wires Over an Homogeneous Earth

and recommend that it be accepted as fulfilling the dissertation requirement for the Degree of Doctor of Philosophy.

	11/13/89 Date
	11/13/89 Date
	11/13/89 Date
	Date
	Date

Final approval and acceptance of this dissertation is contingent upon the candidate's submission of the final copy of the dissertation to the Graduate College.

I hereby certify that I have read this dissertation prepared under my direction and recommend that it be accepted as fulfilling the dissertation requirement.

Dissertation Director	13 NOV 1989 Date

STATEMENT BY AUTHOR

This dissertation has been submitted in partial fulfillment of requirements for an advanced degree at The University of Arizona and is deposited in the University Library to be made available to borrowers under rules of the Library.

Brief quotations from this dissertation are allowable without special permission, provided that accurate acknowledgment of source is made. Requests for permission for extended quotation from or reproduction of this manuscript in whole or in part may be granted by the head of the major department or the Dean of the Graduate College when in his or her judgement the proposed use of the material is in the interests of scholarship. In all other instances, however, permission must be obtained from the author.

SIGNED: 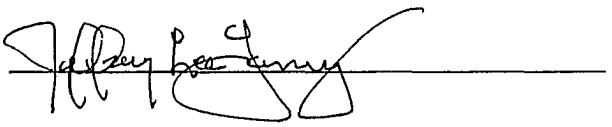

ACKNOWLEDGMENTS

It is a rare opportunity to study under an eminent and distinguished researcher such as Regents Professor James R. Wait. To him I would like to extend my appreciation for his continual support and scholarly advice towards this endeavor. I am also indebted to Dr. D. G. Dudley (for his inestimable electromagnetic instruction), Dr. A. Cangellaris (for his many valuable tutorials), Dr. L. P. Heulsman (for his initial support of my graduate studies) and Dr. W. Fayhey (for his timely counsel).

On the other hand, much of my education has also occured in the *trenches* with colleagues such as J. Anderson, Dr. B. Beartlein, Dr. T. Gruska (pioneer of the Gruska method), R. Lee, Dr. J. Williams and D. Wright – to them I owe much.

Yet this list would be incomplete should I fail to mention Dr. E. Pierce (a constant source of encouragement), Regents Professor H. A. Oberman (an educator par excellence), E. Young (a faithful proof–reader of this text) and the Hughes Aircraft Company (a generous financial supporter of my research).

Finally, words are an inadequate medium in expressing the love and patience I have received from my family, friends and wife.

TABLE OF CONTENTS

TABLE OF CONTENTS – continued

LIST OF ILLUSTRATIONS

LIST OF ILLUSTRATIONS – continued

LIST OF ILLUSTRATIONS – continued

LIST OF ILLUSTRATIONS – continued

LIST OF ILLUSTRATIONS – continued

LIST OF ILLUSTRATIONS – continued

LIST OF ILLUSTRATIONS – continued

ABSTRACT

The electromagnetic response of infinitely long, thin wires over a flat earth is presented for two different applications: the shielding properties of an ensemble of parallel wires excited by a plane wave and the electromagnetic coupling of two perpendicular wires excited by a dipole.

The shielding study begins with the formulation of the boundary value problem for N wires over a lossy half space. A suitable axial impedance operator is applied to obtain a system of equations whose unknowns are the currents flowing on each wire. Once the currents are determined, the aggregate field produced by the ensemble can be computed by summing N Fourier type integrals. For the specialized case of the infinite planar grid, Floquet's Theorem and Poisson's Summation Formula are invoked, transforming the linear system of equations into a closed form expression for the current flowing on each wire. We show that the electromagnetic response of the planar grid of finite extent and the grid of infinite extent are similar. For non–planar configurations, such as the semi–circular shell, shielding values of 60 dB are possible when the structure is of non–resonant dimensions; otherwise, the performance can degrade to 20 dB.

In the case of the crossed wire configuration, the starting point is the development of the integral equations that govern the coupling between wires and the source; the unknowns are the spectral currents flowing in each wire. The equations are given in terms of generalized impedance functions for the situation where the

wires are over a stratified earth. However, for the numerical work, only the case where the wires are in an unbounded, homogeneous medium is considered. Two numerical methods, with overlapping regions of validity, are applied: the method of moments and the method of multiple scatterers. By using the method of moments, we can obtain a matrix equation that will determine the spectral currents for any wire spacing. The multiple scatterer method leads to a more convenient matrix series solution and shows that the coupling strength is proportional to $1/d^2$, where d is the wire separation, plus higher order inverse terms.

CHAPTER 1

INTRODUCTION

Thin wire systems have been a subject of electromagnetic research for many years. The application of such wires is found in everyday use: overhead power cables, microwave ovens, antenna reflectors, and transmission lines. Starting as far back as Lamb [1898] and continuing through the present, prominent and noteworthy investigations have considered propagation, induction, scattering and transient effects. A concise review of the seminal papers follows in the next section. In this dissertation we will primarily focus our attention, with a few minor diversions, on two different yet important thin wire problems; both have practical and immediate application.

First to be considered are the electromagnetic shielding properties of an ensemble of parallel wires in the shape of a semi–circular cage (see Figure 3-17) over an homogeneous earth. From an engineering point of view, such a configuration is attractive since wire ensembles are lighter in weight than their metallic sheet counterpart. Also, the construction of a wire shield in an existing electromagnetic facility (e.g. an electromagnetic compatibility lab) can be accomplished with minimal effort. From a design perspective, shielding behavior of the ensemble will be quantified in terms of overall size, wire radii, mutual wire separation, and earth electrical parameters. This quantification process will deal primarily with numerical results.

Second, the electromagnetic response of two crossing, perpendicular wires will be investigated. There are two particular and relevant cases for this study. The first is found in beacon navigational systems. For instance, with such ship–borne systems, the environs of a radiating antenna are comprised of crossing guy–wires and communication cable links. The former may cause navigational errors, the latter may hinder, obstruct or interfere with communications. An initial study of this kind was performed by Hill and Wait [1977], who investigated such concerns for the single wire case. The second application appears in buried cables and long conductors in tunnels. Hill [1988], in a single wire study, noted that electromagnetic earth probing can be influenced by the presence of the wire. Hence, crossing cables are the next obvious extension for research.

1.1 Background

A modern, introductory treatment regarding the fundamental electromagnetic properties of a single wire can be found in a recent book by Wait [1986a, Ch. 7]. Since much of this dissertation is founded on his development of induction and scattering effects, the reader may look therein for background.

For more advanced topics, individual publications have been consulted. As the scope of thin wire study is so vast, we will arbitarily classify many of these results into four groups: over–head wire propagation, infinite grid configurations, ensembles of a finite number of wires, and crossed wire configurations.

1.1.1 Over–Head Wire Propagation

The modal properties of the over–head power cable have received considerable attention in the literature. Even though the continuous modal spectrum may eventually dominate the discrete components, the discrete modes are usually adequate for finite length structures [Kuester, Chang and Olsen, 1978]. Such modes may be excited, provided that the appropriate aperture field has been selected. With this in mind, we proceed to examine many of the significant contributions that deal with the discrete modal solutions.

The first demonstrative analytical investigation towards the understanding of propagation effects of overhead wire lines was performed by Carson [1926]. Basing his initial assumptions on quasi–static principles, he was able to derive an approximated expression for the propagation constant. Although other investigations furthered Carson's work [Wise, 1934, 1948], it was Wait [1972a] who reconfirmed Carson's results by considering the general electromagnetic boundary value problem. Once establishing the general modal equation, Wait showed more clearly that the *Carson* mode was a perturbation solution to the idealized transmission line modal equation.

Other approximations to this modal equation have been studied. For instance, Coleman [1950] obtained a solution for the specialized case where the wire is located in the air–earth interface. (These results were also confirmed by Wait [1972a].) Starting with Coleman's remarkably simple solution, Chang and Wait [1974] examined the ELF (extremely low frequency) problem in which the wire is slightly elevated. They found that the propagation constant can change dramatically as the wire is elevated from the interface.

Many other investigators [e.g. dos Santos, 1972] have shown the existence of another modal solution through numerical experimentation. This *surface attached* mode [Kuester et al., 1978] may have a lower attenuation rate than the transmission line mode. Kikuchi [1978] studied the high frequency effects of coated wires (particularly, numerical attenuation rates) and showed that, in the higher frequency range, there exists an attenuation minimum for the propagating current.

A paper of significant importance, which will be needed in Chapter Four, is that of Hill and Wait [1977]. Starting with a dipole and an infinite cable over an ideal ground plane, they were able to obtain far field radiation patterns. Particularly, they concluded that the wire plays a significant role in producing a cross polarization component that could effect navigational systems. On the other hand, for a dipole near a leaky coaxial cable, the source can couple very strongly to the monofilar mode.

Finally, the radiation from a semi–infinite wire above ground has been recently investigated [Dudley and Casey, 1989]. Using the classical results of Carson [1926] and Wait [1972a], they used steepest descent to obtain a time history of the far–zone fields.

1.1.2 Infinite Grid Characteristics

Although Fraunhofer is credited with the discovery of the basic optical properties of diffraction gratings (i.e. the grating will decompose the visible white light spectrum into an array of colored spectral lines), it was Lamb [1898] who placed these findings on a firm mathemetical foundation. He demonstrated that, when the electric field vector is parallel to the wires, the strength of the reflected

wave is inversely proportional to the factor $(d/\lambda)\ln(d/2\pi a)$, where d is the distance between mutual wires, λ is the operating wavelength, and a is the wire radius. Unfortunately, Lamb's method was limited in application since static conditions were assumed.

Later investigators [Ignatowsky, 1914; Gans, 1920; Wessel, 1939] refined Lamb's work, but it was MacFarlane [1946] who demonstrated that a grid in free space can be represented by a shunt impedance across an infinite transmission line. Wait [1954a, 1954b, 1957, 1962] showed for a variety of polarizations and configurations that if the grid were parallel to an homogeneous half space, it could be represented by a shunt impedance in a two–segment transmission line. In each of the above cases, the leading and dominating term of the shunt impedance was the aforementioned static expression first developed by Lamb, but with an important correction factor to account for the interaction of the evanescent field with the interface. For numerical results regarding this shunt impedance term, the reader may consult Larsen [1962a] and Young and Wait [1989a] (see also Chapter Three).

The transient effects of an infinite wire grid have been studied by Quintenz and Dudley [1974]. By assuming the input signal to be a double exponential pulse, they showed the high pass filtering characteristics of the grid numerically.

For an encompassing review of wire grid analysis prior to 1962, the reader may refer to Larsen [1962b]. Although wire mesh analysis is not covered in this dissertation, the reader may consult the extensive review by Wait [1978a] and recent paper by Casey [1989].

1.1.3 Thin Wire Ensembles

In this section we begin with Row [1955], since his work exemplifies the foundational principles pertaining to multiple cylindrical scatterers. Considering the two cylinder case (no initial constraints were place on the radii), he obtained an integral equation formulation for the individual currents flowing on the perfectly conducting cylinders. He then expanded the unknowns in the integral equation in terms of their complex Fourier series, thus transforming the integral equation into an infinite set of linear equations with an infinite number of unknowns. Even though his analytical results were completely general, the numerical results were limited to cylinders on the order of $a \approx \lambda/2$ (a is the cylinders' radii and λ is the operating wavelength). Such a size restriction was necessary to justify the truncation of the infinite set of equations.

Thin wire analysis is, in effect, an approximation to the general cylindrical scattering problem where only the first term of the harmonic expansion is used. With this observation in mind, Richmond [1965] analyzed the scattering properties of an arbitrary array of parallel wires. Confining the problem for wires in free space, he demonstrated numerically that the array of wires have scattering properties similar to those of the perfectly conducting counterpart. If the wire configuration is that of a circular shell, a closed form analytical solution is obtainable [Wilson, 1974]. The case of the continuous spherical shell has been exhaustively studied in the frequency domain by Chu, Dudley and Bristol [1969] and in the time domain by Dudley and Quintenz [1975]. The numerical shielding results of a semi-circular cage have also been recently published [Young and Wait, 1989b] (this paper will be expanded on in Chapter Three).

Hitherto, the excitation waveform has been a plane wave. If the wires were excited by a localized source, such as a vertical electric dipole, then the solutions to the wave equation for the field constituents would be given in terms of a double spectral integral representation as demonstrated by Wait [1977b]. The formulation, which is similar to that outlined in Chapter Two, can be formally obtained. However, from a numerical point of view, the problem is formidable, since such a solution would require $N^2 \times M/2$ Sommerfeld evaluations to describe the currents flowing in each wire. Here N is the number of wires and M is the number of sampling points in the discretization process of one of the spectral variables.

1.1.4 Crossed Wire Configurations

Although the complete electromagetic problem concerning crossing, infinite wires has not been addressed in the literature, a few investigations have dealt with crossing earth–return circuits. For instance, Krakowski [1967] investigated the mutual impedance of such circuits when one wire is finite and the other is infinite. (It was assumed that the former was carrying a constant current.) Bannister [1973] expanded on this work by considering image effects at the outset and was able to obtain analytical approximations that correlate well with the more complicated results of Krakowski.

Another set of investigations concentrated on the problem of crossing, non–touching pairs of transmission lines. Giri, Chang and Tesche [1980], formulated the problem by considering a lumped circuit model representation. Such an approximation precludes the possibility of higher order modal coupling and assumes that

all coupling effects are localized near the intersection. The approximation does, however, lead to a tractable solution for the inductive and capacitive coupling coefficients. Kami and Sato [1986] used the same lumped element approximation and provided coupling coefficient curves. Particularly useful in their paper is the confirmation of analytical models with experimental measurement.

From a scattering perspective, King [1975, 1977] obtained an analytical solution for the currents and charges on a perfectly conducting, mutually perpendicular, crossed dipole antenna for a normally incident plane wave. This analysis involved the process of decoupling two Hallén–type integral equations through the iteration technique of multiple scatterers. Numerical solutions, which utilized the moment method technique, were earlier obtained by Taylor et al. [1970] and Butler [1972].

1.2 Dissertation Structure

The design of this dissertation is to give a progressive, but not necessarily all encompassing, theory of thin wire analysis. By starting with first principles (in effect Maxwellian theory) we will present self–contained and complete analytical formulations. The mathematical and numerical results of this dissertation are found in Chapters Two, Three and Four; the numerical analysis is found in Appendix A. This format was chosen to provide continuity of analytical thought from chapter to chapter without interrupting the logical flow for numerical considerations; yet as the appendix shows, the latter are far from trivial.

Chapter Two provides and defines the necessary laws and assumptions pertaining to thin wire analysis (i.e. an expansion of Wait's work [1986a]). A

terse treatment of Maxwellian field theory and Hertzian vector potentials is used to derive the fields of a thin wire (in free space or over a lossy half space). From this, the interior problem is investigated to provide the fundamental definition of the axial impedance operator. A brief definition and justification of thin wire analysis is then given to outline the implicit assumptions thereof. With these minor derivations in place, the fields scattered from a single wire can be calculated. In general, Chapter Two will set the precedent for Chapters Three and Four.

Chapter Three extends the theory of Chapter Two by considering an ensemble of thin wires parallel to each other and an interface. The excitation is assumed to be a plane wave of arbitrary polarization. From this, a general matrix equation is obtained that completely characterizes the currents on each wire; the fields emanating from the overall wire configuration are then easily determined. This general analysis can be directly extended to include the special case of the infinite grid. Several plots are provided that correlate the current and field data for the planar grid of finite extent to the infinite grid case. We also provide several plots that quantify the shielding effectiveness of a given structure for various system parameters such as earth conductivity, number of wires, cage size and incidence angle.

Chapter Four looks at a topic that seems to have received little attention in the literature – namely the electromagnetic response of two perpendicular, infinitely long wires. The general equations will be derived first using Fourier techniques, for the case where the wires are over a stratified earth. This leads to a coupled set of Fredholm integral equations, the unknowns being the spectral currents flowing in each wire. At this time no formal, complete, analytical solution to these equations is available. However, a simplified numerical solution can be

obtained for the case where the wires are in an homogeneous medium (or over an ideal ground plane), using either moment method theory or multiple scattering approximations; both rely on spectral sampling techniques. Once the spectral currents are known, the total field can be calculated at any point. We note that the integral operator is not bounded when the wires are in free space. For this reason, the numerical results will concentrate on the detection problem when the wires are in a lossy, homogeneous earth. The moment method solution and the multiple scatterer solution are compared to point out the salient features of each method.

Chapter Five presents the fundamental conclusions and results of the dissertation. Future research topics are briefly discussed for those who wish to continue in this area of investigation.

Appendix A contains the numerical computation algorithms used to derive the shielding results presented in Chapter Three. Along with these, analytical approximations for the Sommerfeld type integrals are given to validate the numerical test data. The consideration of the quasi–static response of the 2–dimensional Sommerfeld integral introduces a new method for extracting the asymptotic behavior, which expedites the numerical convergence rate for real axis integration.

Appendix B proves that the integral operator, derived in the crossed wire problem, is bounded under certain constraints. Also, for easy reference a glossary is appended at the end which tabulates many of the variables, symbols and nomenclatures peculiar to this dissertation.

CHAPTER 2

PRELIMINARY THIN WIRE CONCEPTS AND EQUATIONS

2.1 Field Theory

At the inception of any electromagnetic problem, a presentation of the fundamental electromagnetic laws for macroscopic quanities, as first compiled by Maxwell [1891], should be given. For an assumed $e^{i\omega t}$ time dependency, the differential form of the four equations in source–free, isotropic, homogeneous media are

$$\nabla \times \mathbf{E} = -i\omega\mu\mathbf{H} \tag{2.1}$$

$$\nabla \times \mathbf{H} = (\sigma + i\omega\epsilon)\mathbf{E} \tag{2.2}$$

$$\nabla \cdot \mathbf{E} = 0 \tag{2.3}$$

$$\nabla \cdot \mathbf{H} = 0 \tag{2.4}$$

where $\mathbf{E}$ is the electric field vector and $\mathbf{H}$ is the magnetic field vector. The three electrical parameters, ϵ, μ and σ are the permittivity, permeability and conductivity of the medium, respectively. In later developments, the results are given in the frequency domain and hence the $e^{i\omega t}$ time factor is suppressed in the antecedent equations and in all subsequent calculations.

For certain geometries, Maxwell's equations do not lend themselves to direct application. For this reason, it is more convenient to introduce some auxiliary vector potential functions which will aid in mathematical analysis. The vector

functions $\mathbf{\Pi}$ and $\mathbf{\Pi}^*$ will be denoted as the electric and magnetic Hertz potentials, respectively. They are related to the field constituents through the rules

$$\mathbf{E} = -i\omega\mu\nabla \times \mathbf{\Pi}^* \tag{2.5}$$

and

$$\mathbf{H} = (\sigma + i\omega\epsilon)\nabla \times \mathbf{\Pi} \tag{2.6}$$

The manipulations of the vector functions into a usable mathematical form have been treated in many excellent texts [e.g. Collin, 1960, §1.6], and will not be duplicated here. It has been found that the potentials are solutions to the homogeneous vector Helmholz equation. For example,

$$(\nabla^2 + k^2)\mathbf{\Pi} = 0 \tag{2.7}$$

where the Laplacian ∇^2 in curvilinear coordinates is defined explicitly by

$$\nabla^2 = grad\ \ div - curl\ \ curl \tag{2.8}$$

With usual convention, k is defined as the wave number of the medium through the relationship $k = \sqrt{-i\omega\mu(\sigma + i\omega\epsilon)}$. Under the assumed time dependence, $\mathrm{Im}[k] < 0$.

If we were treating specific electromagnetic sources in the problem, we would discover that the electric Hertz vector is associated with electric sources, just as the magnetic Hertz vector is associated with magnetic sources. In general, when both sources are present, the superposition of the fields resulting from each source leads to the following relationship between the field constituents and the potential constituents:

$$\mathbf{E} = (k^2 + grad\ \ div)\mathbf{\Pi} - i\omega\mu\ \ curl\mathbf{\Pi}^* \tag{2.9}$$

$$\mathbf{H} = (k^2 + grad\ div)\mathbf{\Pi}^* + (\sigma + i\omega\mu)\ curl\mathbf{\Pi} \tag{2.10}$$

Although physically there are no magnetic sources suchlike, the postulation of the magnetic vector potential will prove in later developments its utility by obtaining an expedient solution for the field constituents. Juxtaposing the forms of (2.9) and (2.10) with the study of wave propagation along thin wires, we observe that the TE (transverse electric) modes are derived from the longitudinal component of $\mathbf{\Pi}^*$ and the TM (transverse magnetic) modes are computed from the longitudinal component of $\mathbf{\Pi}$.

2.2 Thin Wire Analysis

The focus of this monograph is on the electrical characteristics of thin wires which may be located in free space or over a lossy half space. A brief overview of the analytical properties of these wires will set the precedent for ensuing chapters. The dialectical method is similar to Wait's [1986a, Ch. 7], and consequently only the salient features of the analysis are exhibited.

2.2.1 Thin Wire in Free Space

The derivation of the fields emanating from a single wire of radius a in free space resulting from an arbitary current distribution, is considered (see Figure 2-1). The application of Fourier transform methods is utilized to reduce the linear Helmholtz equation into a beneficial algebraic form. The current function $i_y(y)$ is defined as the total spatial current flowing in the y–directed wire. It is presupposed that the current is axially directed without azimuthal variation so that $\partial/\partial\alpha = 0$.

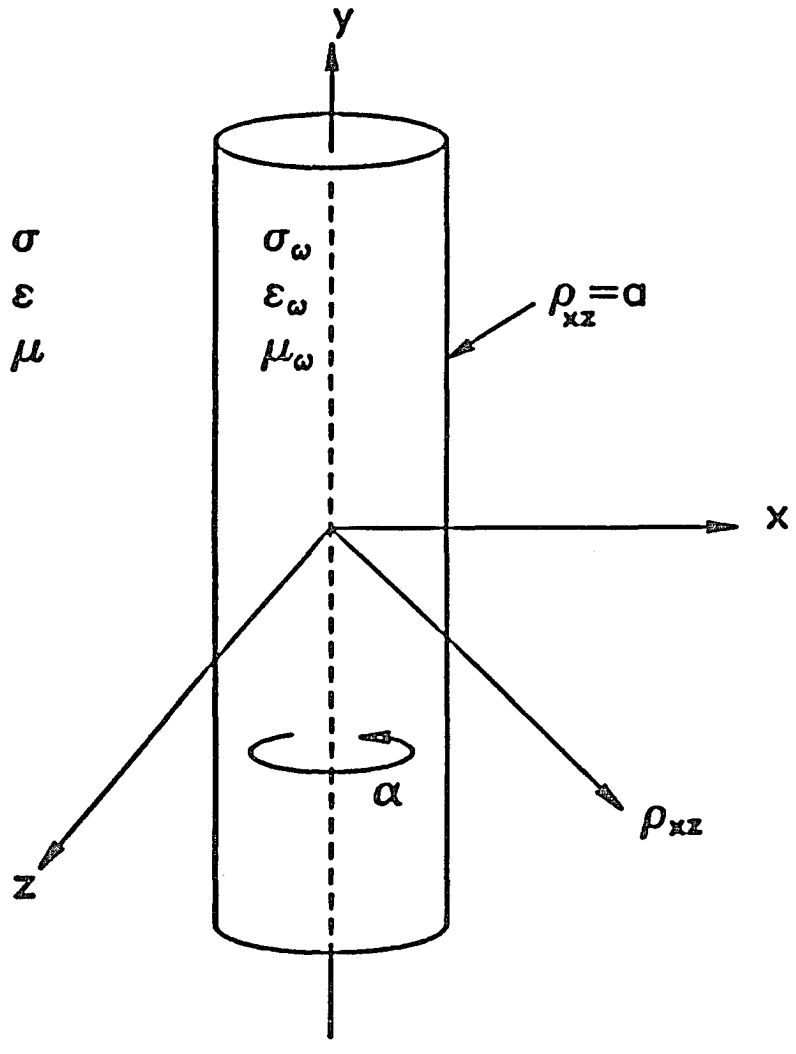

Figure 2-1 A thin wire located in an homogeneous, isotropic medium.

(The basis of such an assumption will be discussed in Section 2.4.) As restricted by Ampere's Law [Wait, 1977a], the Fourier pairs are

$$i_y(y) = \int_{-\infty}^{\infty} I_y(\beta) e^{-i\beta y} d\beta \tag{2.11}$$

and

$$I_y(\beta) = \frac{1}{2\pi} \int_{-\infty}^{\infty} i_y(y) e^{i\beta y} dy \tag{2.12}$$

where $I_y(\beta)$ is the current in the spectral domain.

The foregoing definitions are valid, provided that $i_y(y)$ is absolutely integrable in the open region $(-\infty, \infty)$ [Churchill, 1972, §131]. These transforms will also be applied to both the field functions and the potential functions.

As seen from the geometry, only the y–component of the electric Hertz vector is required to determine completely the field constituents. Applying the transform definition to (2.7), solving the remaining equation in closed form, and finally, taking the inverse transform of the resultant equation, yields the following external solution (i.e. $\rho_{xz} > a$) for the Hertz potential:

$$\Pi_y = \int_{-\infty}^{\infty} A_y(\beta) K_0(v_y \rho_{xz}) e^{-i\beta y} d\beta \tag{2.13}$$

where $v_y = \sqrt{\beta^2 - k^2}$ and $\rho_{xz} = \sqrt{x^2 + z^2}$. The multiple–valued function is rendered single–valued by the stipulation $\mathrm{Re}[v_y] > 0$. The coefficient A_y will be determined below from Ampere's Law. The function K_0, known as the modified Bessel function of the second kind or the MacDonald function, has been chosen

because it exponentially decays as ρ_{xz} increases, thus assuring the radiation condition. The other independent solution, $I_0(v_y\rho_{xz})$, exponentially grows without bound as $\rho_{xz} \to \infty$.

The azimuthal magnetic field, exterior to the wire, can be computed by applying (2.10) to (2.13) to give

$$H_\alpha = (\sigma + i\omega\epsilon)\int_{-\infty}^{\infty} v_y A_y(\beta) K_1(v_y\rho_{xz}) e^{-i\beta y} d\beta \tag{2.14}$$

For a circular path about the wire, Ampere's law relates the total axial current to the azimuthal magnetic field. In the limit as $\rho_{xz} \to 0$ [Wait, 1986a, §7.2],

$$H_\alpha = \frac{i_y(y)}{2\pi\rho_{xz}} \tag{2.15}$$

Taking the transform of (2.15) and equating the integrand with (2.14) yields

$$\frac{I_y(\beta)}{2\pi\rho_{xz}} = \lim_{\rho_{xz}\to 0}(\sigma + i\omega\epsilon) v_y A_y(\beta) K_1(v_y\rho_{xz}) \tag{2.16}$$

The fundamental difficulty associated with the limit of (2.16) is that v_y is a function of β; wherefore, this limit does not exist for all β. This difficulty can be circumvented by considering basic properties of Fourier transform theory. Recall, for the transform of $i_y(y)$ to exist, the current function must be absolutly integrable. That is,

$$\int_{-\infty}^{\infty} |i_y(y)| dy < \infty \tag{2.17}$$

By requiring the current to be a bounded function and assuming it is spatially distributed over much of the wire, we surmise that the spectral distribution will

be closely packed near its origin. Consequently, the limit of (2.16) is obtainable for all significant values of β. From the small argument approximation for the MacDonald function, namely, $K_1(z) \approx 1/z$ for $|z| << 1$, it follows that

$$A_y(\beta) = \frac{I_y(\beta)}{2\pi(\sigma + i\omega\epsilon)} \tag{2.18}$$

Thus, for a thin wire, the integral representation for the electric vector potential (which has been previously derived by Hill and Wait [1977]) is

$$\Pi_y = \frac{1}{2\pi(\sigma + i\omega\epsilon)} \int_{-\infty}^{\infty} I_y(\beta) K_0(v_y \rho_{xz}) e^{-i\beta y} d\beta \tag{2.19}$$

If the integral representation for K_0 [Gradshtein and Ryzhik, 1980, # 3.961.2] is employed, namely,

$$K_0(v_y \rho_{xz}) = \frac{1}{2} \int_{-\infty}^{\infty} \frac{e^{-uz}}{u} e^{-i\lambda x} d\lambda \tag{2.20}$$

where, $u = \sqrt{\lambda^2 + v_y^2}$, with the proper Riemann sheet specified by $\mathrm{Re}[u] > 0$, an alternate representation for (2.19) is obtained:

$$\Pi_y = \frac{1}{4\pi(\sigma + i\omega\epsilon)} \int_{-\infty}^{\infty} I_y(\beta) e^{-i\beta y} \int_{-\infty}^{\infty} \frac{e^{-uz}}{u} e^{-i\lambda x} d\lambda d\beta \tag{2.21}$$

The electric field component, longitudinal to the wire, is obtained by the application of (2.9) to (2.19). This results in the following expression for the electric field component in the y–direction:

$$E_y = \frac{-1}{2\pi(\sigma + i\omega\epsilon)} \int_{-\infty}^{\infty} v_y^2 I_y(\beta) K_0(v_y \rho_{xz}) e^{-i\beta y} d\beta \tag{2.22}$$

2.2.2 Thin Wire over a Lossy Half Space

A more involved calculation arises when the wire is located in a heterogeneous medium. The case of a y–directed thin wire of radius a parallel to a lossy half space at a height h from the interface is now considered. Again, it is assumed that the wire is carrying an arbitrary current distribution, $i_y(y)$. The region for which $z > 0$ is characterized by the electrical parameters ϵ_1 and μ_1; for $z < 0$, the subscript "one" is replaced with the subscript "two". The situation is depicted in Figure 2-2. In general, ϵ and μ may be complex to account for dissipative losses.

As with any scattering problem, the total electric potential may be decomposed into a primary part, Π_y^p, and a secondary part, Π_y^s. In particular, for $z > 0$,

$$\Pi_y = \Pi_y^p + \Pi_y^s \tag{2.23}$$

The primary part is similar to (2.21), with the exception that a height dependency in the integrand must be included:

$$\Pi_y^p = \frac{1}{4\pi i\omega\epsilon_1}\int_{-\infty}^{\infty} I_y(\beta)e^{-i\beta y}\int_{-\infty}^{\infty}\frac{e^{-u_1|z-h|}}{u_1}e^{-i\lambda x}d\lambda d\beta \tag{2.24}$$

where $u_1 = \sqrt{\lambda^2+\beta^2-k_1^2}$ and $k_1 = \omega\sqrt{\mu_1\epsilon_1}$ with $\mathrm{Re}[u_1] > 0$ and $\mathrm{Im}[k_1] < 0$. The secondary part is constructed from the form of (2.24), but modified to account for the lower half space as follows:

$$\Pi_y^s = \frac{1}{4\pi i\omega\epsilon_1}\int_{-\infty}^{\infty} I_y(\beta)e^{-i\beta y}\int_{-\infty}^{\infty}R_y(\lambda,\beta)\frac{e^{-u_1(z+h)}}{u_1}e^{-i\lambda x}d\lambda d\beta \tag{2.25}$$

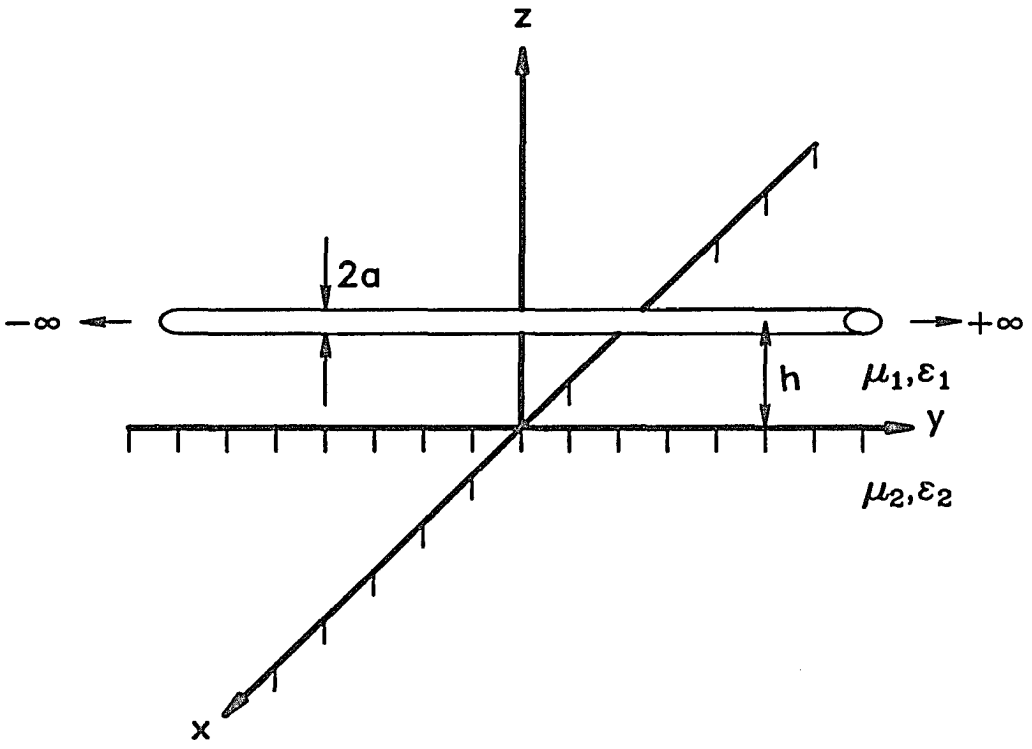

Figure 2-2 A thin wire located over an homogeneous half space.

where R_y is to be determined. The transmitted potential, Π_y^t, valid for $z < 0$, is also constructed from these same forms to yield

$$\Pi_y^t = \frac{1}{4\pi i\omega\epsilon_1}\int_{-\infty}^{\infty} I_y(\beta)e^{-i\beta y}\int_{-\infty}^{\infty} T_y(\lambda,\beta)\frac{e^{u_2 z}e^{-u_1 h}}{u_1}e^{-i\lambda x}d\lambda d\beta \tag{2.26}$$

where $u_2 = \sqrt{\lambda^2+\beta^2-k_2^2}$, with $\mathrm{Re}[u_2] > 0$ and $k_2 = \omega\sqrt{\mu_2\epsilon_2}$.

A quick check can be executed to demonstrate that there is a deficiency in the number of coefficients (i.e. R_y and T_y) necessary to satisfy the continuity relations of the tangential fields at the interface. For this reason we introduce the magnetic Hertz potentials, which are also constructed from the form of (2.24). In particular for $z > 0$,

$$\Pi_y^* = \frac{1}{4\pi i\omega\epsilon_1}\int_{-\infty}^{\infty} I_y(\beta)e^{-i\beta y}\int_{-\infty}^{\infty} M_y(\lambda,\beta)e^{-u_1(z+h)}\frac{e^{-i\lambda x}}{u_1}d\lambda d\beta \tag{2.27}$$

and for $z < 0$,

$$\Pi_y^* = \frac{1}{4\pi i\omega\epsilon_1}\int_{-\infty}^{\infty} I_y(\beta)e^{-i\beta y}\int_{-\infty}^{\infty} N_y(\lambda,\beta)e^{u_2 z}e^{-u_1 h}\frac{e^{-i\lambda x}}{u_1}d\lambda d\beta \tag{2.28}$$

From (2.9) and (2.10), the horizontal field constituents are given explicitly when $z > 0$ by

$$E_x = \frac{\partial^2}{\partial x\partial y}\Pi_y + i\omega\mu_1\frac{\partial}{\partial z}\Pi_y^* \tag{2.29}$$

$$H_x = \frac{\partial^2}{\partial x\partial y}\Pi_y^* - i\omega\epsilon_1\frac{\partial}{\partial z}\Pi_y \tag{2.30}$$

$$E_y = \left(k_1^2 + \frac{\partial^2}{\partial y^2}\right)\Pi_y \tag{2.31}$$

$$H_y = \left(k_1^2 + \frac{\partial^2}{\partial y^2}\right)\Pi_y^* \tag{2.32}$$

The forms for $z < 0$ can be obtained by replacing the subscript "one" with the subscript "two". Application of these definitions to the potential functions and the match of like field components at the interface yields the following equations of four unknowns:

$$(k_1^2 - \beta^2)(1 + R_y) = (k_2^2 - \beta^2)T_y \tag{2.33}$$

$$(k_1^2 - \beta^2)M_y = (k_2^2 - \beta^2)N_y \tag{2.34}$$

$$i\lambda\beta(1 + R_y) - \mu_1\omega u_1 M_y = i\lambda\beta T_y + \mu_2\omega u_2 N_y \tag{2.35}$$

$$i\lambda\beta M_y - \epsilon_1\omega u_1(1 - R_y) = i\lambda\beta N_y - \epsilon_2\omega u_2 T_y \tag{2.36}$$

By solving for R_y and M_y, we obtain the following expressions [Wait, 1972a]:

$$R_y = \frac{\lambda^2\beta^2(1 - K_y)^2 + \omega^2(\epsilon_1 u_1 - \epsilon_2 u_2 K_y)(\mu_1 u_1 + \mu_2 u_2 K_y)}{-\lambda^2\beta^2(1 - K_y)^2 + \omega^2(\epsilon_1 u_1 + \epsilon_2 u_2 K_y)(\mu_1 u_1 + \mu_2 u_2 K_y)} \tag{2.37}$$

and

$$M_y = \frac{2i\omega\lambda\beta(1 - K_y)\epsilon_1 u_1}{-\lambda^2\beta^2(1 - K_y)^2 + \omega^2(\epsilon_1 u_1 + \epsilon_2 u_2 K_y)(\mu_1 u_1 + \mu_2 u_2 K_y)} \tag{2.38}$$

where

$$K_y = \frac{k_1^2 - \beta^2}{k_2^2 - \beta^2} \tag{2.39}$$

The results herein, for the external fields, can also be extended for a stratified earth. The only difference lies in the form of the coefficients, such as R_y and M_y.

The total electric field in the y–direction is computable by applying (2.31) to (2.23) which gives

$$E_y^w = E_y^p + E_y^s \tag{2.40}$$

where

$$E_y^p = \frac{-1}{2\pi i\omega\epsilon_1}\int_{-\infty}^{\infty} v_1^2 I_y(\beta) K_0(v_1\hat{\rho}_{xz}) e^{-i\beta y} d\beta \tag{2.41}$$

and

$$E_y^s = \frac{-1}{4\pi i\omega\epsilon_1}\int_{-\infty}^{\infty} v_1^2 I_y(\beta) e^{-i\beta y} \int_{-\infty}^{\infty} R_y(\lambda,\beta)\frac{e^{-u_1(z+h)}}{u_1} e^{-i\lambda x} d\lambda d\beta \tag{2.42}$$

The geometrical optical distance $\hat{\rho}_{xz}$ is given by $\hat{\rho}_{xz} = \sqrt{x^2+(z-h)^2}$. Also, $v_1 = \sqrt{\beta^2 - k_1^2}$ with $\mathrm{Re}[v_1] > 0$.

Equations (2.41) and (2.42) represent a continuous summation of plane waves over real and complex angles [Wait, 1985, §4.14]. These forms will be needed in the analysis presented in Chapter 4. For the plane wave shielding problem, which will be discussed in Chapter 3, only a single spatial frequency term is excited. This is illustrated by letting $i_y(y) = I_w e^{ik_y y}$ where I_w is a constant and k_y is some specified wave number. Recognising that the transform of this current excitation is the Dirac delta function, we find that (2.41) and (2.42) reduce to

$$E_y^p = \frac{-v_a^2}{2\pi i\omega\epsilon_1} I_w e^{ik_y y} K_0(v_a\hat{\rho}_{xz}) \tag{2.43}$$

and

$$E_y^s = \frac{-v_a^2}{4\pi i\omega\epsilon_1} I_w e^{ik_y y} \int_{-\infty}^{\infty} R_y(\lambda,k_y)\frac{e^{-u_a(z+h)}}{u_a} e^{-i\lambda x} d\lambda \tag{2.44}$$

Here $v_a = \sqrt{k_y^2 - k_1^2}$, $u_a = \sqrt{\lambda^2 + v_a^2}$ and $u_b = \sqrt{\lambda^2 + k_y^2 - k_2^2}$. The reflection term is obtained by replacing u_1 with u_a and u_2 with u_b in (2.37). Again, the proper Riemann sheet is specified by the requirements $\mathrm{Re}[v_a] > 0$, $\mathrm{Re}[u_a] > 0$ and $\mathrm{Re}[u_b] > 0$. (The integration contour of (2.44) must bypass the branch point singularities on the real axis, for k_1 entirely real, according to the branch cut definitions.)

For the case where $k_y = 0$ (i.e. no longitudinal phase variation), the final results are similar, within a multiplicative constant, to the classic 2–D Green's function problem. Particularly, when $\mu_1 = \mu_2$ [Wait, 1985, §4.14],

$$E_y^p = \frac{-i\omega\mu_1}{2\pi} I_w K_0(ik_1\hat{\rho}_{xz}) \tag{2.45}$$

and

$$E_y^s = \frac{-i\omega\mu_1}{4\pi} I_w \int_{-\infty}^{\infty} \left[\frac{w_1 - w_2}{w_1 + w_2}\right] \frac{e^{-w_1(z+h)}}{w_1} e^{-i\lambda x} d\lambda \tag{2.46}$$

where $w_1 = \sqrt{\lambda^2 - k_1^2}$ and $w_2 = \sqrt{\lambda^2 - k_2^2}$, with $\mathrm{Re}[w_1] > 0$ and $\mathrm{Re}[w_2] > 0$.

2.3 Axial Impedance Operator

In this section the internal problem of an homogeneous wire, whose electrical parameters are ϵ_w, μ_w and σ_w, is addressed. As before, the current is assumed to be axially directed so that $\partial/\partial\alpha = 0$. In general, if the wire is *close* to some other structure, say an adjacent wire or a half space, the azimuthal variance may have appreciable effect. Again, these concerns will be addressed more fully in Section 2.4.

For the case where $\rho_{xz} < a$, Π_y is a solution of

$$(\nabla^2 - \gamma_w^2)\Pi_y = 0 \tag{2.47}$$

where $\gamma_w = \sqrt{i\omega\mu_w(\sigma_w + i\omega\epsilon_w)}$ with $\mathrm{Re}[\gamma_w] > 0$. The only non-singular solution to (2.47) is

$$\Pi_y = \int_{-\infty}^{\infty} B_y(\beta) I_0(v_w \rho_{xz}) e^{-i\beta y} d\beta \tag{2.48}$$

where I_0 is the modified Bessel function of the first kind, $v_w = \sqrt{\beta^2 + \gamma_w^2}$ ($\mathrm{Re}[v_w] > 0$) and B_y is to be determined. The resulting axial electric field and the azimuthal magnetic field, as computed from (2.9) and (2.10), with k^2 replaced by $-\gamma_w^2$, are

$$E_y = -\int_{-\infty}^{\infty} v_w^2 B_y(\beta) I_0(v_w \rho_{xz}) e^{-i\beta y} d\beta \tag{2.49}$$

and

$$H_\alpha = -(\sigma_w + i\omega\mu_w) \int_{-\infty}^{\infty} v_w B_y(\beta) I_1(v_w \rho_{xz}) e^{-i\beta y} d\beta \tag{2.50}$$

Again, noting that the total current flowing in the wire is $2\pi a H_\alpha|_{\rho_{xz}=a}$, requires

$$B_y(\beta) = \frac{-I_y(\beta)}{2\pi a(\sigma_w + i\omega\epsilon_w) v_w I_1(v_w a)} \tag{2.51}$$

The insertion of (2.51) into (2.49) yields the formal definition for the axial impedance operator [Wait, 1977a]:

$$E_y\Big|_{\rho_{xz}=a} = \int_{-\infty}^{\infty} I_y(\beta) Z_w(\beta) e^{-i\beta y} d\beta \tag{2.52}$$

where

$$Z_w(\beta) = \frac{v_w}{2\pi a(\sigma_w + i\omega\epsilon_w)} \frac{I_0(v_w a)}{I_1(v_w a)} \tag{2.53}$$

The function Z_w is defined as the spatially dispersive axial impedance of a thin, bare wire.

For the particular case where $i_y = I_w e^{ik_y y}$, the axial impedance operator is [Schelkunoff, 1943, Ch. 8],

$$E_y\Big|_{\rho_{xz}=a} = I_w Z_w(k_y) e^{ik_y y} \tag{2.54}$$

where

$$Z_w(k_y) = \frac{q_w}{2\pi a(\sigma_w + i\omega\epsilon_w)} \frac{I_0(q_w a)}{I_1(q_w a)} \tag{2.55}$$

with $q_w = \sqrt{k_y^2 + \gamma_w^2}$ ($\mathrm{Re}[q_w] > 0$). For the usual case where the wires are highly conducting (i.e. $\sigma_w > \omega\epsilon_w$) along with $|\gamma_w| >> |k_y|$ and $|q_w a| >> 1$, (2.55) is well approximated by

$$Z_w = \frac{1+i}{2\pi a}\sqrt{\frac{\omega\mu_w}{2\sigma_w}} \tag{2.56}$$

Hence, under these constraints, the axial impedance is independent of the wave number, k_y.

2.4 The Validity of the Thin Wire Approximation

To quantify what is meant by a thin wire, a modal analysis (which includes all of the azimuthal modes) of a general homogeneous cylinder in free space should be considered. We present the case where $\partial/\partial y = 0$. If $|k_1|a << 1$, Wait [1986a, §7.6] showed that the general expression does indeed collapse into the solution given in the preceding sections. The amplitude ratio of the zero order mode A_0 to the mth order mode A_m for a highly conducting wire, is [Wait, 1986a]

$$\left|\frac{A_0}{A_m}\right| = \frac{(ka)^{2m}}{m!(m-1)!2^{2m-1}} \left|\frac{1}{\ln(ka/2) + .5773}\right| \tag{2.57}$$

For example, if $ka = .01$ then $|A_0/A_1| \approx 1 \times 10^{-5}$.

When the wire is placed over a lossy interface, the complexity of the problem is significantly increased. The general problem was addressed for propagating currents of the form $e^{ik_y y}$ by Pogorzelski and Chang [1977]. They compared the first–order azimuthal current components to the zero order or axially directed currents. If A_0, A_1 and M_1 are defined as the amplitude of the zero–order electric, first–order electric and first–order magnetic multipoles, respectively, then

$$\frac{A_1}{A_0} = \frac{(v_a a)^2}{2(v_a h)} \left[i + \frac{1 + (v_b/v_a)^2}{K^2 + 1}\right] \tag{2.58}$$

and

$$\frac{M_1}{A_0} = \frac{(v_a a)^2}{2(v_a h)} \left(\frac{k_1}{k_y}\right) \left[2i + \frac{1 + (v_b/v_a)^2}{K^2 + 1}\right] \tag{2.59}$$

where $K^2 = k_2^2/k_1^2$ and $v_b = \sqrt{k_y^2 - k_2^2}$. The above expressions are valid when $|v_a h| << 1$ and $|k_2 h| << 1$.

Although (2.58) and (2.59) were derived under specific conditions, they will nevertheless be used as a general rule of thumb for all remaining analysis in this treatise.

2.5 Scattering From a Single Wire

An example pertaining to the wave scattering from a single thin wire over a lossy half space will now be given. The geometry of the problem is depicted in Figure 2–3. The current induced on the wire is calculated from the impedance operator given by (2.54); knowing this current, we can determined the fields at any location. Although almost any source can be used to excite a current on the wire, it is prudent at this juncture to choose one which will expeditiously lead to a closed–form solution. Without any loss of generality, the upper half space is assumed lossless; the lower may be dissipative.

For this reason, a plane wave is chosen that includes both polarizations: parallel (vertical) and perpendicular (horizontal). Parallel polarization denotes that the electrical field is parallel to the plane of incidence; similarly, perpendicular polarization signifies that the electrical field is perpendicular to this same plane. For all remaining discussions, the plane of incidence will be defined as the plane which is perpendicular to the wire and parallel to the interfacial normal vector. The incident field will originate from the upper medium with energy flow directed opposite to the spherical radial vector. In Cartesian coordinates, the y–component of the incident electric field is given by

$$E_y^{inc} = [E_h \cos\phi_0 + E_v \sin\phi_0 \cos\theta_0]\, e^{ik_x x} e^{ik_y y} e^{ik_{1z} \cos\theta_0} \qquad (2.60)$$

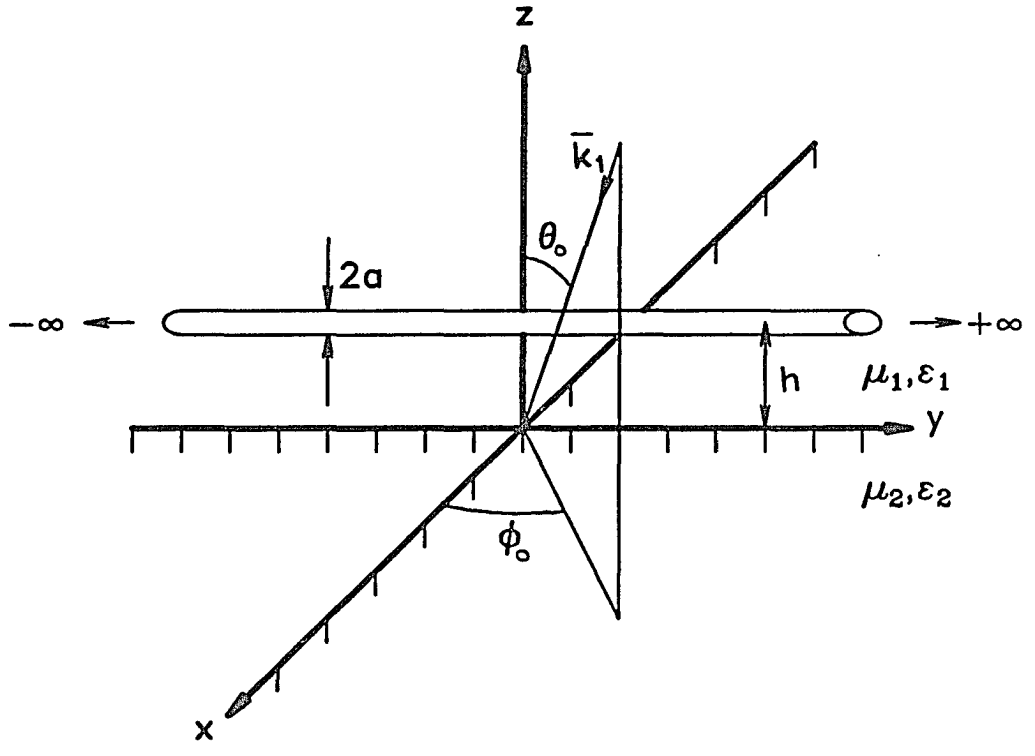

Figure 2-3 A thin wire located over an homogeneous half space when excited by a plane wave of arbitrary incidence and polarization.

where $k_x = k_1 \sin\theta_0 \cos\phi_0$ and $k_y = k_1 \sin\theta_0 \sin\phi_0$. We denote E_v and E_h as the amplitudes of the vertical and horizontal components which are related by $E_h^2 + E_v^2 = 1$. This last criteria is given to insure that the power density transmitted by the wave is constant for any polarization. Standard spherical notation has been used so that the zenith angle θ_0 is measured from the z–axis and the azimuthal angle ϕ_0 is referenced from the x–axis.

The reflected wave is of the same form as (2.60), but modified to account for its outgoing nature and weighted in strength so that the interfacial boundary conditions are satisfied. Hence,

$$E_y^{ref'l} = [E_h R_h \cos\phi_0 - E_v R_v \sin\phi_0 \cos\theta_0]\, e^{ik_x x} e^{ik_y y} e^{-ik_1 z \cos\theta_0} \tag{2.61}$$

where the Fresnel reflection coefficients are given by [Jordan and Balmain, 1968, §5.12]

$$R_h = \frac{\cos\theta_0 - \sqrt{K^2 - \sin\theta_0}}{\cos\theta_0 + \sqrt{K^2 - \sin\theta_0}} \tag{2.62}$$

and

$$R_v = \frac{K^2\cos\theta_0 - \sqrt{K^2 - \sin\theta_0}}{K^2\cos\theta_0 + \sqrt{K^2 - \sin\theta_0}} \tag{2.63}$$

The complex index of refraction K is again given by $K = k_2/k_1$. For later chapters, an alternative definition for K^2, valid only when $\mu_1 = \mu_2$, is $K^2 = N_d^2(1 - i\tan\delta_2)$, where $\tan\delta_2$ is the loss tangent given by $\sigma_2/(\omega\epsilon_2)$ and N_d is the dielectrical index of refraction given by $N_d = \sqrt{\epsilon_2/\epsilon_1}$.

The current induced on the wire can be readily computed from (2.54). Before applying this operator to the problem, we note from the source excitation that

the current must be of the form $I_w e^{ik_y y}$, where I_w is a constant to be determined. Since it is assumed that there is negligible azimuthal variation around the wire, the matching points for the impedance operator are chosen to be $x = 0$ and $z = h + a$. From this, the impedance operator becomes

$$\left[E_y^{inc} + E_y^{ref'l} + E_y^w\right]_{x=0,z=h+a} = I_w Z_w(k_y) e^{ik_y y} \tag{2.64}$$

where E_y^w is given by (2.40), along with (2.43) and (2.44). Application of Ohm's law from circuit theory yields an alternative representation for E_y^w in terms of an external impedance function and the induced current. At the matching points,

$$E_y^w(0, y, h + a) = -I_w Z_e e^{ik_y y} \tag{2.65}$$

where the external impedance function, Z_e, is given explicitly by the aggregation of the primary and secondary terms:

$$Z_e(k_y) = Z_e^p(k_y) + Z_e^s(k_y) \tag{2.66}$$

where

$$Z_e^p(k_y) = \frac{v_a^2}{2\pi i\omega\epsilon_1} K_0(av_a) \tag{2.67}$$

and

$$Z_e^s(k_y) = \frac{v_a^2}{4\pi i\omega\epsilon_1} \int_{-\infty}^{\infty} R_y(\lambda, k_y) \frac{e^{-u_a(2h+a)}}{u_a} d\lambda \tag{2.68}$$

From (2.60) and (2.61) the current I_w is thus found to be [Olsen and Chang, 1974],

$$I_w = \left\{E_h \cos\phi_0 \left[e^{ik_1 h\cos\theta_0} + R_h e^{-ik_1 h\cos\theta}\right]\right.$$
$$\left. + E_v \sin\phi_0 \cos\theta_0 \left[e^{ik_1 h\cos\theta_0} - R_v e^{-ik_1 h\cos\theta}\right]\right\}\left\{Z_w(k_y) + Z_e(k_y)\right\}^{-1} \tag{2.69}$$

Equation (2.69) is similar to the equation representing a series circuit with two impedance elements, where the circuit is driven by a voltage source. Thus, the current induced on a single wire is inversely proportional to the sum of the external and series impedances. The scattered field, longitudinal to the wire, may be computed by substituting (2.65) into (2.43) and (2.44).

It is desirable to plot graphically the functional dependency of the current on the zenith angle θ_0 and on the earth's conductivity σ_2. In Figures 2–4 and 2–5, we plot the magnitude of the current function for horizontal polarization (i.e $\phi_0 = 0$) and vertical polarization (i.e. $\phi_0 = 90^o$), respectively. The following parameters are chosen: $h = 6$ meters, $a = 0.01$ meters, $\epsilon_2 = 10$, $f = 500$ kHz, and $\sigma_w = 5.8 \times 10^7$; all other electrical parameters are set to the free space values. For horizontal polarization, the current function decreases monotonically as θ_0 is increased. For vertical polarization, a maximium occurs for large θ_0; this maximum tends to $\theta_0 = 90^o$ as σ_2 is increased. These results and conclusions were previously made by Yatom and Ruppin [1983]. (The reader may refer to Appendix A, for the numerical approach used to obtain these results.)

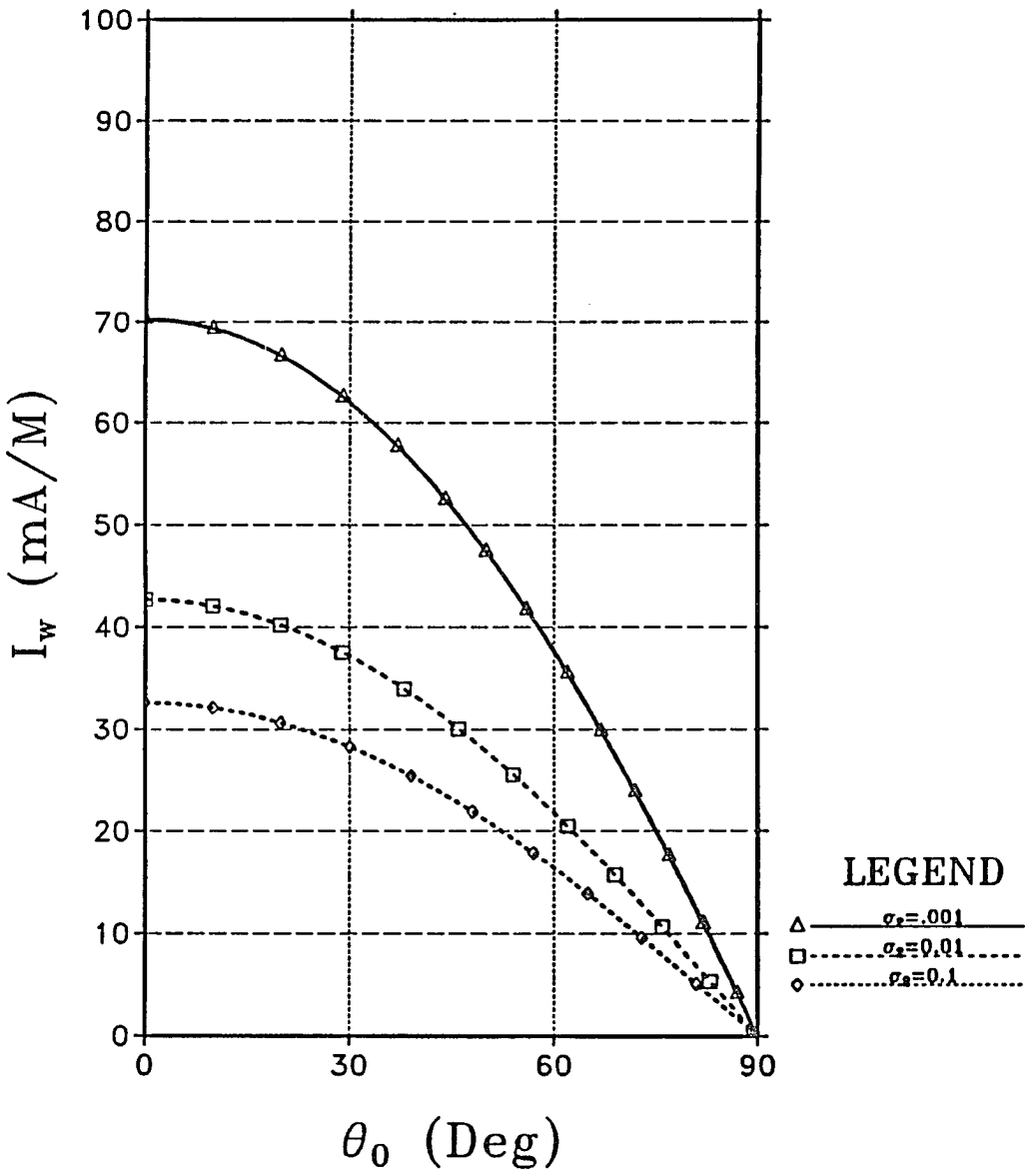

Figure 2-4 Induced current on a thin bare wire over a lossy interface for horizontal polarization. The relevant parameters are: $h = 6$ m, $a = 0.01$ m, $\epsilon_2 = 10\epsilon_0$, $f = 500$ kHz, and $\sigma_w = 5.8 \times 10^7$ S/m; all other electrical parameters are set to the free space values.

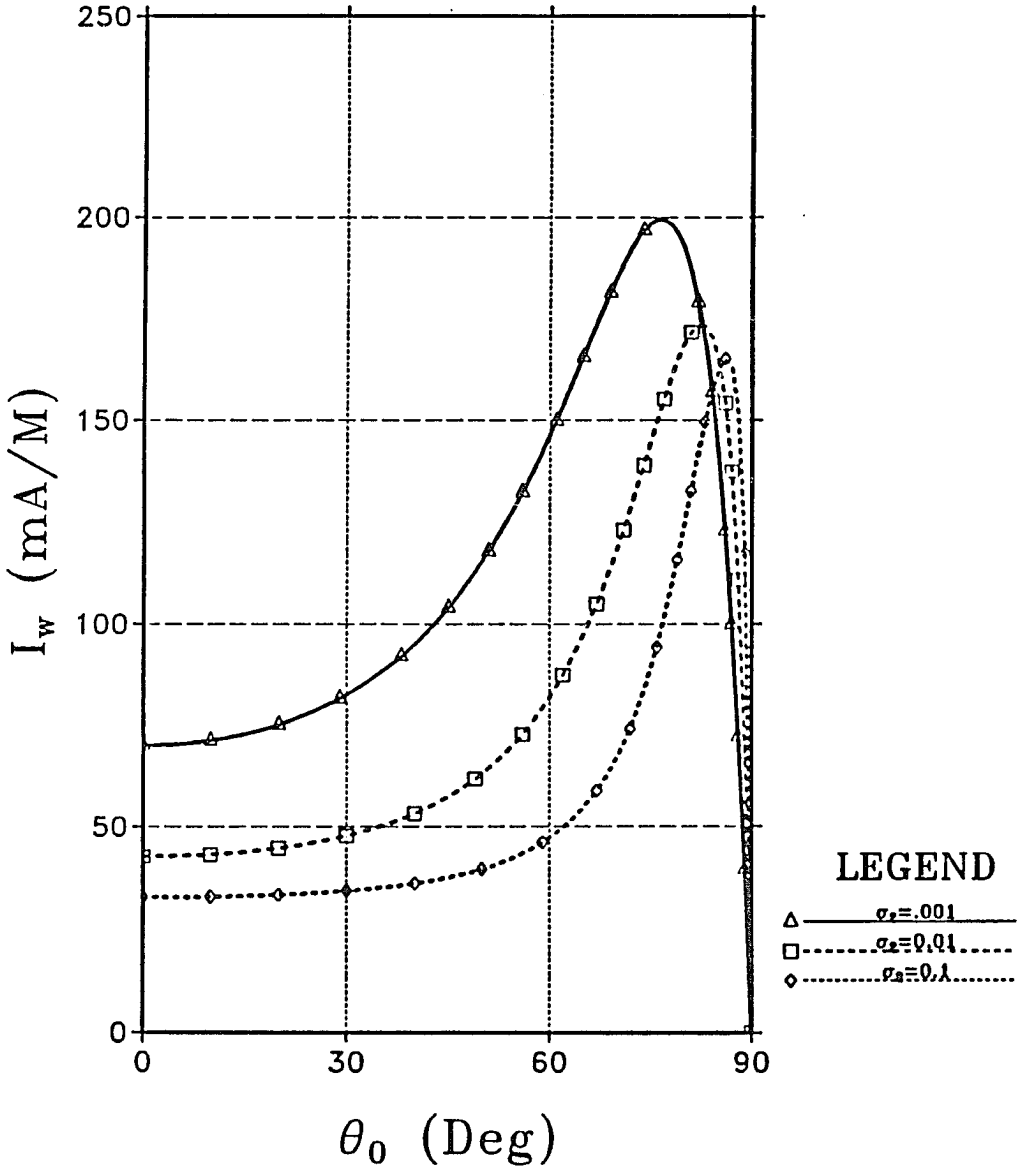

Figure 2-5 Induced current on a thin bare wire over a lossy interface for vertical polarization. The relevant parameters are: $h = 6$ m, $a = 0.01$ m, $\epsilon_2 = 10\epsilon_0$, $f = 500$ kHz, and $\sigma_w = 5.8 \times 10^7$ S/m; all other electrical parameters are set to the free space values.

CHAPTER 3

SHIELDING PROPERTIES OF AN ENSEMBLE OF THIN WIRES

In this chapter, the electromagnetic properties of an array of parallel wires in the presence of a half space are examined. The focus of this investigation is on the *interior* problem: the shielding of unwanted electromagnetic signals by the use of wire structures. Using Chapter Two as the starting point, we derive the complete analytical expressions that determine the induced currents flowing in each wire and the field scattered from the ensemble.

The analysis in which Wait [1954b, 1962] presented a rigorous solution to the boundary value problem, using Floquet's Theorem for the infinite grid structure, is confirmed in this chapter by the employment of an independent method. We begin with the solution for the finite grid (given in terms of a Fourier spectral integral), extend the results to the infinite grid case, and apply Poisson's Summation Formula to show explicitly how the infinite wire grid discretizes the continuous spectrum. Through numerical experimentation, an equivalent physical optics interpretation for the wire grid structure is formulated by comparing the infinite grid to the finitely extended grid.

Many of the results presented in this chapter have been documented in the literature and, consequently, appropriate references will be given. Such derivations are presented with the fundamental intent of bringing the multiplicity of publications and books into a single, concise document. The primary contribution of this work, however, is with numerical results – that is, a detailed examination of the

electromagnetic mechanisms and parameters that govern the shielding response of thin wire ensembles, through the use of numerical experimentation.

3.1 Ensemble of Thin Wire Scatterers

In Chapter 2, the problem of the single wire over a lossy half space was addressed. That analysis is now extended to included multiple wire configurations. In general, N wires are located at (x_n, z_n) $(n = 1, 2, \ldots, N)$ with a radius a and an axial impedance Z_w; this situation is depicted Figure 3–1. The restriction $z_n > 0$ will be made; the $z_n < 0$ case will immediately follow. The ensemble is excited by a plane wave of arbitrary incidence with arbitrary polarization, as diagrammed earlier in Figure 2–3. Although unnecessary, it will be analytically economical to assume that the electrical parameters of each wire, ϵ_w, μ_w and σ_w, are identical. The objective is to determine the individual currents on each wire and the total resulting field, namely, the shielding of the source wave inside the ensemble. Except for the thin wire approximation, no other assumptions are requisite. That is, the complete boundary value problem will be presented which includes all interactions between the mutual wires and the interface. The subsequent analytical presentation is similar to that provided in Chapter 2.

To solve this scattering problem, the total electric field is decomposed for the region $z > 0$ into three parts: an incident wave, a reflective wave and a scattered field:

$$E_y^{tot} = E_y^{inc} + E_y^{refl} + \sum_{n=1}^{N} E_{y_n}^{scat} \tag{3.1}$$

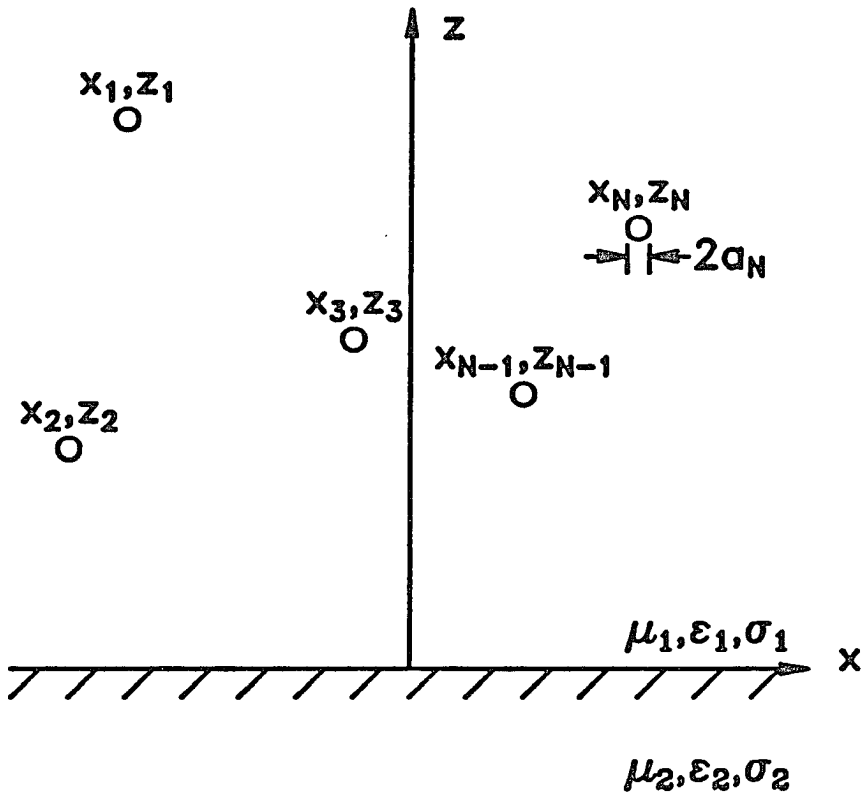

Figure 3-1 An ensemble of N wires over an homogeneous half space.

The summation term represents the aggregate of the fields scattered from the individual wires. As before, the incident wave and the reflected wave are given by (2.60) and (2.61), respectively. The field contribution of the nth wire E_{yn}^{scat} is a composite of the primary component E_{yn}^{p} and the secondary component E_{yn}^{s}. The corresponding expressions are given by (2.43) and (2.44), but with minor substitutions: I_w is replaced by I_n, h is replaced by z_n and x is replaced by $x - x_n$. From this, the primary and scattered fields, in integral form, are

$$E_{yn}^{p} = \frac{-v_a^2}{4\pi i\omega\epsilon_1} I_n e^{ik_y y} \int_{-\infty}^{\infty} \frac{e^{-u_a|z-z_n|}}{u_a} e^{-i\lambda(x-x_n)} d\lambda \tag{3.2}$$

and

$$E_{yn}^{s} = \frac{-v_a^2}{4\pi i\omega\epsilon_1} I_n e^{ik_y y} \int_{-\infty}^{\infty} R_y(\lambda, k_y) \frac{e^{-u_a(z+z_n)}}{u_a} e^{-i\lambda(x-x_n)} d\lambda \tag{3.3}$$

where, from the source excitation, $k_y = k_1 \sin\theta_0 \sin\phi_0$. Implicit in these forms for the incident, reflected and scattered fields are the satisfaction of the continuity conditions of tangential fields at the interface.

The last boundary condition to invoke is the relationship between the total field present at the surface of the wire and the induced current flowing in the wire. When the axial impedance operator given by (2.54) is applied, the total current flowing in the nth wire is

$$E_y^{tot}\Big|_{\rho_n=a} = I_n Z_w(k_y) e^{ik_y y} \tag{3.4}$$

where $\rho_n = \sqrt{(x-x_n)^2 + (z-z_n)^2}$, E_y^{tot} is given by (3.1), and Z_w is given by (2.55). The matching points will be chosen such that $x = x_n$ and $z = z_n + a$.

Applying (3.4) at the surface of each wire (i.e. including all self and mutual wire interactions) yields the following equation, which is similar to Wait's [1977b]:

$$E_y^{inc}(x_m, y, z_m) + E_y^{refl}(x_m, y, z_m) - \sum_{n=1}^{N} I_n Z_{n,m} e^{+ik_y y} = Z_w I_m e^{+ik_y y} \qquad (3.5)$$

Here $m = 1, 2, \ldots, N$. Once again, the impedance notation is used such that

$$Z_{n,m} = Z_{n,m}^p + Z_{n,m}^s \qquad (3.6)$$

with

$$Z_{n,m}^p = \frac{v_a^2}{4\pi i\omega\epsilon_1} \int_{-\infty}^{\infty} \frac{e^{-u_a|z_m - z_n + a_n|}}{u_a} e^{-i\lambda(x_m - x_n)} d\lambda \qquad (3.7)$$

and

$$Z_{n,m}^s = \frac{v_a^2}{4\pi i\omega\epsilon_1} \int_{-\infty}^{\infty} R_y(\lambda, k_y) \frac{e^{-u_a(z_m + z_n)}}{u_a} e^{-i\lambda(x_m - x_n)} d\lambda \qquad (3.8)$$

Since the wires are assumed thin, the a dependency has been neglected for $n \neq m$; as a result, the linear system of equations is symmetric.

Equation (3.5) may be viewed from the circuit interpretation of generalized impedances, currents and voltages [Harrington, 1968, §5-1]. The impedance term, which includes the axial impedance expression and the summation term, are geometrically and frequency dependent, but independent of the applied source. The zeros of the determinant of the impedance matrix are the natural frequencies of the system. Thus, the entire time domain response to a unit impulse is buried in (3.5). The impressed field determines the voltage excitation from which the currents in each wire can be obtained.

Since (3.5) represents a system of N equations with N unknowns, the induced currents on each wire can be obtained. Unfortunately, regardless of the difficulty in loading the $Z_{n,m}$ matrix, this system must be solved by numerical matrix methods for a generalized wire configuration. In the next section, the infinite grid will be analyzed; this will yield a closed–form expression for the individual currents. Nevertheless, once the currents are known, the total field can be determined at any point from (3.1).

3.2 Infinite Grid

With respect to a Cartesian coordinate system, the wire grid is contained in the plane $z = h$ and is parallel to a plane interface at $z = 0$, as shown in Figure 3–2. The grid is composed of an array of infinite wires parallel to the y axis and spaced a distance d between centers. Again, the wires are taken to be of circular cross section and the diameter $2a$ is assumed to be small compared to d and h. The media in both half spaces are homogeneous and lossless, with permittivity ϵ_1, for $x > 0$ and permittivity ϵ_2, for $x < 0$. The magnetic permeability is assumed to be the free space value μ_0, everywhere. The non–dissipative assumptions are consistent with frequency selective surface theory; without any loss of generality, the results can include dissipation effects by making the permittivity and the permeability complex. All other definitions and constraints are the same as in the previous section.

For this geometry, $x_n = nd$ and $z_n = h$ so that (3.5) becomes

$$E_y^{inc}(md, y, h) + E_y^{refl}(md, y, h) - \sum_{n=-\infty}^{\infty} I_n Z_{n,m} e^{+ik_y y} = Z_w I_m e^{+ik_y y} \qquad (3.9)$$

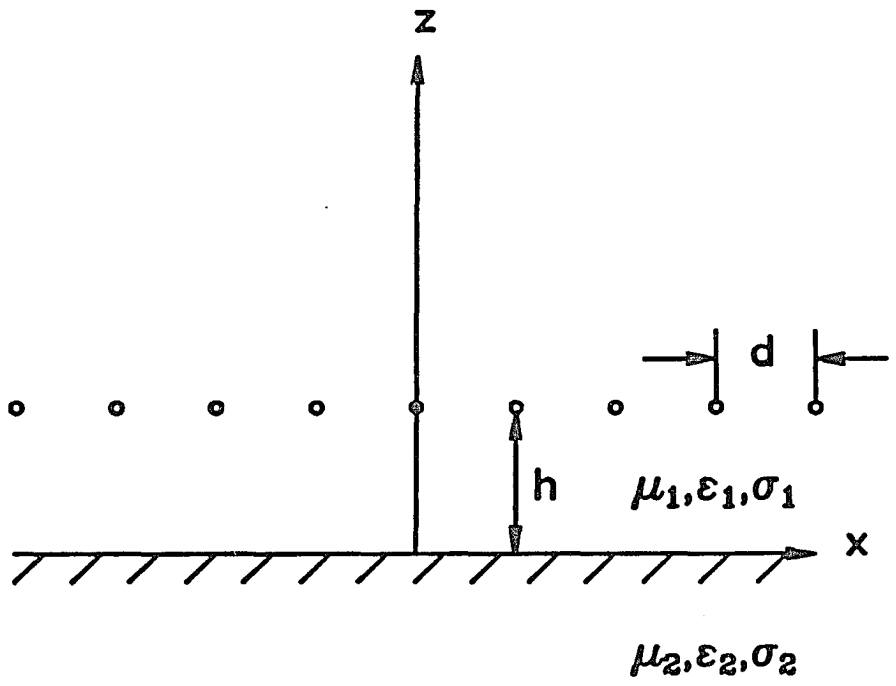

Figure 3-2 A planar grid of parallel wires over an homogeneous half space.

A closed form solution is obtainable for (3.9) by the invocation of Floquet's Theorem. Due to the periodicity of the grid, the current is invariant in amplitude from wire to wire, whereas the phase is linearly progressive by the amount associated with the wire separation, d, and the propagation delay along x (i.e. k_x). For this reason, the equality $I_n = I_w e^{indk_x}$ is justifiable (recall from Chapter Two that $k_x = k_1 \sin\theta_0 \cos\phi_0$). Hence,

$$I_w e^{+ik_y y} = \frac{E_y^{inc}(md, y, h) + E_y^{refl}(md, y, h)}{Z_w e^{+imk_x d} + \sum_{n=-\infty}^{\infty} Z_{n,m} e^{+indk_x}} \tag{3.10}$$

The above equation is valid for all m so that, without any loss of generality, it is convenient to set $m = 0$. The result is

$$I_w e^{+ik_y y} = \frac{E_y^{inc}(0, y, h) + E_y^{refl}(0, y, h)}{Z_w + S_0} \tag{3.11}$$

where

$$S_0 = \sum_{n=-\infty}^{\infty} Z_{n,0} e^{+indk_x} \tag{3.12}$$

From (3.7) and (3.8), the above summation may be written as the composition of two other series, say, S_1 and S_2 (i.e. $S_0 = S_1 + S_2$) where

$$S_1 = \frac{v_a^2}{4\pi i\omega\epsilon_1} \sum_{n=-\infty}^{\infty} e^{+indk_x} \int_{-\infty}^{\infty} \frac{e^{-au_a}}{u_a} e^{-ind\lambda} d\lambda \tag{3.13}$$

and

$$S_2 = \frac{v_a^2}{4\pi i\omega\epsilon_1} \sum_{n=-\infty}^{\infty} e^{+indk_x} \int_{-\infty}^{\infty} R_y(\lambda, k_y) \frac{e^{-2u_a h}}{u_a} e^{-ind\lambda} d\lambda \tag{3.14}$$

In theory, (3.11) is the closed form solution for the current amplitudes in each wire. The infinite summation involves the computation of Sommerfeld type integrals, which is undesireable. However, by following a similar development as Bremmer [1949 §9.3] and applying the Cesaro series, we find that for some arbitrary, yet piecewise smooth, bounded function, say $F(\lambda)$, the following identity holds true:

$$\sum_{n=-\infty}^{\infty} e^{indk_x} \int_{-\infty}^{\infty} F(\lambda) e^{ind\lambda} d\lambda = \frac{2\pi}{d} \sum_{n=-\infty}^{\infty} F(\lambda)\Big|_{\lambda=\frac{2n\pi}{d}-k_x} \tag{3.15}$$

Equation (3.15) is an extension of the Poisson Summation Formula. The validity of (3.15) is guaranteed provided that $F(\lambda)$ is piecewise continuous, vanishes at $\lambda = \pm\infty$ and the integral, $\int_{-\infty}^{\infty} |F| d\lambda$ is finite [Stakgold, 1979].

The application of (3.15) and the performance of some basic algebraic steps, yields an alternative representation for S_1 and S_2 [Wait, 1954b, 1962]:

$$S_1 = \frac{v_a^2}{4\pi i\omega\epsilon_1} \sum_{n=-\infty}^{\infty} \frac{e^{-2\pi(a/d)U_n}}{U_n} \tag{3.16}$$

and

$$S_2 = \frac{v_a^2}{4\pi i\omega\epsilon_1} \sum_{n=-\infty}^{\infty} R_n \frac{e^{-4\pi(h/d)U_n}}{U_n} \tag{3.17}$$

When $\mu_1 = \mu_2$,

$$R_n = \frac{(n - k_x d/(2\pi))^2 k_y^2 (1-K_a)^2 + (k_1^2 U_n - k_2^2 U_n' K_a)(U_n + U_n' K_a)}{-(n - k_x d/(2\pi))^2 k_y^2 (1-K_a)^2 + (k_1^2 U_n + k_2^2 U_n' K_a)(U_n + U_n' K_a)} \tag{3.18}$$

where $K_a = v_a/v_b$ with

$$U_n = \sqrt{n^2 - 2nD_1 \sin\theta_0 \cos\phi_0 - D_1^2 \cos^2\theta_0} \tag{3.19}$$

and

$$U_n' = \sqrt{n^2 - 2nD_1 \sin\theta_0 \cos\phi_0 + D_1^2 \sin^2\theta_0 - D_2^2} \tag{3.20}$$

The factors $D_{1,2}$ are normalized dimensions with respect to wavelength, for lossless media, such that $D_{1,2} = d/\lambda_{1,2}$, or equivalently, $D_{1,2} = k_{1,2}d/(2\pi)$. Equation (3.11), in conjunction with (3.16) and (3.17), is an alternative closed form solution for the current amplitude.

The final step is to extract the quasi–static behavior from the series S_1 and S_2; this will improve their convergence rate. First, it is noted that

$$\begin{aligned} \lim_{n\to\infty} U_n &= \lim_{n\to\infty} |n| \\ \lim_{n\to\infty} U_n' &= \lim_{n\to\infty} |n| \\ \lim_{n\to\infty} R_n &= R^{(0)} \end{aligned} \tag{3.21}$$

where $R^{(0)} = R_n$ when $d = 0$. Explicitly,

$$R^{(0)} = \frac{k_y^2(1-K_a)^2 + (k_1^2 - k_2^2 K_a)(1+K_a)}{-k_y^2(1-K_a)^2 + (k_1^2 + k_2^2 K_a)(1+K_a)} \tag{3.22}$$

Recalling that $(a/d) << 1$ and using the information of (3.21), we may write the series of (3.16) and (3.17) in the form

$$S_1 = \frac{-v_a^2}{2\omega\epsilon_1 k_1 d\cos\theta_0} + \frac{v_a^2}{4\pi i\omega\epsilon_1}\left\{S_a + \sum_{n=-\infty, n\neq 0}^{\infty}\left[\frac{1}{U_n} - \frac{1}{|n|}\right]\right\} \tag{3.23}$$

and

$$S_2 = \frac{-v_a^2}{2\omega\epsilon_1 k_1 d\cos\theta_0} R_0 e^{-2ik_1 h\cos\theta_0} + \frac{v_a^2}{4\pi i\omega\epsilon_1}\left\{S_b + \sum_{n=-\infty, n\neq 0}^{\infty}\left[R_n \frac{e^{-4\pi(h/d)U_n}}{U_n} - R^{(0)}\frac{e^{-4\pi|n|(h/d)}}{|n|}\right]\right\} \tag{3.24}$$

where

$$S_a = 2\sum_{n=1}^{\infty}\frac{e^{-2\pi n(a/d)}}{n} \tag{3.25}$$

and

$$S_b = 2R^{(0)}\sum_{n=1}^{\infty}\frac{e^{-4\pi n(h/d)}}{n} \tag{3.26}$$

The series of (3.25) and (3.26) are summable [Wheelon, 1968]:

$$\sum_{n=1}^{\infty}\frac{e^{-\alpha m}}{m} = -\ln\left(1-e^{-\alpha}\right) \approx -\ln(\alpha) \qquad for\ \ \alpha << 1 \tag{3.27}$$

Now since $a << d$, the quasi-static leading term is

$$S_a = 2\ln\left(\frac{d}{2\pi a}\right) \tag{3.28}$$

Similarly,

$$S_b = -2R^{(0)}\ln\left(1-e^{-4\pi(h/d)}\right) \tag{3.29}$$

With these previous derivations in place, the final expression for the current can be written in the following compact form [Wait, 1962]:

$$I_w e^{+ik_y y} = \frac{d[E_y^{inc}(0,y,h) + E_y^{refl}(0,y,h)]}{Z_g - \frac{v_a^2}{2\omega\epsilon_1 k_1 \cos\theta_0}\left\{1 + R_0 e^{-2ik_1 h\cos\theta_0}\right\}} \tag{3.30}$$

where

$$Z_g = \frac{v_a^2 d}{2\pi i\omega\epsilon_1}\left[\ln\frac{d}{2\pi a} - R^{(0)}\ln\left(1 - e^{-4\pi|h/d|}\right) + \Delta\right] + dZ_w \tag{3.31}$$

The quantity Δ is defined as the correction factor to the logarithmic terms and is given by

$$\Delta = \frac{1}{2}\sum_{n=-\infty, n\neq 0}^{\infty}\left[\frac{1 + R_n e^{-4\pi|h/d|U_n}}{U_n} - \frac{1 + R^{(0)} e^{-4\pi|h/d||n|}}{|n|}\right] \tag{3.32}$$

If the grid were placed below the interface, the shunt impedance expression would still be given by (3.31) and (3.32) with subscripts one and two interchanged; this accounts for the magnitude signs around the h. Wait [1962] has shown that the impedance term Z_g acts as a shunt impedance in an equivalent, two-segment transmission line.

Once the current is known, the primary and scatttered fields are computable from (3.2) and (3.3). Summing over all n, and again applying the Summation Formula of (3.15), yields (for $z > 0$),

$$E_y^p = \frac{-v_a^2}{4\pi i\omega\epsilon} I_w e^{ik_x x} e^{ik_y y}\sum_{n=-\infty}^{\infty} e^{-(2\pi/d)|z-h|U_n}\frac{e^{-i(2n\pi/d)x}}{U_n} \tag{3.33}$$

and

$$E_y^s = \frac{-v_a^2}{4\pi i\omega\epsilon} I_w e^{ik_x x} e^{ik_y y} \sum_{n=-\infty}^{\infty} R_n e^{-(2\pi/d)(z+h)U_n} \frac{e^{-i(2n\pi/d)x}}{U_n} \tag{3.34}$$

Therefore, for an infinite grid, the total field is

$$E_y^{tot} = E_y^{inc} + E_y^{ref'l} + E_y^p + E_y^s \tag{3.35}$$

Inherent in (3.33) and (3.34) is the re-radiation of wave types from the grid. For values of n for which U_n is entirely imaginary, the re-radiation wavefronts are simple plane waves corresponding to real angles of reflectance. As n increases, U_n will become entirely real so that the re-radiated wavefronts are evanescent. For these values of n, the grating produces an inductive storage field in its vicinity [MacFarlane, 1946].

The preceeding analysis illuminates the important physical concepts that underlie wire grid structures. The method given herein has general applicability to more complex periodic structures. For example, if the grid were in or over a stratified earth, then the only analytical task would be to derive an expression for the wave function (for the single wire) in terms of a continuous spectral integral. The application of Poisson's Summation Formula would give directly the solution for the grid. Thus, a whole class of problems of this type can be solved with little effort.

3.2.1 Parallel Incidence

If the plane of incidence is defined as the yz plane, then for parallel (or vertical) polarization (i.e $\phi_0 = \pi/2$), $k_x = 0$ and $k_y = k_1 \sin\theta_0$, with $U_n = \sqrt{n^2 - D_1^2 \cos^2\theta_0}$ and $U_n' = \sqrt{n^2 - D_1^2 \sin^2\theta_0 - D_2^2}$. As a result, the expressions in the previous section collapse into those of Wait [1962]:

$$I_w = \frac{E_v d \cos\theta_0 \left(e^{ik_1 h\cos\theta_0} - R_v e^{-ik_1 h\cos\theta_0}\right)}{\frac{1}{2}\eta_1 \cos\theta_0 \left\{1 - R_v e^{-2ik_1 h\cos\theta_0}\right\} + Z_g^v} \tag{3.36}$$

where R_v is given by (2.63) and

$$Z_g^v = dZ_w + \frac{i\omega\mu d\cos^2\theta_0}{2\pi}\left(\ln\frac{d}{2\pi a} - R^{(0)}\ln\left(1 - e^{-4\pi|h/d|}\right) + \Delta^v\right) \tag{3.37}$$

with

$$\Delta^v = \sum_{n=1}^{\infty}\left[\frac{1 + R_n^v e^{-4\pi|h/d|\sqrt{n^2 - D_1^2\cos^2\theta_0}}}{\sqrt{n^2 - D_1^2\cos^2\theta_0}} - \frac{1 + R^{(0)}e^{-4\pi|h/d|n}}{n}\right] \tag{3.38}$$

and

$$R_n^v = \frac{n^2 k_y^2 (1 - K_a)^2 + (k_1^2 U_n - k_2^2 U_n' K_a)(U_n + U_n' K_a)}{-n^2 k_y^2 (1 - K_a)^2 + (k_1^2 U_n + k_2^2 U_n' K_a)(U_n + U_n' K_a)} \tag{3.39}$$

In (3.36), we defined the intrinsic impedance of region one η_1 by $\eta_1 = \sqrt{\mu_1/\epsilon_1}$.

From (3.33) and (3.34), the primary and scattered fields are then

$$E_y^p = \frac{-i\omega\mu_1\cos^2\theta_0}{4\pi} I_w e^{ik_y y} \sum_{n=-\infty}^{\infty} \frac{e^{-(2\pi/d)|z-h|\sqrt{n^2 - D_1^2\cos^2\theta_0}}}{\sqrt{n^2 - D_1^2\cos^2\theta_0}} e^{-i(2n\pi/d)x} \tag{3.40}$$

and

$$E_y^s = \frac{-i\omega\mu_1 d\cos^2\theta_0}{4\pi} I_w e^{ik_y y} \sum_{n=-\infty}^{\infty} R_n^v \frac{e^{-(2\pi/d)(z+h)\sqrt{n^2 - D_1^2\cos^2\theta_0}}}{\sqrt{n^2 - D_1^2\cos^2\theta_0}} e^{-i(2n\pi/d)x} \tag{3.41}$$

3.2.2 Perpendicular Incidence

If the plane of incidence is defined as the xz plane, then for perpendicular (or horizontal) polarization (i.e $\phi_0 = 0$), $k_y = 0$, and $k_x = k_1 \sin\theta_0$. From this, the general results derived in Section 3.2 reduce those of Wait [1957]:

$$I_w = \frac{E_h d \left(e^{ik_1 h\cos\theta_0} + R_h e^{-ik_1 h\cos\theta_0}\right)}{\frac{\eta_1}{2\cos\theta_0}\left\{1 + R_h e^{-2ik_1 h\cos\theta_0}\right\} + Z_g^h} \tag{3.42}$$

where R_h is given by (2.62) and

$$Z_g^h = dZ_w + \frac{i\omega\mu_0 d}{2\pi}\left(\ln\frac{d}{2\pi a} + \Delta^h\right) \tag{3.43}$$

Here

$$\begin{aligned}\Delta^h =& \frac{1}{2}\sum_{n=1}^{\infty}\left[\frac{1 + R_n^h \exp[-4\pi|h/d|\sqrt{(n - D_1\sin\theta_0)^2 - D_1^2}]}{\sqrt{(n - D_1\sin\theta_0)^2 - D_1^2}}\right.\\ &+ \left.\frac{1 + R_{-n}^h \exp[-4\pi|h/d|\sqrt{(n + D_1\sin\theta_0)^2 - D_1^2}]}{\sqrt{(n + D_1\sin\theta_0)^2 - D_1^2}} - \frac{2}{n}\right]\end{aligned} \tag{3.44}$$

and

$$R_n^h = \frac{\sqrt{(n - D_1\sin\theta_0)^2 - D_1^2} - \sqrt{(n - D_1\sin\theta_0)^2 - D_2^2}}{\sqrt{(n - D_1\sin\theta_0)^2 - D_1^2} + \sqrt{(n - D_1\sin\theta_0)^2 - D_2^2}} \tag{3.45}$$

where R_{-n}^h is obtained by replacing n with $-n$. For this polarization, $R^{(0)}$ is identically zero.

Finally, the resulting primary and secondary electric fields are

$$E_y^p = \frac{-i\omega\mu_1}{4\pi} I_w e^{ik_x x} \sum_{n=-\infty}^{\infty} \frac{e^{-(2\pi/d)|z-h|\sqrt{(n-D_1\sin\theta_0)^2-D_1^2}}}{\sqrt{(n-D_1\sin\theta_0)^2-D_1^2}} e^{-i(2n\pi/d)x} \tag{3.46}$$

and

$$E_y^s = \frac{-i\omega\mu_1}{4\pi} I_w e^{ik_x x} \sum_{n=-\infty}^{\infty} R_n \frac{e^{-(2\pi/d)(z+h)\sqrt{(n-D_1\sin\theta_0)^2-D_1^2}}}{\sqrt{(n-D_1\sin\theta_0)^2-D_1^2}} e^{-i(2n\pi/d)x} \tag{3.47}$$

Before investigating the numerical characteristics of Δ^h, we will look at a limiting case. The quantities Δ^∞ and $\Delta^{-\infty}$ are denoted as the value of the correction factor, Δ^h, when $h \to \pm\infty$, respectively. When $\theta_0 = 0$, (3.44) reduces to

$$\Delta^\infty = \sum_{n=1}^{\infty} \frac{1}{\sqrt{n^2 - D_1^2}} - \frac{1}{n} \tag{3.48}$$

and

$$\Delta^{-\infty} = \sum_{n=1}^{\infty} \frac{1}{\sqrt{n^2 - (KD_1)^2}} - \frac{1}{n} \tag{3.49}$$

Now let $D_1^4 << 1$ and $|KD_1|^4 << 1$; the difference of (3.48) from (3.49) is well approximated by

$$\Delta^\infty - \Delta^{-\infty} \approx \frac{1}{2} D_1^2 (1-K^2) \sum_{n=1}^{\infty} \frac{1}{n^3} \tag{3.50}$$

But, $\sum_{n=1}^{\infty} 1/n^3 = 1.20206\ldots$ [Wheelon, 1968] so that

$$\Delta^\infty - \Delta^{-\infty} \approx 0.601 D_1^2 (1-K^2) \tag{3.51}$$

Equation (3.51) is consistent with a similar formula given by Wait [1957].

3.3 Numerical Results

The multiplicity of parameters that governs the electromagnetic response of thin wire sytems prevents a thorough numerical investigation into every possible case. In order to avoid a profusion of plots, the following results have been chosen to explicate the important electromagnetic features and phenomena.

For all calculations, an operating frequency of 1 MHz, an incident field strength of 1 V/m and a lossless free space for region one are assumed. The copper wires are chosen to be identical with the following parameters: $\epsilon_w = \epsilon_0$, $\mu_w = \mu_0$, $\sigma_w = 5.8 \times 10^7$ S/m and $k_1 a = 10^{-2}$. (For all practical purposes, the wire is essentially perfectly conducting for these wire parameters.) The lower half space will be characterized by the complex index of refraction K^2 so that the parameters ω, μ_2 (the permeability will assume the free space value), ϵ_2 and σ_2 will be given by a single number, K^2. As an example, for a 1 MHz signal with $\epsilon_2 = 8\epsilon_0$ and $\sigma_2 = 10^{-3}$ S/m, $K^2 = 8.00 - i17.98$. Thus, the specification of $k_1 a$ and K renders the results more general.

Our numerical field results were first tested against previously published scattering results [Richmond, 1965; Wait, 1986a; Ragheb and Hamid, 1988]. However, stronger validation tests can be established by comparing the responses of the infinitely extended grid with the finitely extended grid; these results are given in a later section.

To avoid confusion, the term parallel (or vertical) polarization is used to denote that the electric field is entirely parallel to the yz plane. Perpendicular (or horizontal) polarization will denote that electric field vector is perpendicular to the

xz plane. The former will excite travelling currents on the wires (i.e. $\frac{\partial}{\partial y} \neq 0$); the latter will excite only stationary currents (i.e. $\frac{\partial}{\partial y} = 0$).

For later discussions, it is convenient to define a shielding figure of merit or shielding efficiency expression in dB as follows:

$$S = 20\log_{10}\left|\frac{E_y}{E_y^{ref}}\right|$$

where E_y is the computed field with the shielding structure present and E_y^{ref} is the reference field at the same location without the shielding structure.

The numerical method for the computation of the Sommerfeld type integrals is given in detail in Appendix A. This method is similar to that proposed by Johnson and Dudley [1983].

3.3.1 Impedance Correction Factor: Perpendicular Polarization

Before proceeding to the general results, we may gain some insight by examining at a few plots of the correction factor for perpendicular polarization when the lower half space is lossless or perfectly conducting. (The case for parallel polarization has already been investigated in detail [Larsen, 1962a].) Although the infinite grid equations are completely general for all values of D_1, its value in subsequent computations will be restricted such that the relations, $D_1 < (1/(1 + \sin|\theta_0|)$ and $D_1 < (1/N_d(1 + \sin|\theta_0|)$ are satisfied. That is, grating lobes will not be allowed to occur for all values of d and h.

For a perfectly conducting lower half space, the correction factor Δ^h is plotted in Figures 3–3 and 3–4 as a function of H (here $H = h/\lambda_1$) for various values of D_1 when $\theta_0 = 0$ and 45 degrees, respectively; the results are in general agreement with those sketched in an earlier study [Wait, 1954a]. As expected, when $H \geq 1$, Δ^h approaches the value for the case where the wires are in free space [MacFarlane, 1946].

Similar results are shown in Figures 3–5 and 3–6 when $N_d^2 = 1.57$. Figure 3–7 shows the correction factor when region one is the denser medium (i.e. $N_d^2 = 1/1.57$) and $\theta_0 = 0$. The general shape of the curves shown in Figures 3–5, 3–6 and 3–7 is predicted by (3.51). The numerical data in Figure 3–7 supersedes and extends an earlier investigation [Wait, 1957].

3.3.2 Infinite Grid vs. Finitely Extended Grid

At this point it is desirable to compare the electromagnetic properties of the the finite grid with the infinite grid. The results will prove useful for two reasons. First, they will verify the numerical programming of each of the equations in this chapter. That is, by starting with two different analytical solutions (one containing infinite sums, the other containing infinite integrals) we may test the numerical implementations against each other. Second, they will delineate and correlate the indigenous electromagnetic response of each structure.

In this numerical example, both structures will have the same characteristic dimensions: $D_1 = 0.1$ and $h = 0.2\lambda_1$. The finite grid is centered at the origin with a total of 41 wires, so that its overall length is $4\lambda_1$. The fields will be computed along a horizontal plane at a height of 0.1λ.

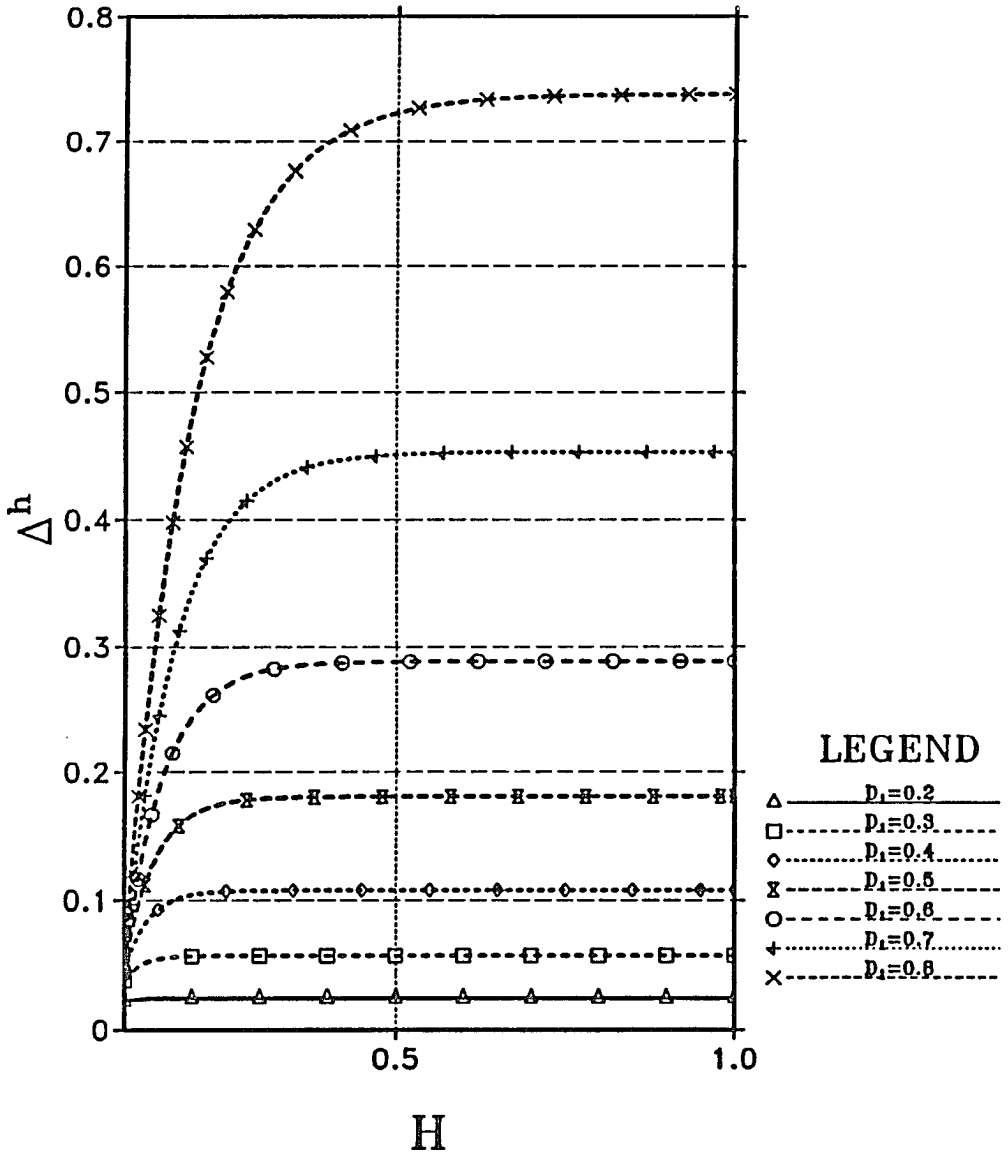

Figure 3-3 The impedance correction factor, Δ^h, as a function of the normalized distance H ($H = h/\lambda_1$) for various values of D_1 ($D_1 = d/\lambda_1$). Here we assume an incident plane wave with horizontal polarization and let $\theta_0 = 0$, $\phi_0 = 0$ and $\sigma_2 \rightarrow \infty$.

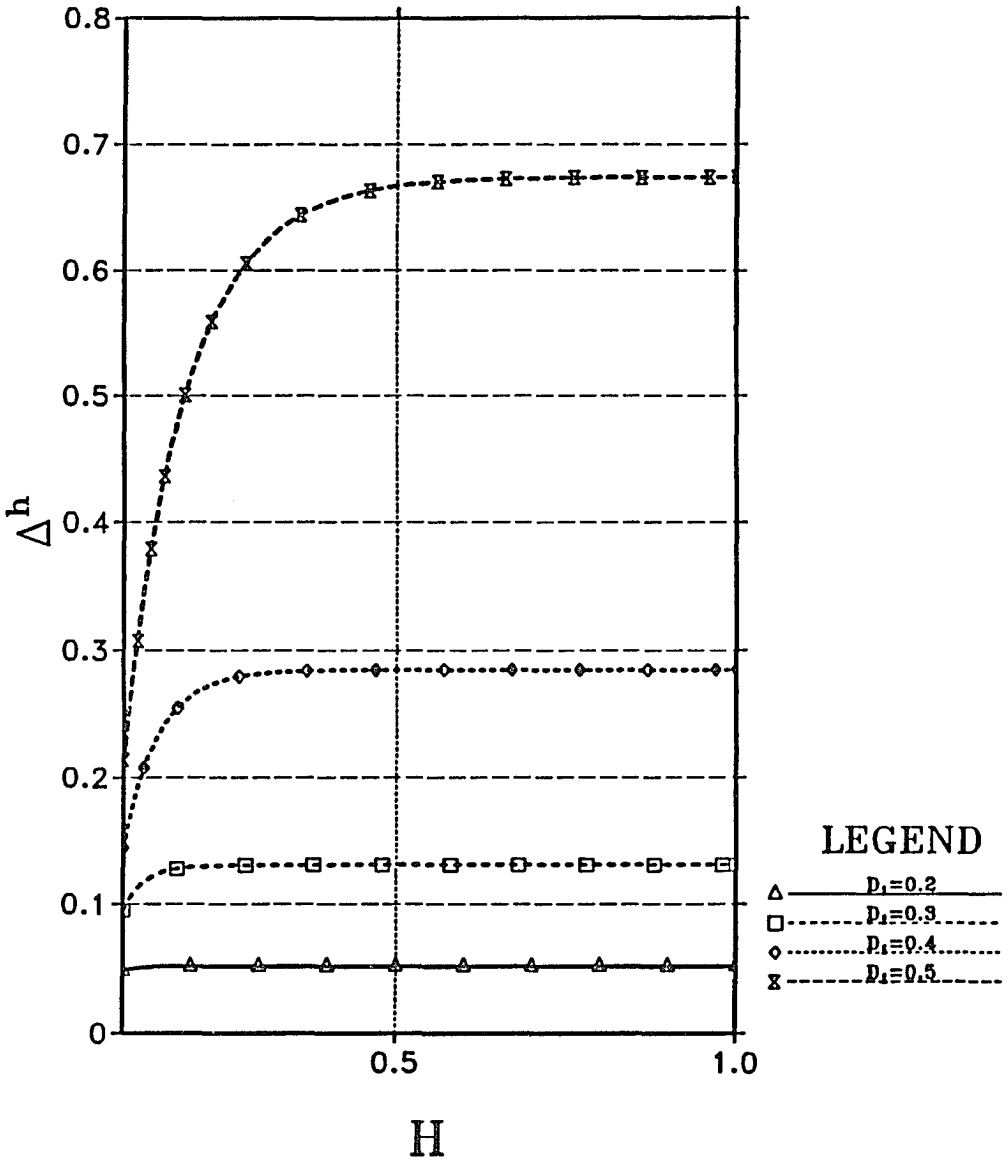

Figure 3-4 The impedance correction factor, Δ^h, as a function of the normalized distance H ($H = h/\lambda_1$) for various values of D_1 ($D_1 = d/\lambda_1$). Here we assume an incident plane wave with horizontal polarization and let $\theta_0 = 45^o$, $\phi_0 = 0$ and $\sigma_2 \rightarrow \infty$.

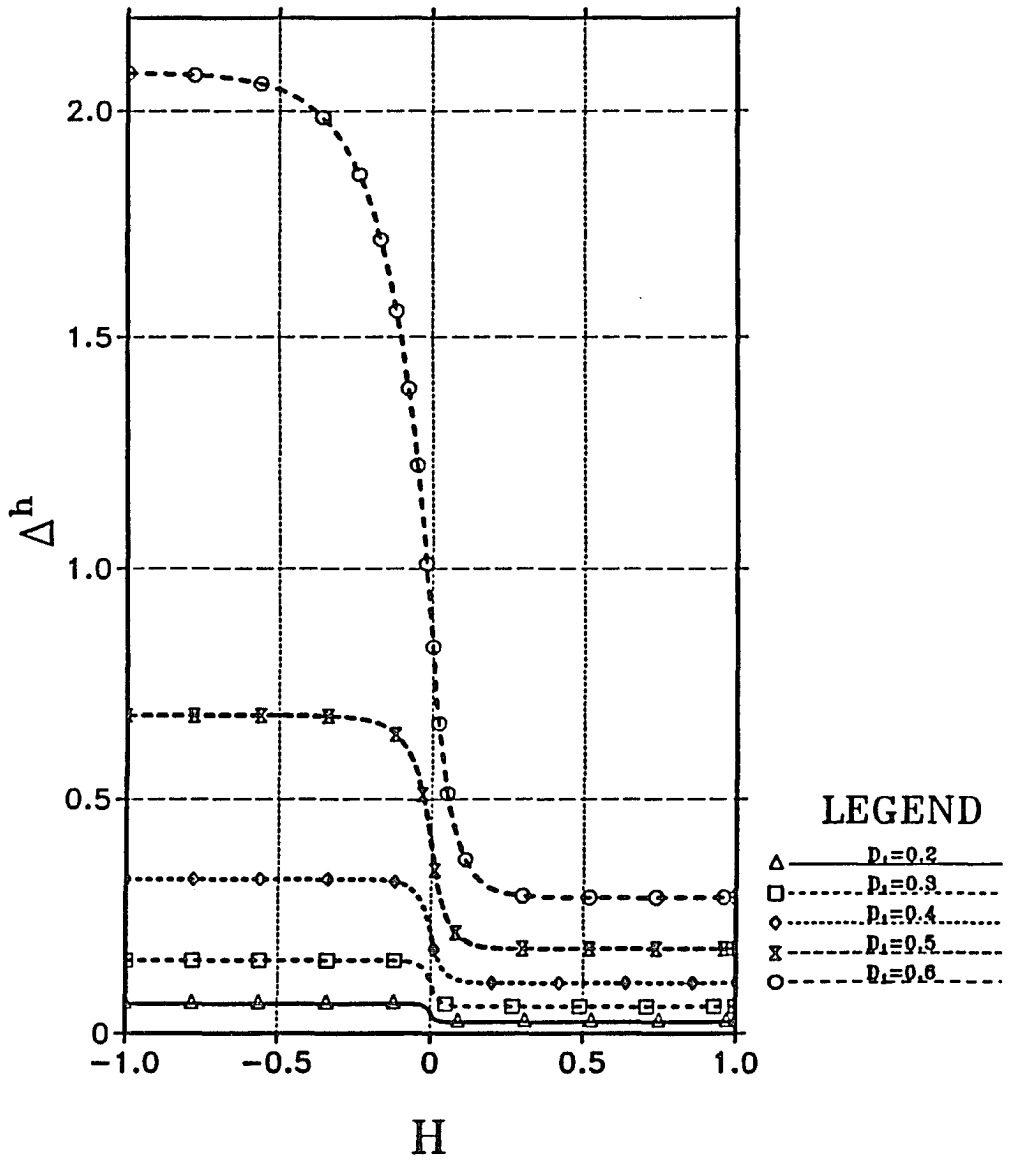

Figure 3-5 The impedance correction factor, Δ^h, as a function of the normalized distance H ($H = h/\lambda_1$) for various values of D_1 ($D_1 = d/\lambda_1$). Here we assume an incident plane wave with horizontal polarization and let $\theta_0 = 0$, $\phi_0 = 0$ and $N_d = 1.57$.

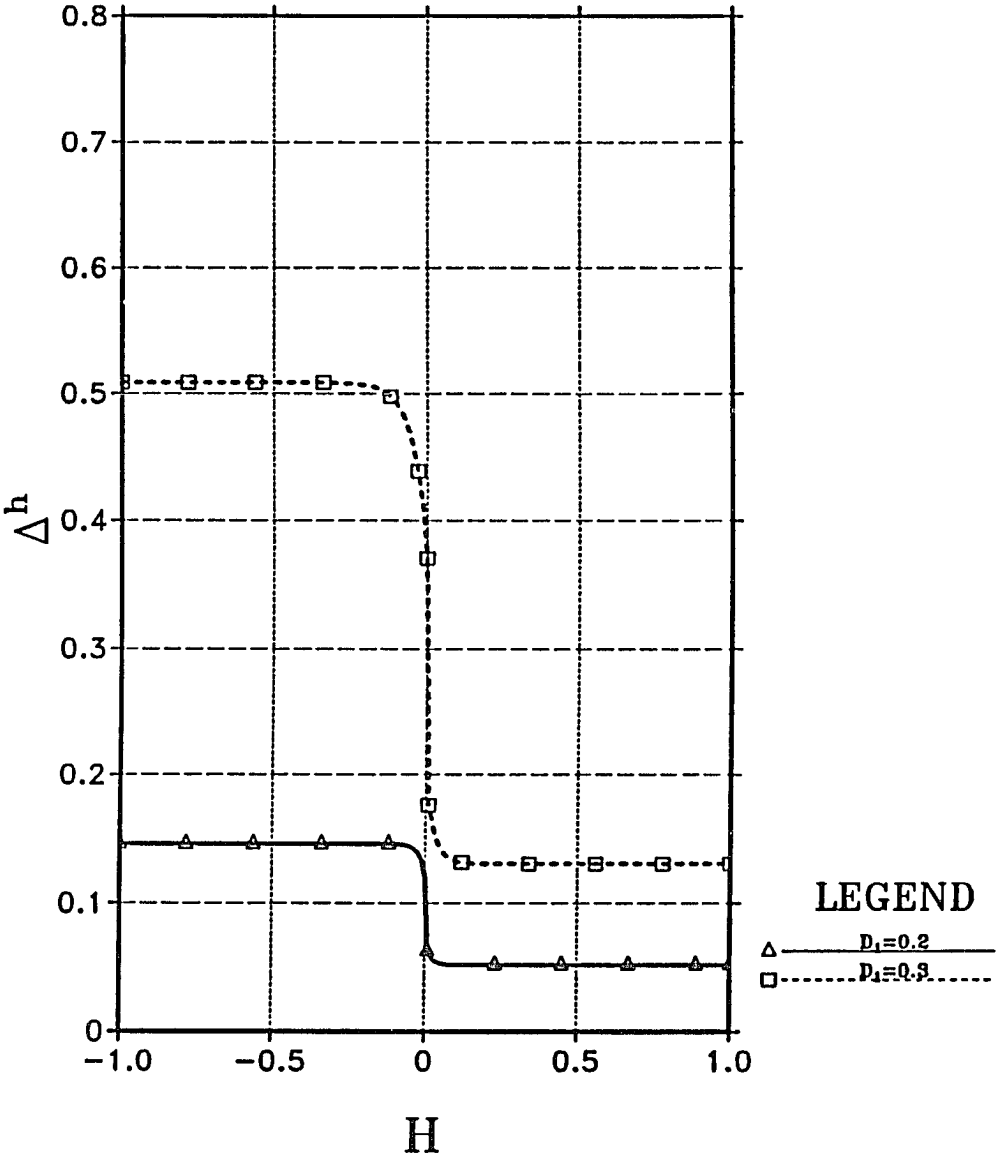

Figure 3-6 The impedance correction factor, Δ^h, as a function of the normalized distance H ($H = h/\lambda_1$) for various values of D_1 ($D_1 = d/\lambda_1$). Here we assume an incident plane wave with horizontal polarization and let $\theta_0 = 45°$, $\phi_0 = 0$ and $N_d = 1.57$.

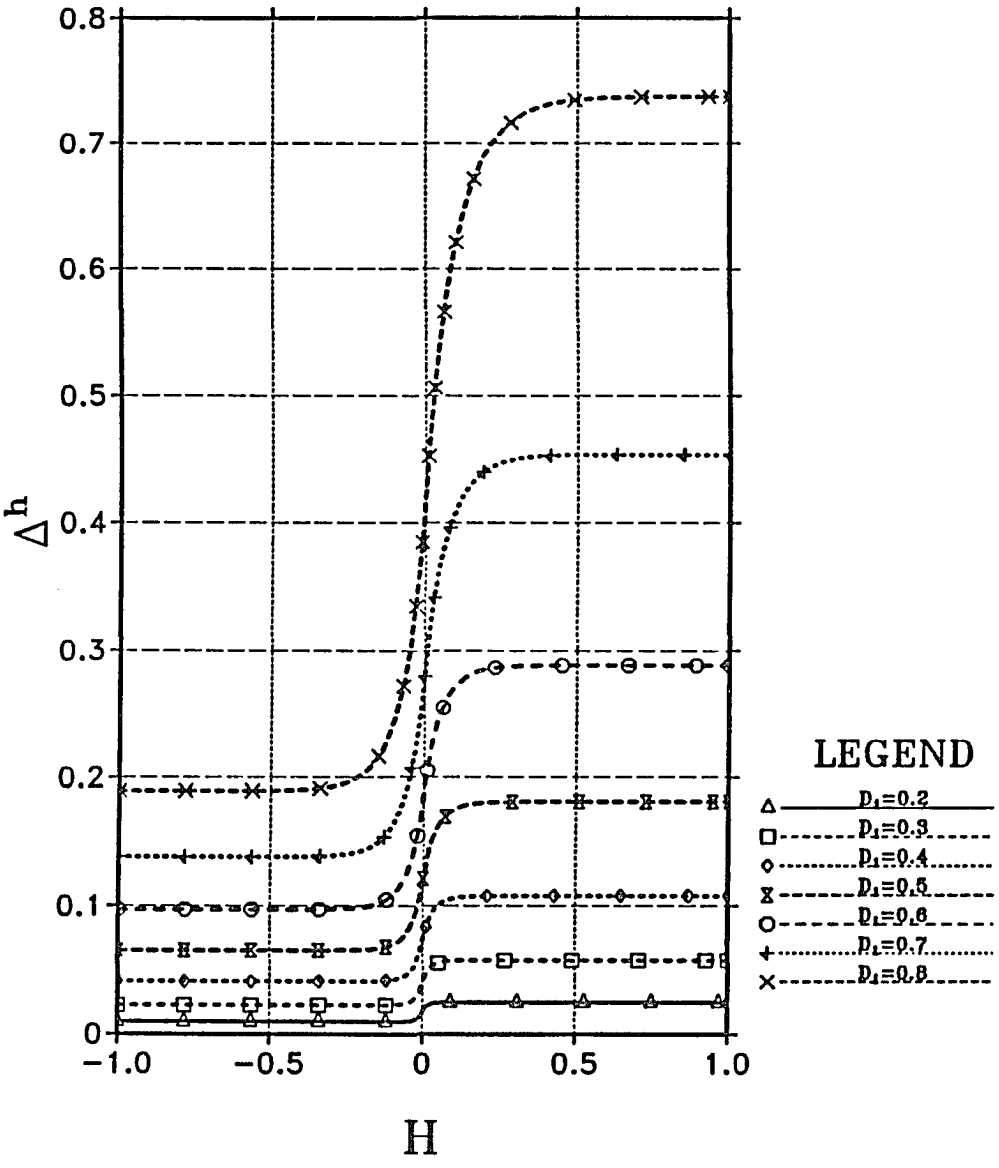

Figure 3-7 The impedance correction factor, Δ^h, as a function of the normalized distance H ($H = h/\lambda_1$) for various values of D_1 ($D_1 = d/\lambda_1$). Here we assume an incident plane wave with horizontal polarization and let $\theta_0 = 0$, $\phi_0 = 0$ and $N_d = 1/1.57$.

Figures 3–8 through 3–11 superimpose the total field response data, for perpendicular polarization, calculated from (3.1) and (3.35). The following parameters have been chosen: for Figure 3–8 region two is free space and $\theta_1 = 0$; Figure 3–9 is the same, but $\theta_0 = 30^o$; for Figure 3–10, $\theta_0 = 0$ and $K^2 = 8.00 - i17.98$; for Figure 3–11, the same earth parameters are kept, but $\theta_0 = 30^o$. In all four figures there are good correlations between field responses in the shadow region. The field response in the transition region is similar to phenomena observed for the continuous finite metalic strip resulting from the current edge singularity. The earth appears to smooth much of the oscillations observed in the free space case.

The former numerical experiment is repeated, but with parallel polarization. For Figures 3–12 and 3–13, the grid is in free space, with $\theta_0 = 30^o$ and $\theta_0 = 45^o$, respectively; Figures 3–14 and 3–15 assume that the grid is over a lossy earth ($K^2 = 8.00 - i17.98$), with the same aforementioned zenith parameters. In general, there are no new phenomena observed for this polarization.

For the data shown in Figure 3–16, for the finitely extended grid, we assume that $I_n = I_w \exp(-ink_1 d \sin\theta_0)$, where I_w is the computed value determined from (3.30). Such an approximation is equivalent to the physical optics approximation for the continuous conducting strip. The corresponding field response is plotted and then compared with the exact solution when $\theta_0 = 0$ and $K^2 = 8.00 - i17.98$. Except for the overshoot in the transition region, this approximation seems to give a good estimate for determining the field response in the shadow region. The advantage of such an approximation is the prediction of I_n without having to load and invert large matrices. It is found, for typical values of d and h, that the expression for Δ converges after the summation of about 100 terms. In contrast, the numerical evaluation of $Z_{n,m}$ can be on the order of 100 to 1000 terms, if the

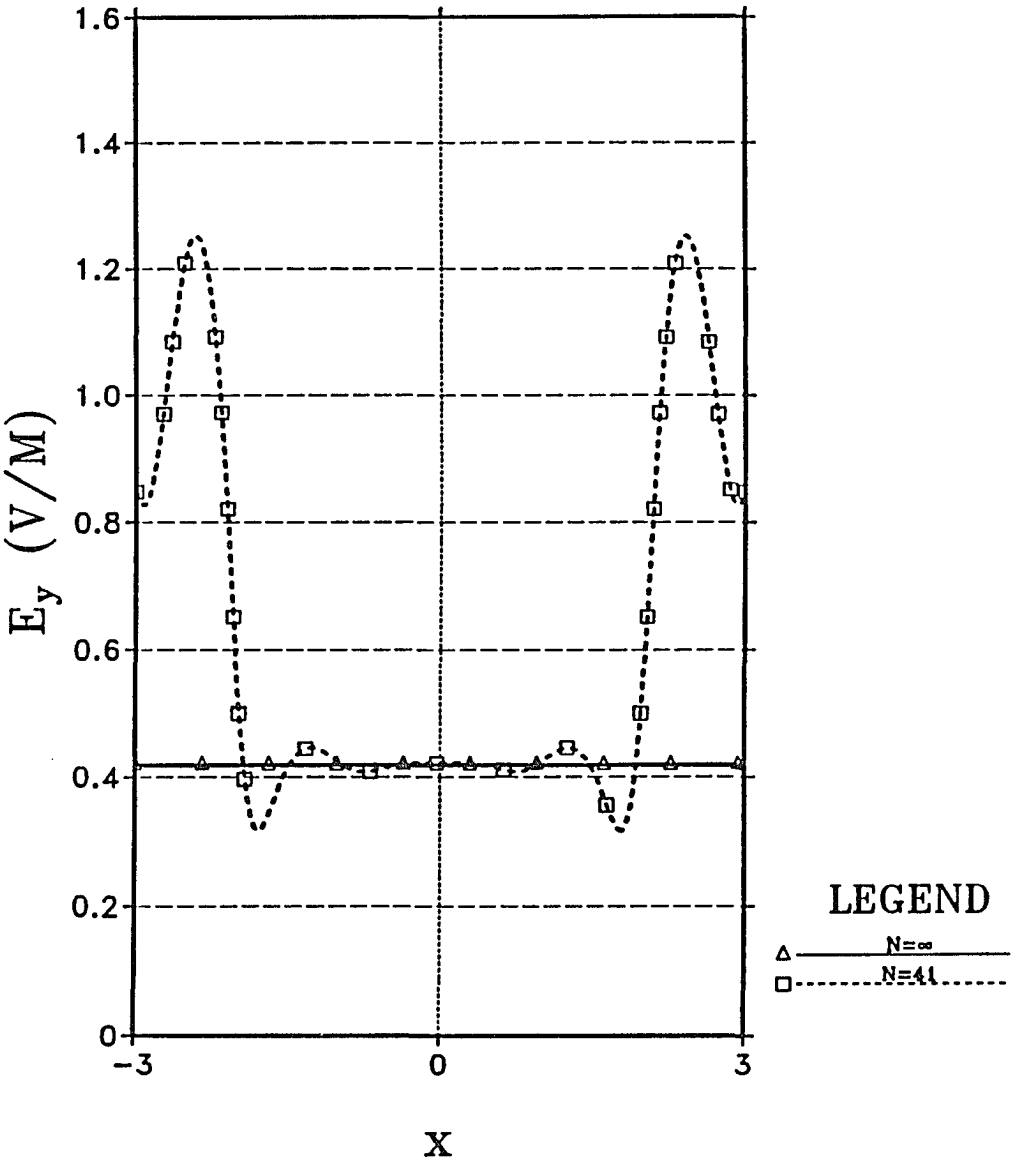

Figure 3-8 The electric field response below the finite and infinite wire grid in free space as a function of the horizontal distance x (x is normalized to free space wavelength) for a normally incident plane wave when $\theta_0 = 0$, $\phi_0 = 0$, $h = 0.2\lambda_1$, $d = .1\lambda_1$, $z = .1\lambda_1$ and $E_0 = 1$ V/m.

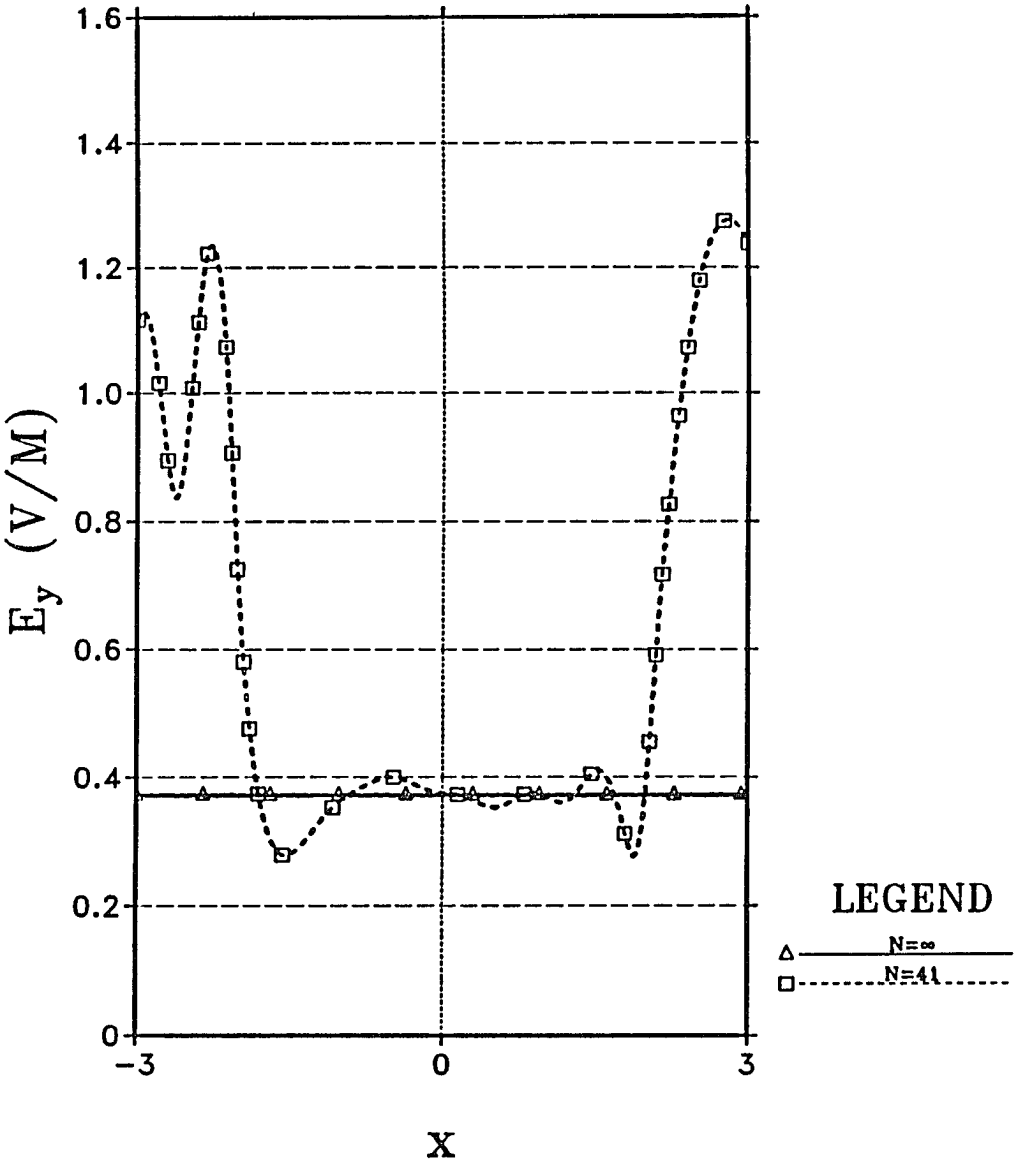

Figure 3-9 The electric field response below the finite and infinite wire grid in free space as a function of the horizontal distance x (x is normalized to free space wavelength) for perpendicular polarization when $\theta_0 = 30°$, $\phi_0 = 0$, $h = 0.2\lambda_1$, $d = .1\lambda_1$, $z = .1\lambda_1$ and $E_0 = 1$V/m.

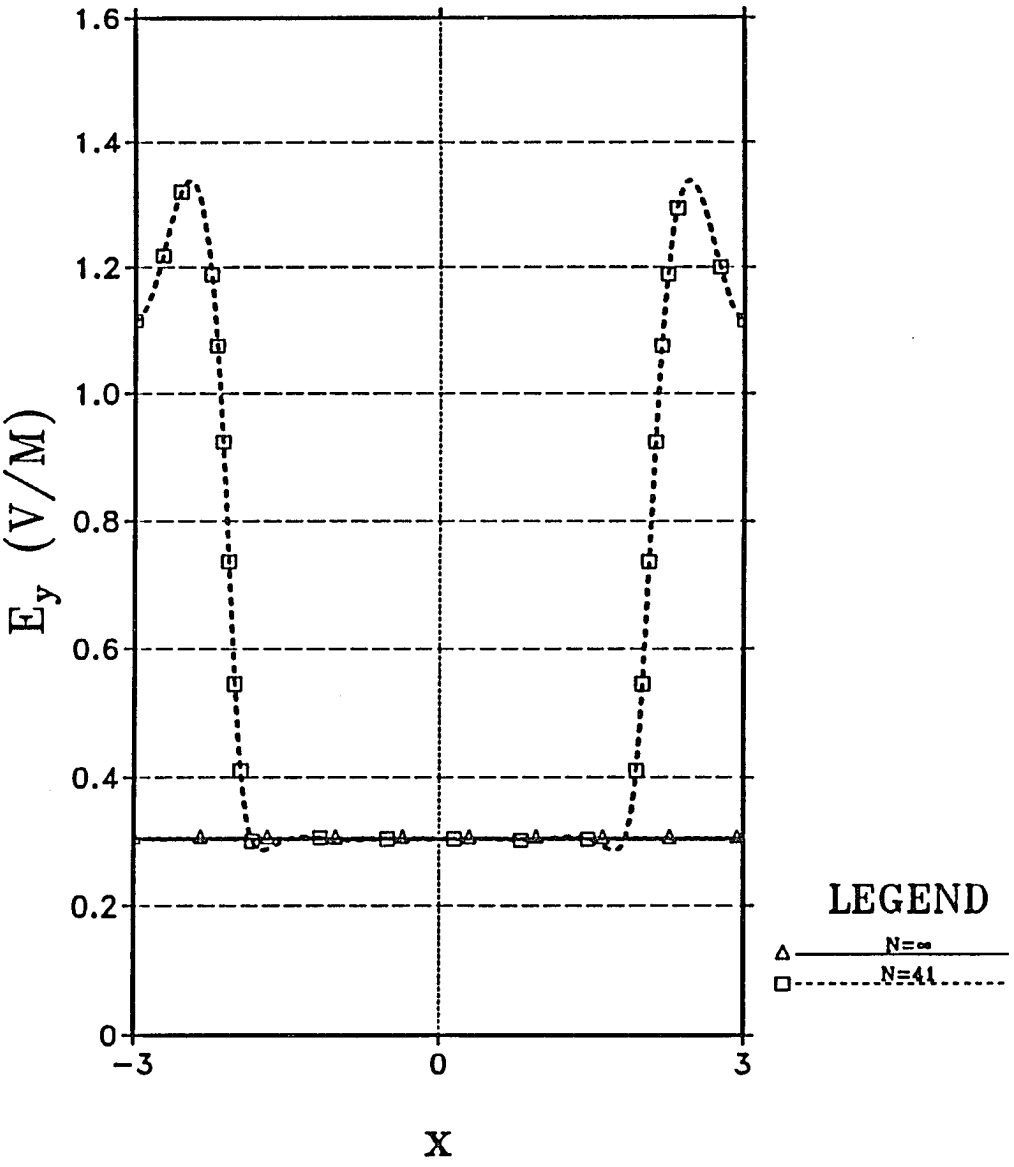

Figure 3-10 The electric field response below the finite and infinite wire grid over a lossy half space as a function of the horizontal distance x (x is normalized to free space wavelength) for a normally incident plane wave when $\theta_0 = 0$, $\phi_0 = 0$, $h = 0.2\lambda_1$, $d = .1\lambda_1$, $z = .1\lambda_1$, $K^2 = 8.00 - i17.89$ and $E_0 = 1\text{V/m}$.

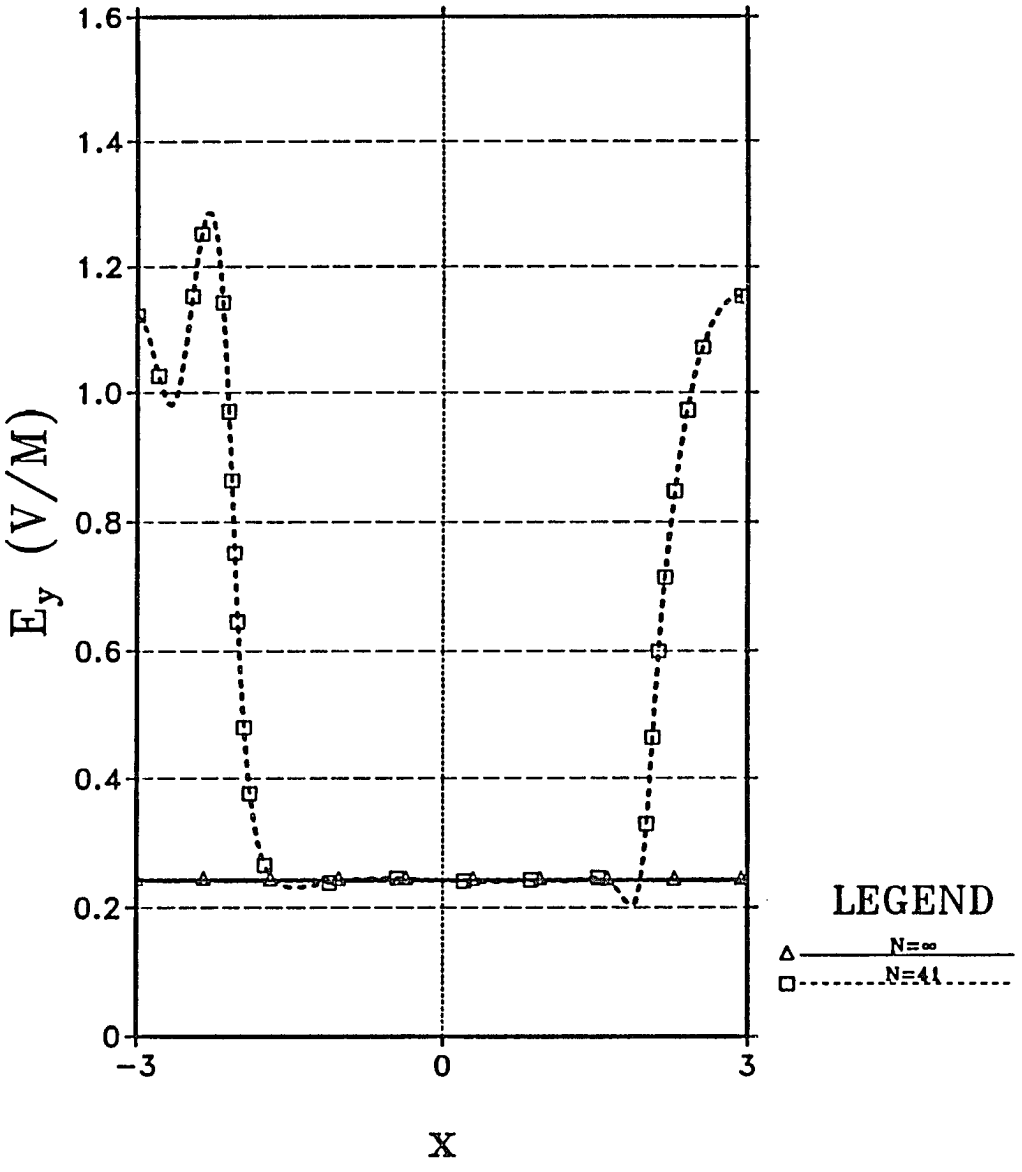

Figure 3-11 The electric field response below the finite and infinite wire grid over a lossy half space as a function of the horizontal distance x (x is normalized to free space wavelength) for perpendicular polarization when $\theta_0 = 30°$, $\phi_0 = 0$, $h = 0.2\lambda_1$, $d = .1\lambda_1$, $z = .1\lambda_1$, $K^2 = 8.00 - i17.89$ and $E_0 = 1\text{V/m}$.

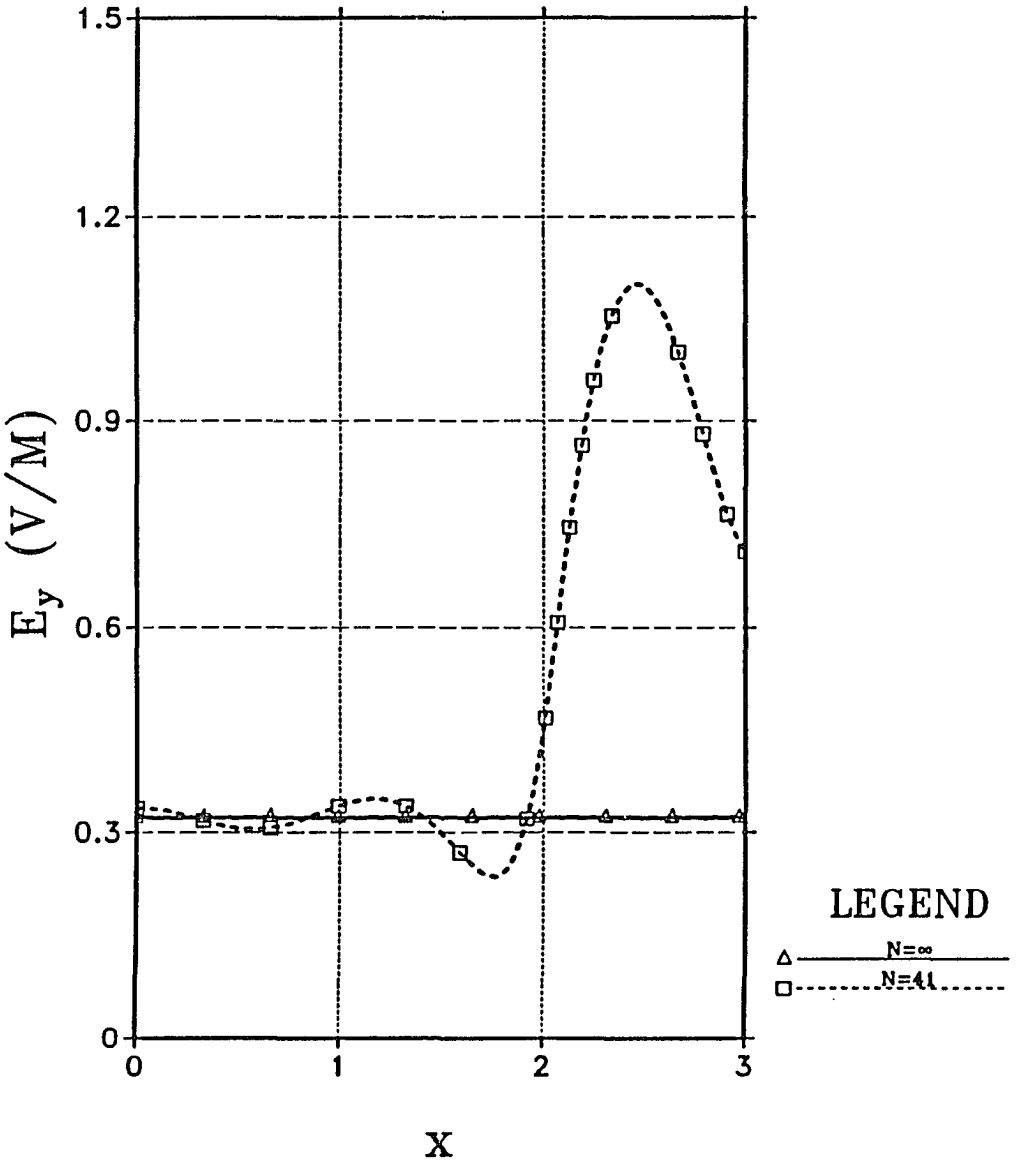

Figure 3-12 The electric field response below the finite and infinite wire grid in free space as a function of the horizontal distance x (x is normalized to free space wavelength) for parallel polarization when $\theta_0 = 30°$, $\phi_0 = 90°$, $h = 0.2\lambda_1$, $d = .1\lambda_1$, $z = .1\lambda_1$ and $E_0 = 1$V/m.

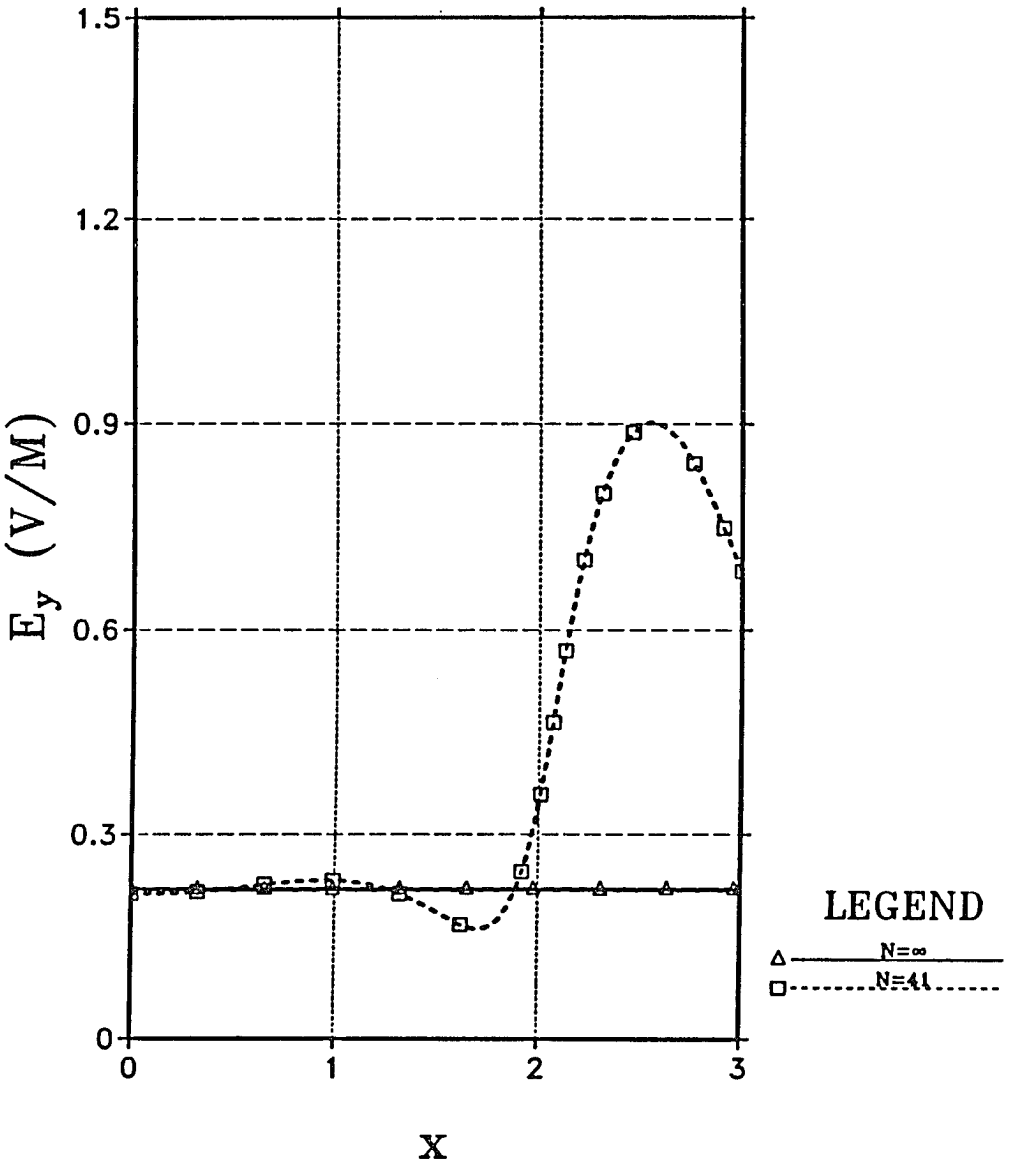

Figure 3-13 The electric field response below the finite and infinite wire grid in free space as a function of the horizontal distance x (x is normalized to free space wavelength) for parallel polarization when $\theta_0 = 45°$, $\phi_0 = 90°$, $h = 0.2\lambda_1$, $d = .1\lambda_1$, $z = .1\lambda_1$ and $E_0 = 1$V/m.

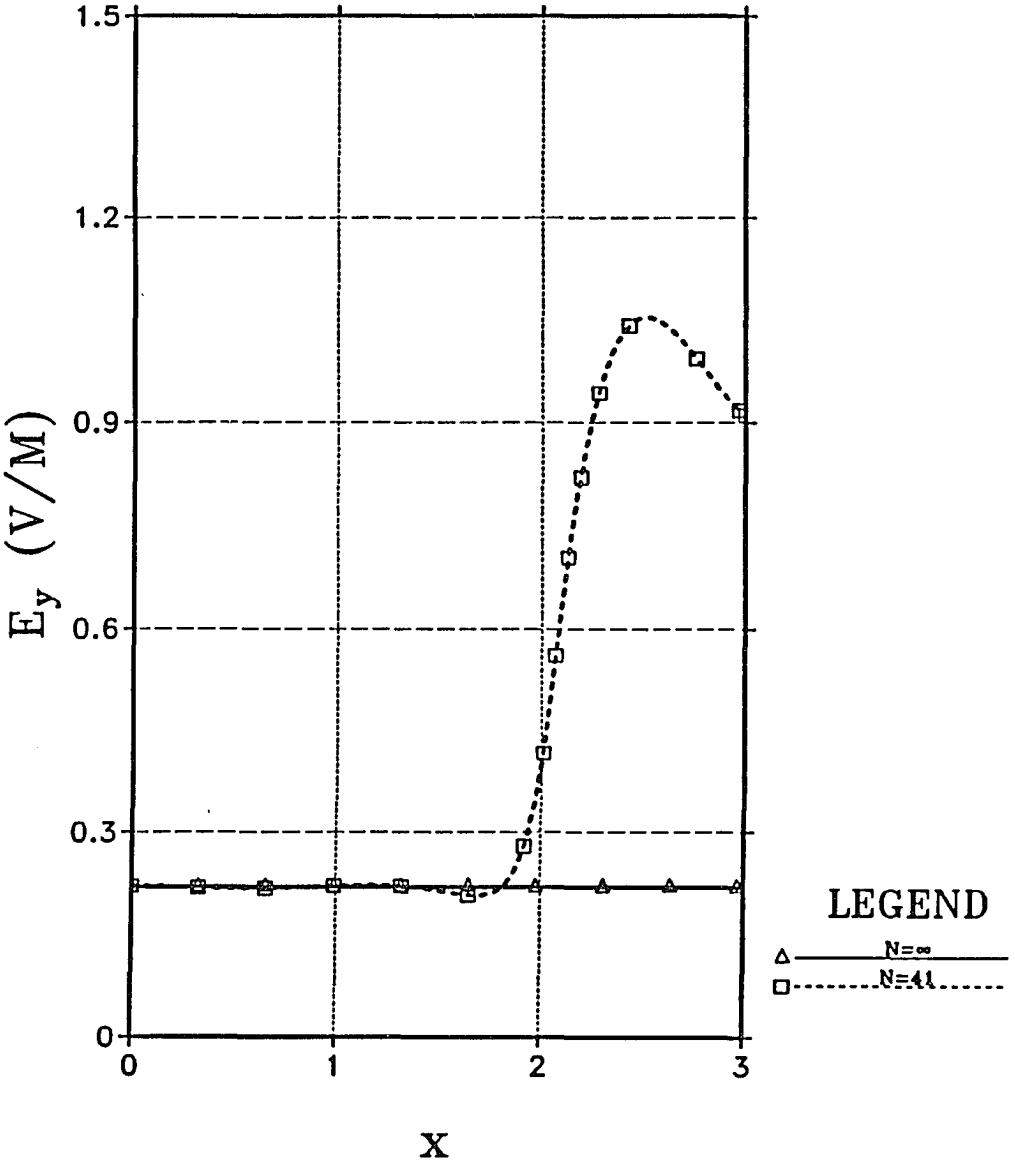

Figure 3-14 The electric field response below the finite and infinite wire grid over a lossy half space as a function of the horizontal distance x (x is normalized to free space wavelength) for parallel polarization when $\theta_0 = 30^o$, $\phi_0 = 90^o$, $h = 0.2\lambda_1$, $d = .1\lambda_1$, $z = .1\lambda_1$, $K^2 = 8.00 - i17.89$ and $E_0 = 1\text{V/m}$.

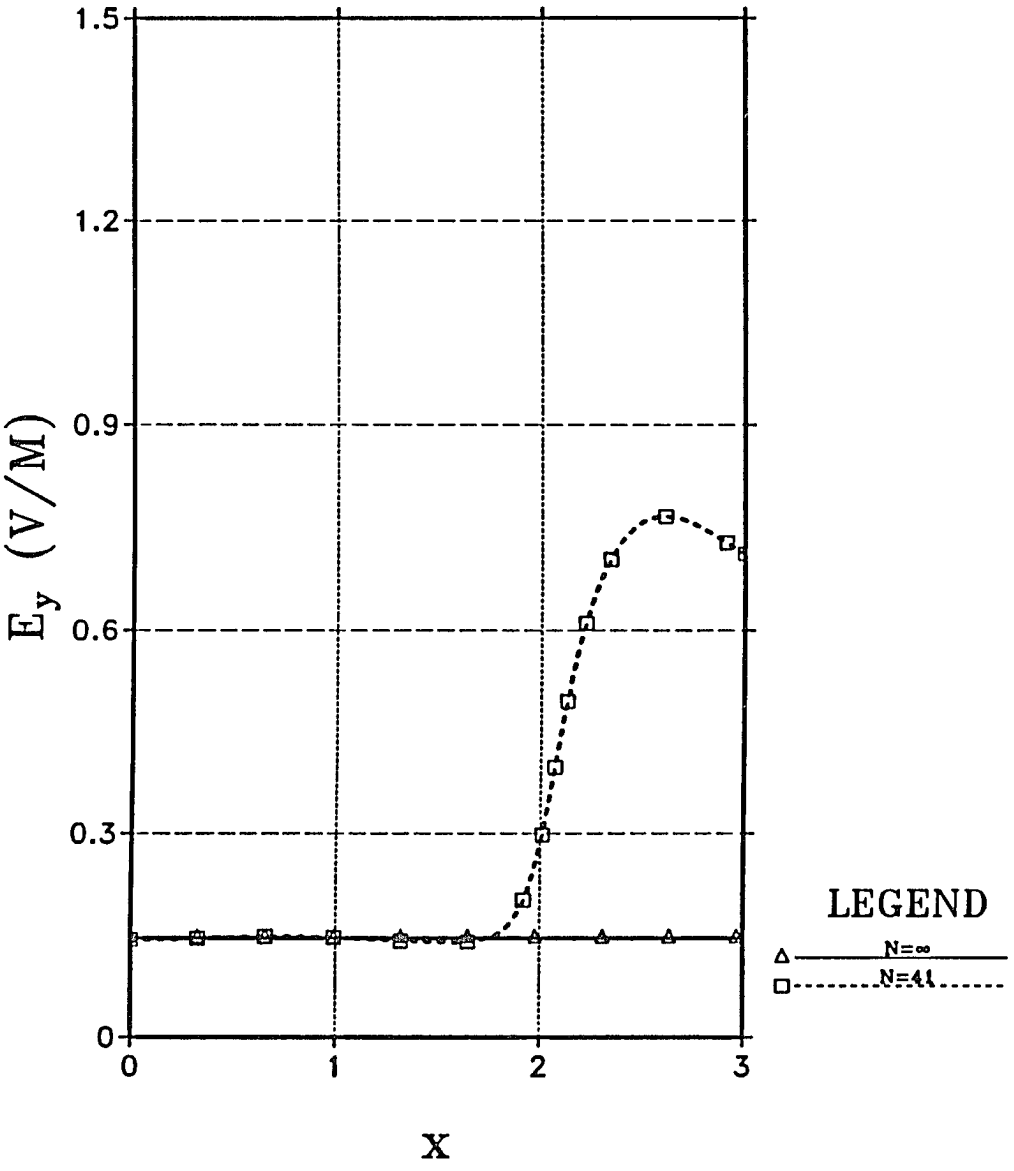

Figure 3-15 The electric field response below the finite and infinite wire grid over a lossy half space as a function of the horizontal distance x (x is normalized to free space wavelength) for parallel polarization when $\theta_0 = 45°$, $\phi_0 = 90°$, $h = 0.2\lambda_1$, $d = .1\lambda_1$, $z = .1\lambda_1$, $K^2 = 8.00 - i17.89$ and $E_0 = 1\text{V/m}$.

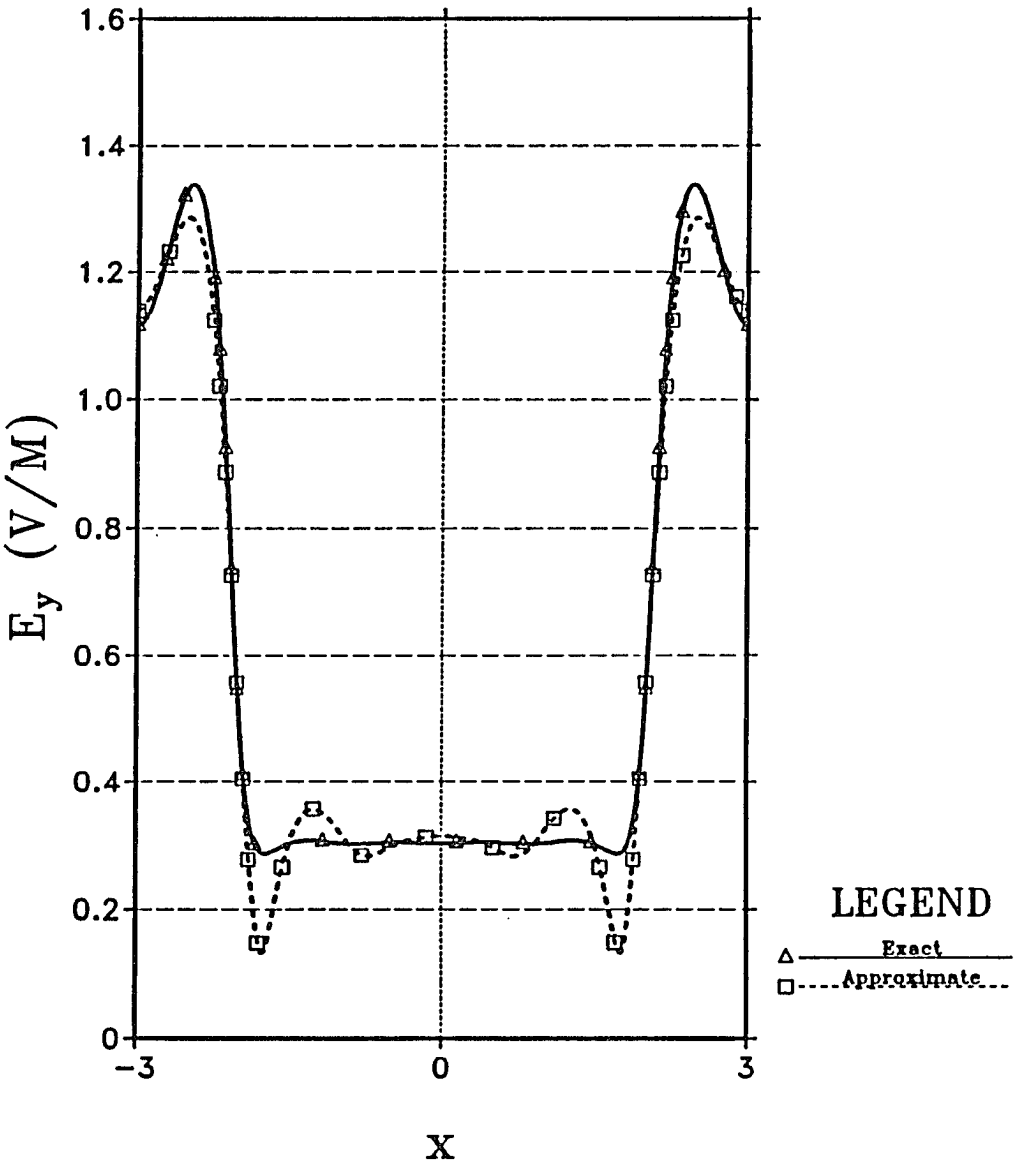

Figure 3-16 The electric field response produced by the finite grid over a lossy half space using two different current distributions for normal incidence. The solid curve represents the exact value computed from (3.5); the dashed curve assumes a constant current distribution whose value is given fom (3.30). The relevant parameters are: $\theta_0 = 0$, $\phi_0 = 90^o$, $h = 0.2\lambda_1$, $d = .1\lambda_1$, $z = .1\lambda_1$, $K^2 = 8.00 - i17.89$ and $E_0 = 1$V/m.

approach outlined in Appendix A is used. Thus, an estimation can be obtained for the total current distribution of the grid by using (3.30) in the same time that (or time less than) it would take to load one matrix element given in (3.5). For N wires, this corresponds to a savings of roughly $N^2/2$ evaluations of (3.7) and (3.8).

3.3.3 Shielding Studies: Perpendicular Polarization

The semi–circular cage of radius b with equally spaced wires was chosen for the structure under investigation as indicated in Figure 3–17. The cage is centered at $x = 0$ and a height of $h = 0.02\lambda_1$. Our primary concern is the functional dependency of a, b, N, σ_2 and θ_0 on S when the incident field is perpendicularly polarized; all other parameters not mentioned will be kept constant. The fields will be numerically observed along a horizontal cut at a height of $0.1\lambda_1$, unless otherwise noted.

A family of curves demonstrating the functional dependency of S on the distance x in wavelengths is shown in Figure 3–18 for various numbers of wires N with $\theta_0 = 0$, $b = 0.25\lambda$, $K^2 = 8.00 - i17.98$, and $k_1 a = .01$. As expected, the shielding effectiveness improves as N increases. At $x = 0$, S decreases from -26 dB for $N = 25$ (i.e 32 wires per wavelength) to -42 dB for $N = 50$ (i.e. 64 wires per wavelength) to -67 dB for $N = 75$ (i.e 96 wires per wavelength). The discontinuities at the transition regions result from probing close to the wire. For all practical purposes, the wire's axial impedance is near zero at this frequency, causing the E–field to vanish at its surface. Figure 3–19 shows the logarithmic electric field contour plot when $N = 75$ for this same structure; the contours are

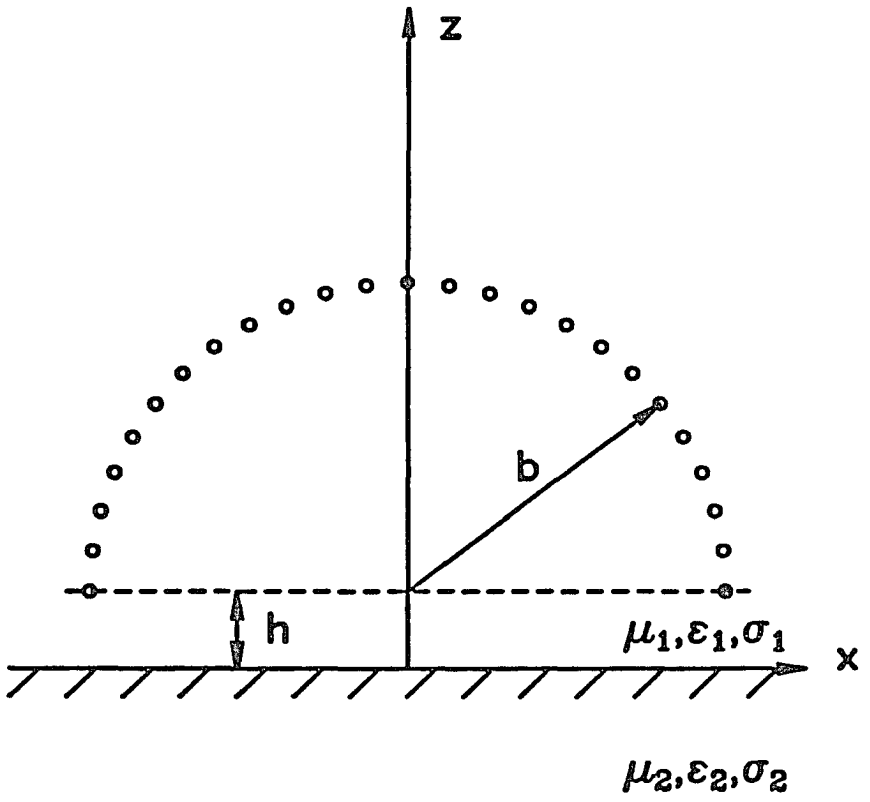

Figure 3-17 A semi-circular cage of radius b at a height h from the interface.

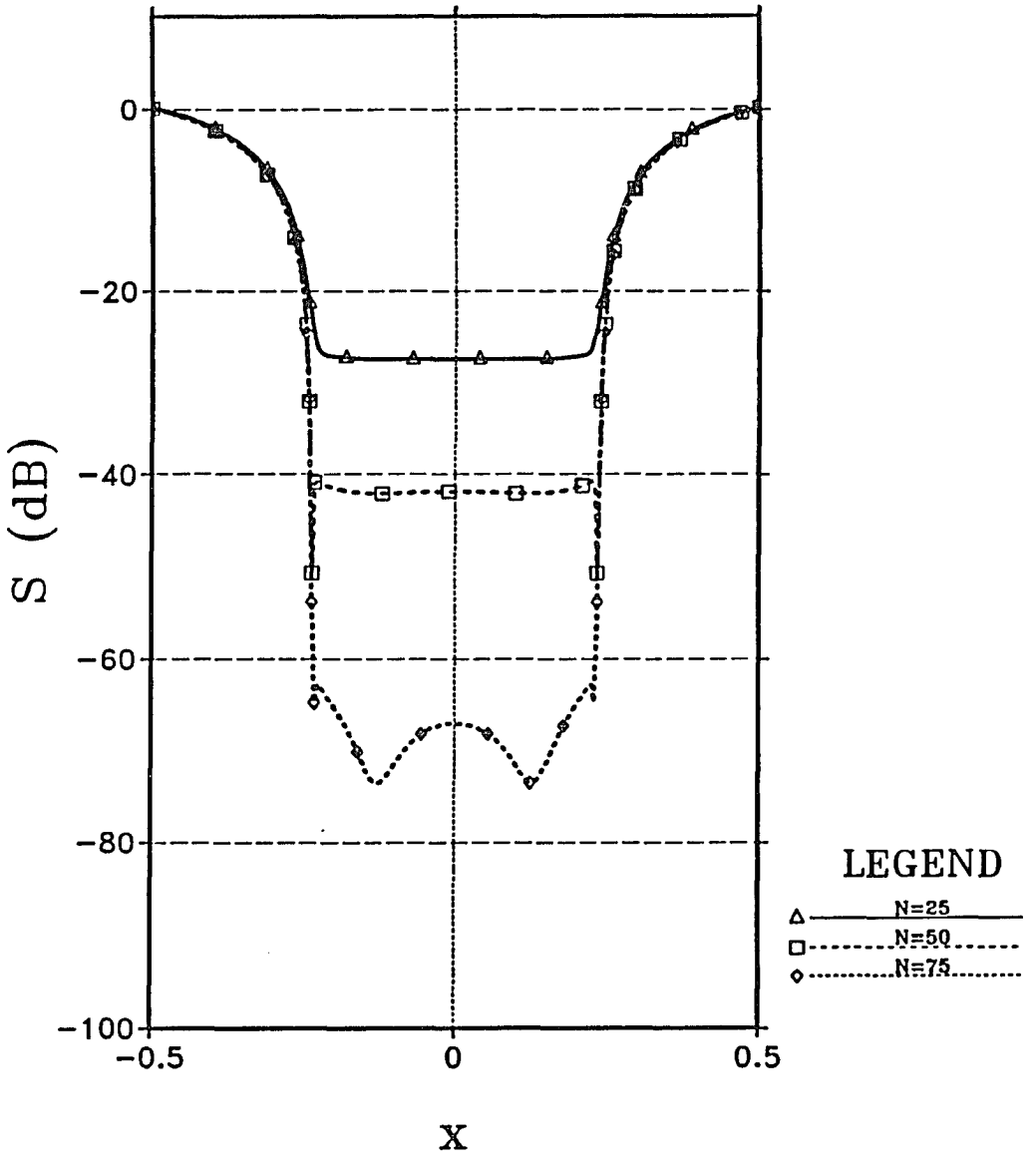

Figure 3-18 A plot of the shielding efficiency, S, as a function of x when varying N for the semi-circular cage. The shielding effectiveness is measured along a horizontal cut at a height of $0.1\lambda_1$ above the half space; x is measured in wavelengths. The relevant parameters are $h = .02\lambda_1$, $b = .25\lambda_1$, $E_0 = 1$ V/m, $K^2 = 8.00 - i17.98$, $k_1 a = 0.01$, $\theta_0 = 0$ and $\phi_0 = 0$.

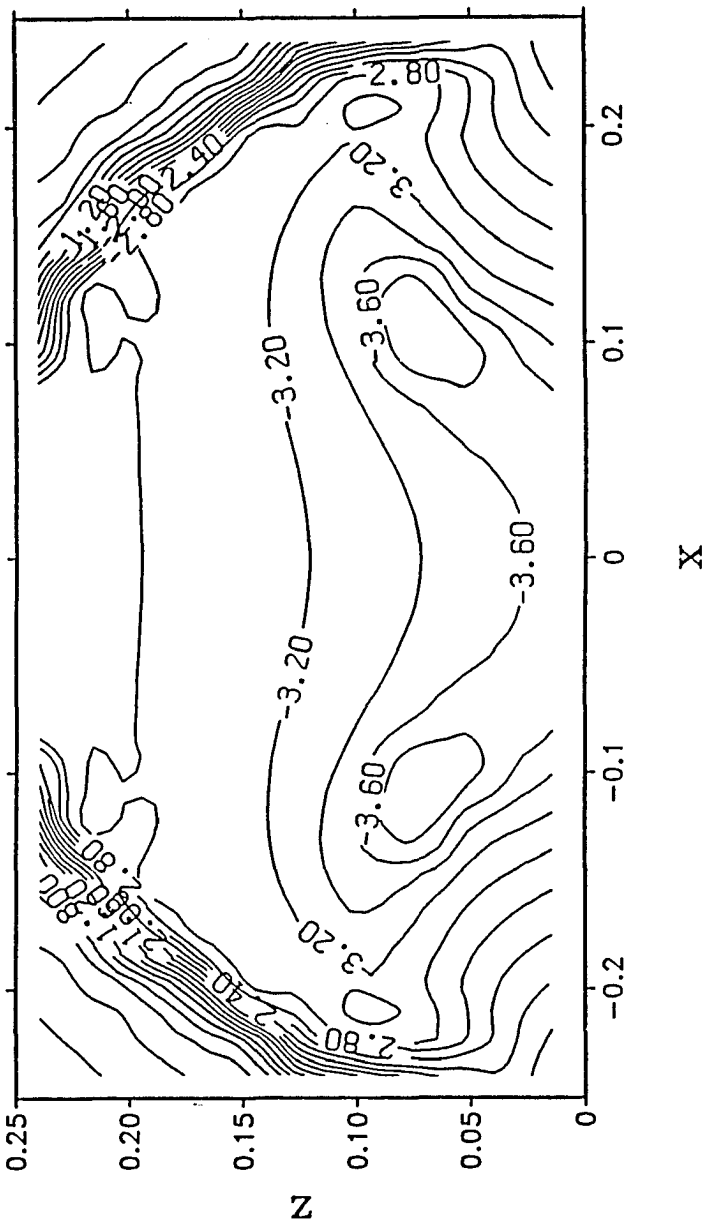

Figure 3-19 A contour plot of the logarithm of the E-field (i.e. $\log_{10}|E_y^{tot}|$) on the xz–plane for the semi–circular cage; x and z are measured in wavelengths. The relevant parameters are $h = .02\lambda_1$, $b = .25\lambda_1$, $E_0 = 1$ V/m, $K^2 = 8.00 - i17.98$, $k_1 a = 0.01$, $\theta_0 = 0$ and $\phi_0 = 0$.

the constant values of $\log_{10}|E_y^{tot}|$. In general, the internal variation of the E–field is minimal throughout the cage; in contrast, a rapid spatial rate–of–change in the field occurs as the numerical probe passes from the internal region to the external. Other than the leakage that occurs between the interface and the cage, the structure shields very well. It was designed not to support any internal field resonances; Figure 3–19 confirms that this is indeed the case.

The foregoing calculations are repeated for oblique incidence with $\theta_0 = 45°$; Figure 3–20 confirms that S is no longer constant inside the structure. A close comparison of Figure 3–20 with Figure 3–18 shows that the fields at $x = 0$ are modified slightly. Figure 3–21 exhibits the functional dependency of θ_0 on S. Particularly, the shielding improves as x increases and the E–field gradient is effectively in the direction of the incident plane wave. As expected for this angle of incidence, resonances are not excited.

The presence of the half space modifies the shielding characteristics for various values of N as seen in Figures 3–22 through 3–27. The three special cases of interest are when $K^2 = 1$, $K^2 \to \infty$ and $K^2 = 8$. In all three cases, normal incidence is assumed. The results in Figures 3–22 and 3–23 ($K^2 = 1$) demonstrate that the interface is necessary if any shielding is to be accomplished, regardless of the number of wires used. Yet, whether the lower half space is lossless, as seen in Figures 3–26 and 3–27, or perfectly conducting, as seen Figures 3–24 and 3–25, the shielding effectiveness is left virtually unaffected. The contour plots of Figures 3–25 and 3–27 demonstrate that the earth's conductivity plays an important role in smoothing the shielding distribution inside the cage, particularly when N is large. This same phenonmenon was observed for the planar grid cases.

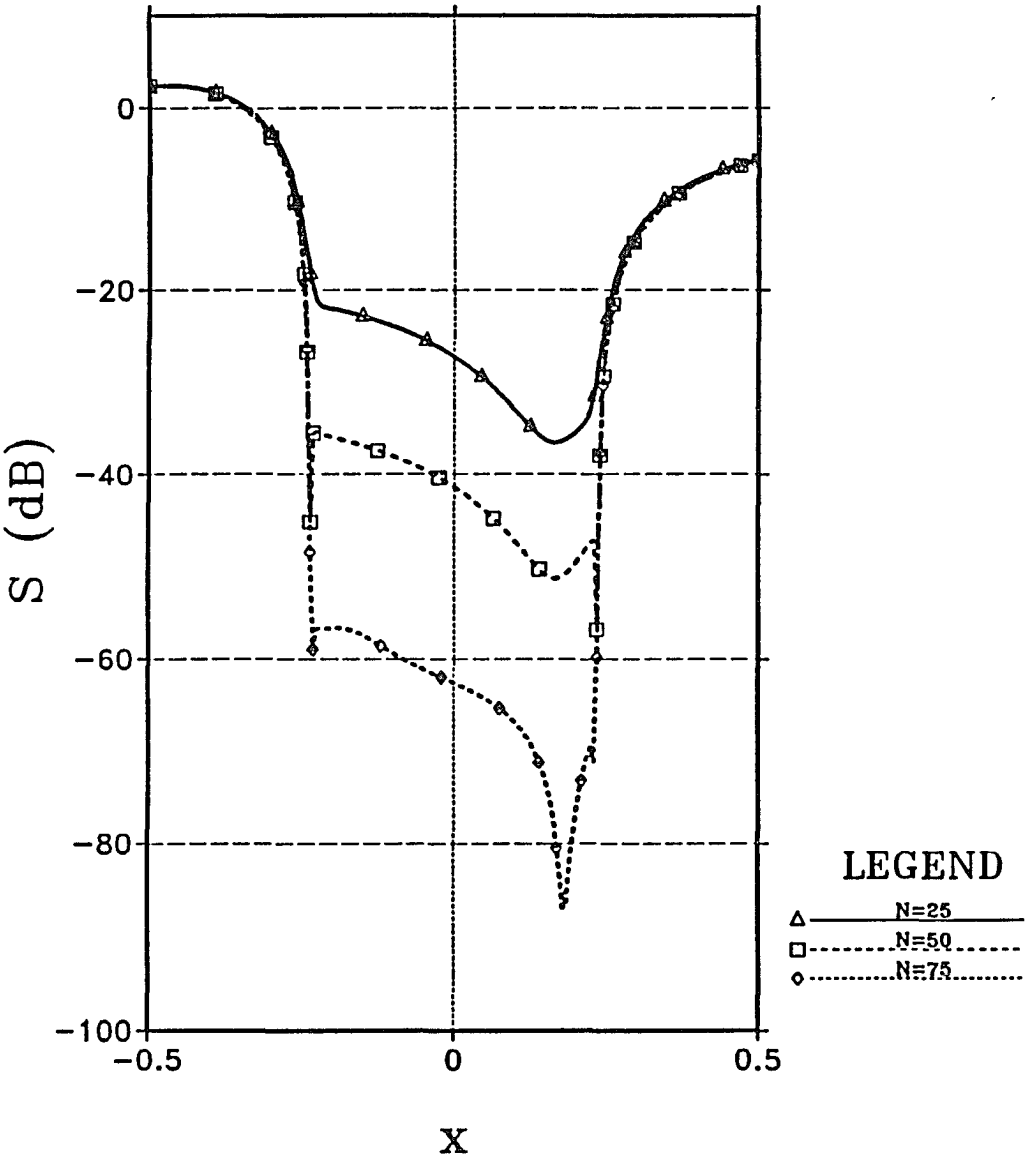

Figure 3-20 A plot of the shielding efficiency, S, as a function of x when varying N for the semi–circular cage. The shielding effectiveness is measured along a horizontal cut at a height of $0.1\lambda_1$ above the half space; x is measured in wavelengths. The relevant parameters are $h = .02\lambda_1$, $b = .25\lambda_1$, $E_0 = 1$ V/m, $K^2 = 8.00 - i17.98$, $k_1 a = 0.01$, $\theta_0 = 45^o$ and $\phi_0 = 0$.

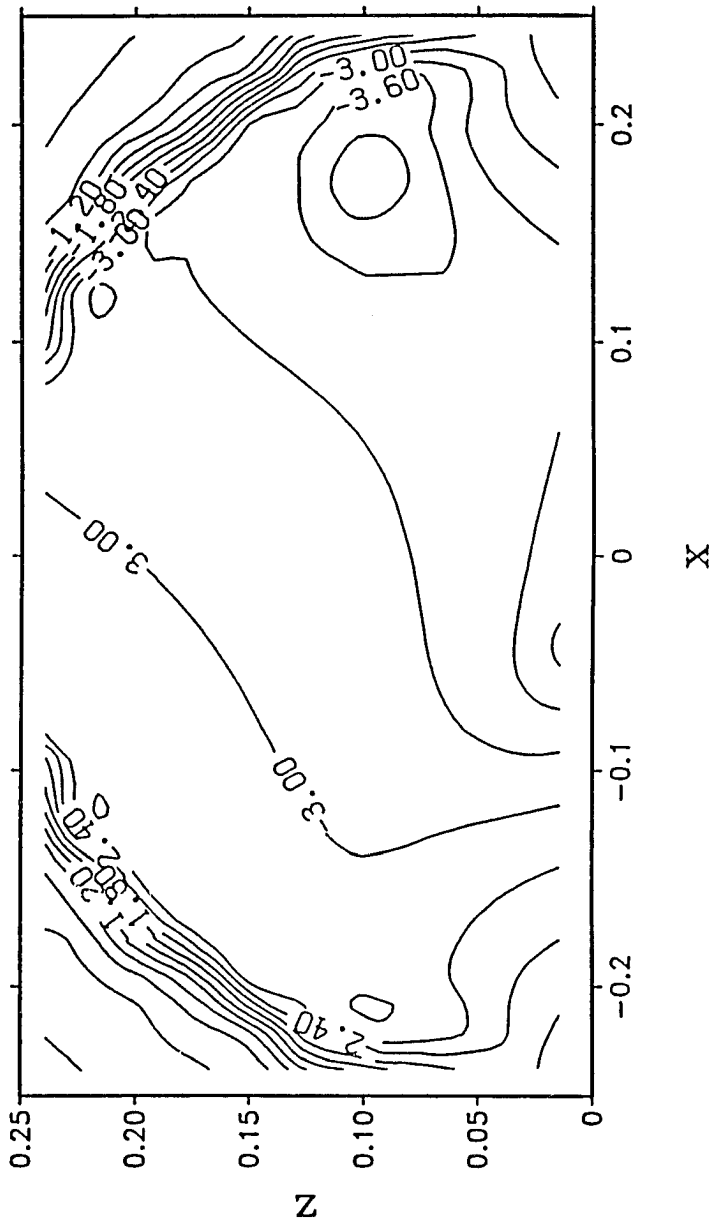

Figure 3-21 A contour plot of the logarithm of the E–field (i.e. $\log_{10}|E_y^{tot}|$) on the xz–plane for the semi–circular cage; x and z are measured in wavelengths. The relevant parameters are $h = .02\lambda_1$, $b = .25\lambda_1$, $E_0 = 1$ V/m, $K^2 = 8.00 - i17.98$, $k_1 a = 0.01$, $\theta_0 = 45^o$ and $\phi_0 = 0$.

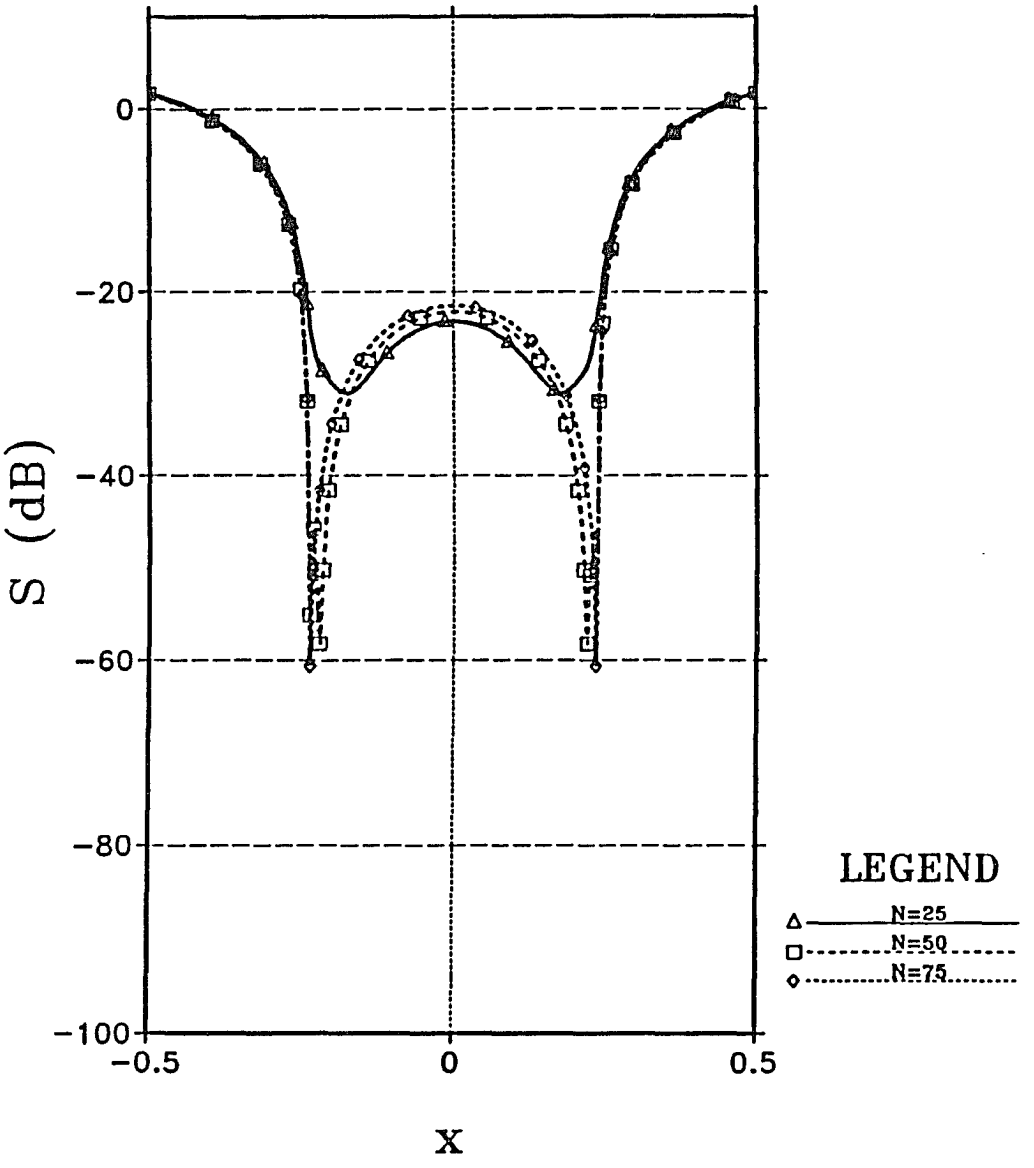

Figure 3-22 A plot of the shielding efficiency, S, as a function of x when varying N for the semi-circular cage. The shielding effectiveness is measured along a horizontal cut at a height of $0.1\lambda_1$ above the half space; x is measured in wavelengths. The relevant parameters are $h = .02\lambda_1$, $b = .25\lambda_1$, $E_0 = 1$ V/m, $K^2 = 1$, $k_1 a = 0.01$ $\theta_0 = 0$ and $\phi_0 = 0$.

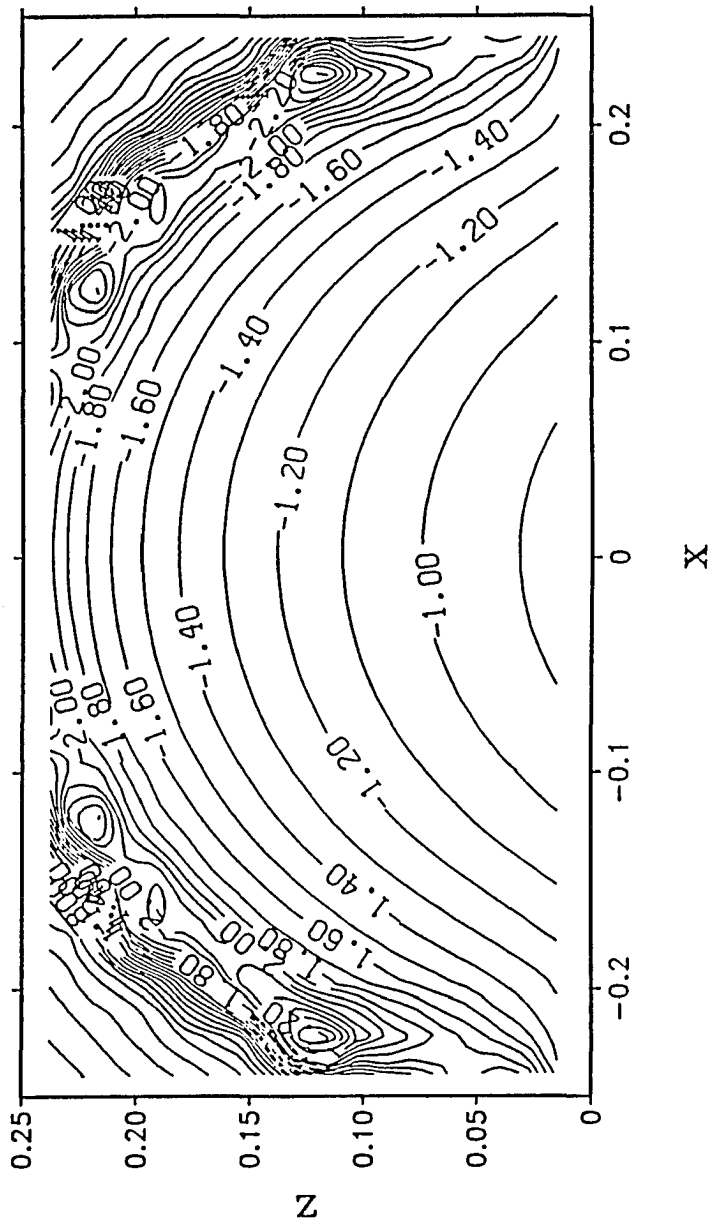

Figure 3-23 A contour plot of the logarithm of the E-field (i.e. $\log_{10}|E_y^{tot}|$) on the xz-plane for the semi-circular cage; x and z are measured in wavelengths. The relevant parameters are $h = .02\lambda_1$, $b = .25\lambda_1$, $E_0 = 1$ V/m, $K^2 = 1$, $k_1 a = 0.01$, $\theta_0 = 0$ and $\phi_0 = 0$.

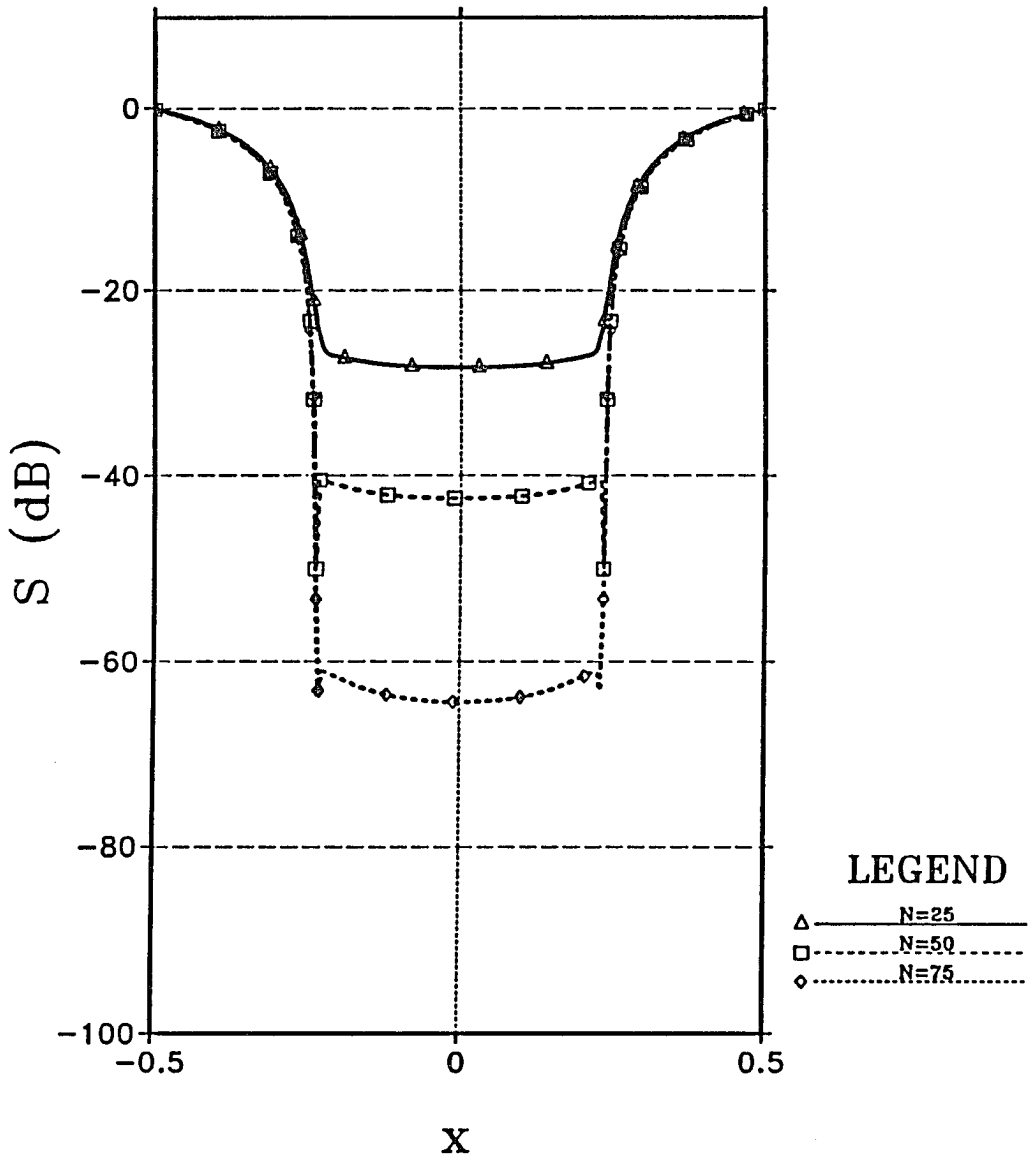

Figure 3-24 A plot of the shielding efficiency, S, as a function of x when varying N for the semi-circular cage. The shielding effectiveness is measured along a horizontal cut at a height of $0.1\lambda_1$ above the half space; x is measured in wavelengths. The relevant parameters are $h = .02\lambda_1$, $b = .25\lambda_1$, $E_0 = 1$ V/m, $K^2 \to \infty$, $k_1 a = 0.01$, $\theta_0 = 0$ and $\phi_0 = 0$.

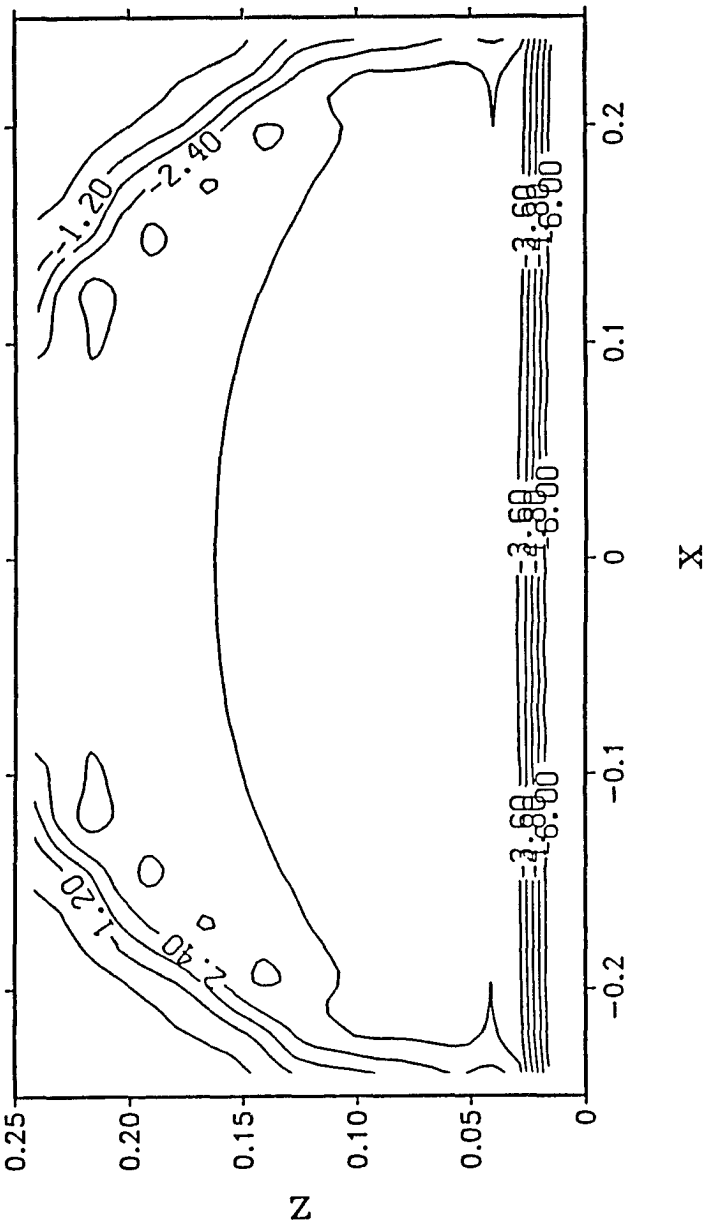

Figure 3-25 A contour plot of the logarithm of the E-field (i.e. $\log_{10}|E_y^{tot}|$) on the xz-plane for the semi-circular cage; x and z are measured in wavelengths. The relevant parameters are $h = .02\lambda_1$, $b = .25\lambda_1$, $E_0 = 1$ V/m, $K^2 \to \infty$, $k_1 a = 0.01$, $\theta_0 = 0$ and $\phi_0 = 0$.

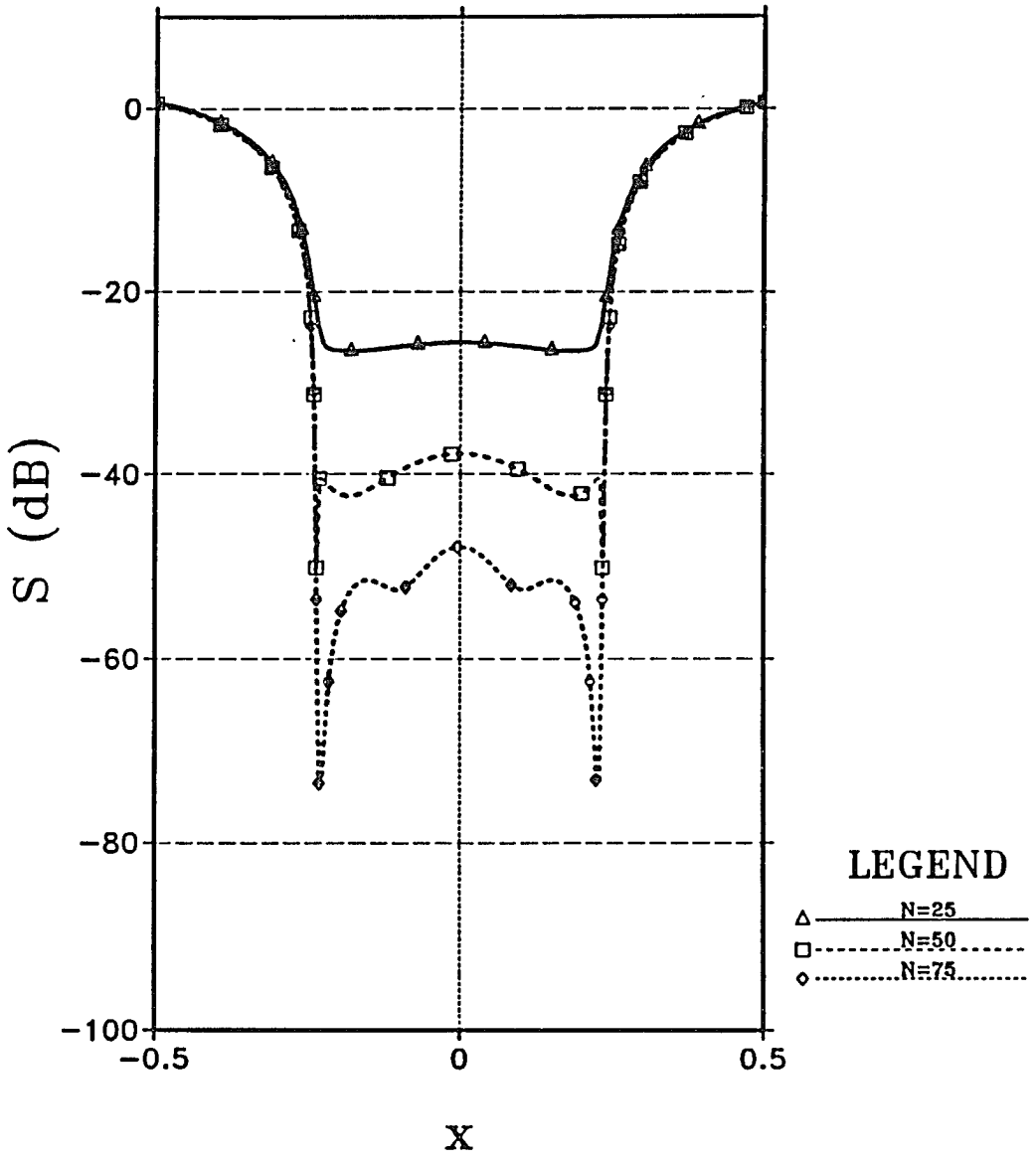

Figure 3-26 A plot of the shielding efficiency, S, as a function of x when varying N for the semi-circular cage. The shielding effectiveness is measured along a horizontal cut at a height of $0.1\lambda_1$ above the half space; x is measured in wavelengths. The relevant parameters are $h = .02\lambda_1$, $b = .25\lambda_1$, $E_0 = 1$ V/m, $K^2 = 8$, $k_1 a = 0.01$, $\theta_0 = 0$ and $\phi_0 = 0$.

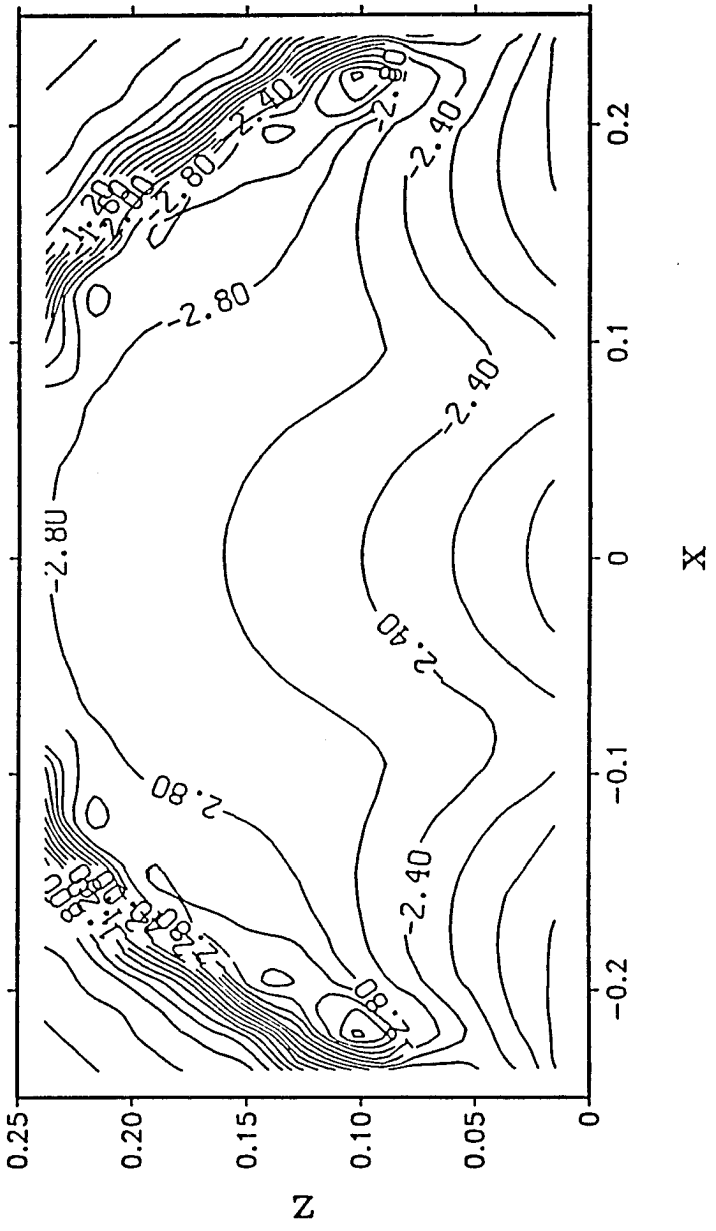

Figure 3-27 A contour plot of the logarithm of the E–field (i.e. $\log_{10}|E_y^{tot}|$) on the xz–plane for the semi–circular cage; x and z are measured in wavelengths. The relevant parameters are $h = .02\lambda_1$, $b = .25\lambda_1$, $E_0 = 1$ V/m, $K^2 = 8$, $k_1 a = 0.01$, $\theta_0 = 0$ and $\phi_0 = 0$.

The preceeding conclusion is exemplified in Figures 3–28 and 3–29 when $\theta_0 = 0$ and $\theta_0 = 45$, respectively. For this case, $N = 50$ and the loss tangent, $\tan \delta_2$, is varied from 0.1 (i.e. low loss) to 10.0 (i.e. high loss) in 0.5 base ten logarithmic steps. For $\theta_0 = 0$, the shielding distribution becomes flatter as the conductivity of the lower medium is increased. This can be understood from the electromagnetic imaging effect. For large values of conductivity, the wires above the ground are imaged well by the half space. That is, the image currents are almost equal in magnitude and opposite in phase to the primary current. Since, from geometrical considerations, the computational cut is almost along a plane of symmetry, the corresponding shielding distribution tends to be flat. However, when $\theta_0 = 45°$, this cut is not along such a symmetrical plane, and consequently, the distribution is less even.

Up to this point, the structures under investigation did not support internal resonances because of the relatively small overall dimensions in terms of wavelength. We next consider the resonant effects which become important for larger structural dimensions. For example, Figures 3–30, 3–31 and 3–32 show the shielding effects of the semi-circular cage with a wire distribution of 66 wires per wavelength for a highly conductive earth ($K^2 = 8.0 - i179.8$). Each figure shows the logarithmic field contour lines as b is increased. The dimension b was chosen to either satisfy the 2–D ideal resonant cavity equation, $J_m(k_1 b) = 0$, or some point in between resonances. (J_m denotes the Bessel function of the first kind.) For Figure 3–30, b corresponds to the first zero of $J_0(k_1 b)$ (i.e. $b = 0.3827\lambda_1$); for Figure 3–32, b corresponds to the second zero of $J_1(k_1 b)$ (i.e. $b = 0.6098\lambda_1$); for Figure 3–31, we arbitarily choose a point between the other two, say, $b = 0.5\lambda_1$. Since the ground is highly conducting, the E–field will diminish in value as the

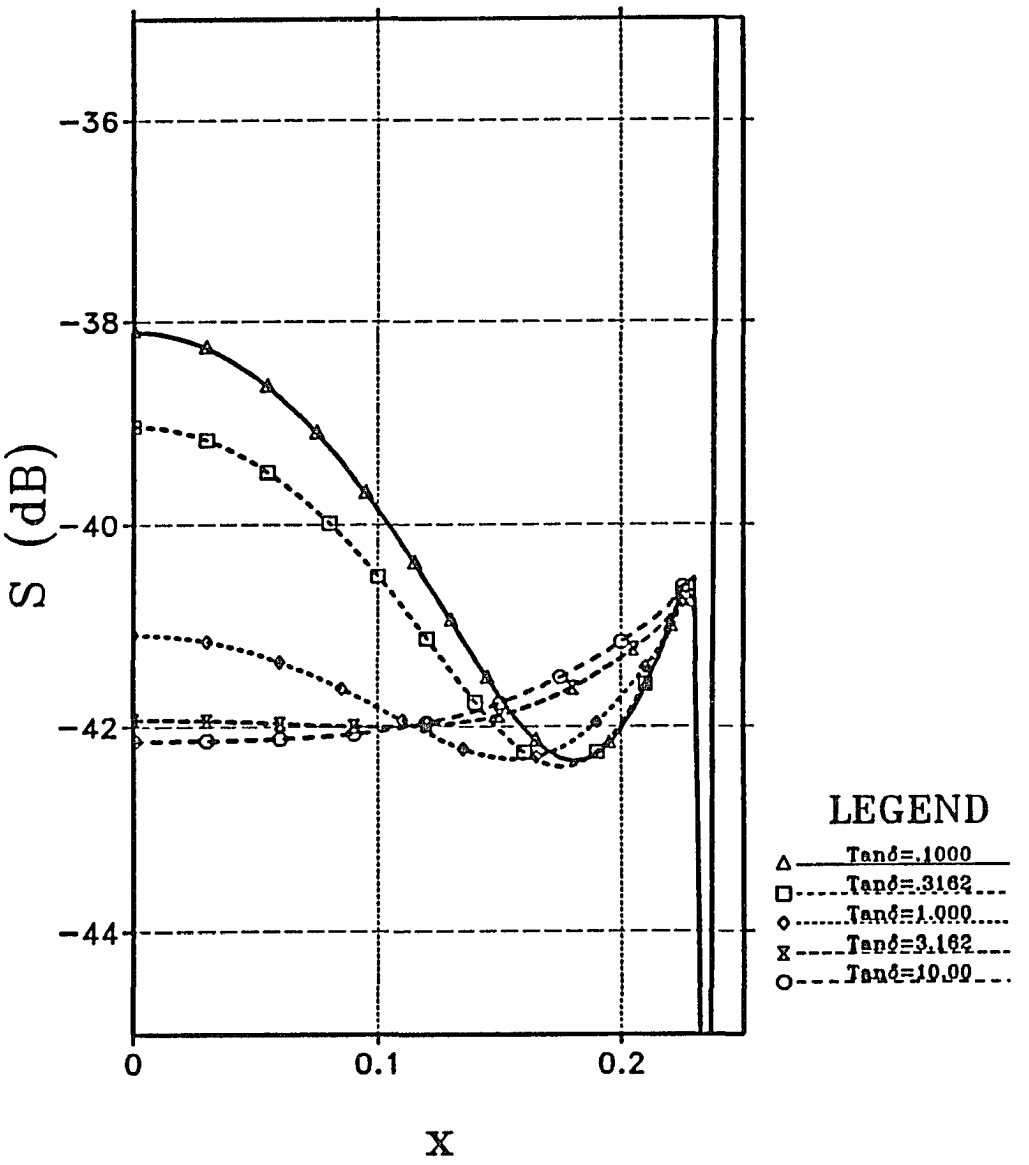

Figure 3-28 A plot of the shielding efficiency, S, as a function of x when varying $\tan\delta_2$ for the semi-circular cage. The shielding effectiveness is measured along a horizontal cut at a height of $0.1\lambda_1$ above the half space; x is measured in wavelengths. The relevant parameters are $h = .02\lambda_1$, $b = .25\lambda_1$, $E_0 = 1$ V/m, $k_1 a = 0.01$, $\theta_0 = 0$ and $\phi_0 = 0$.

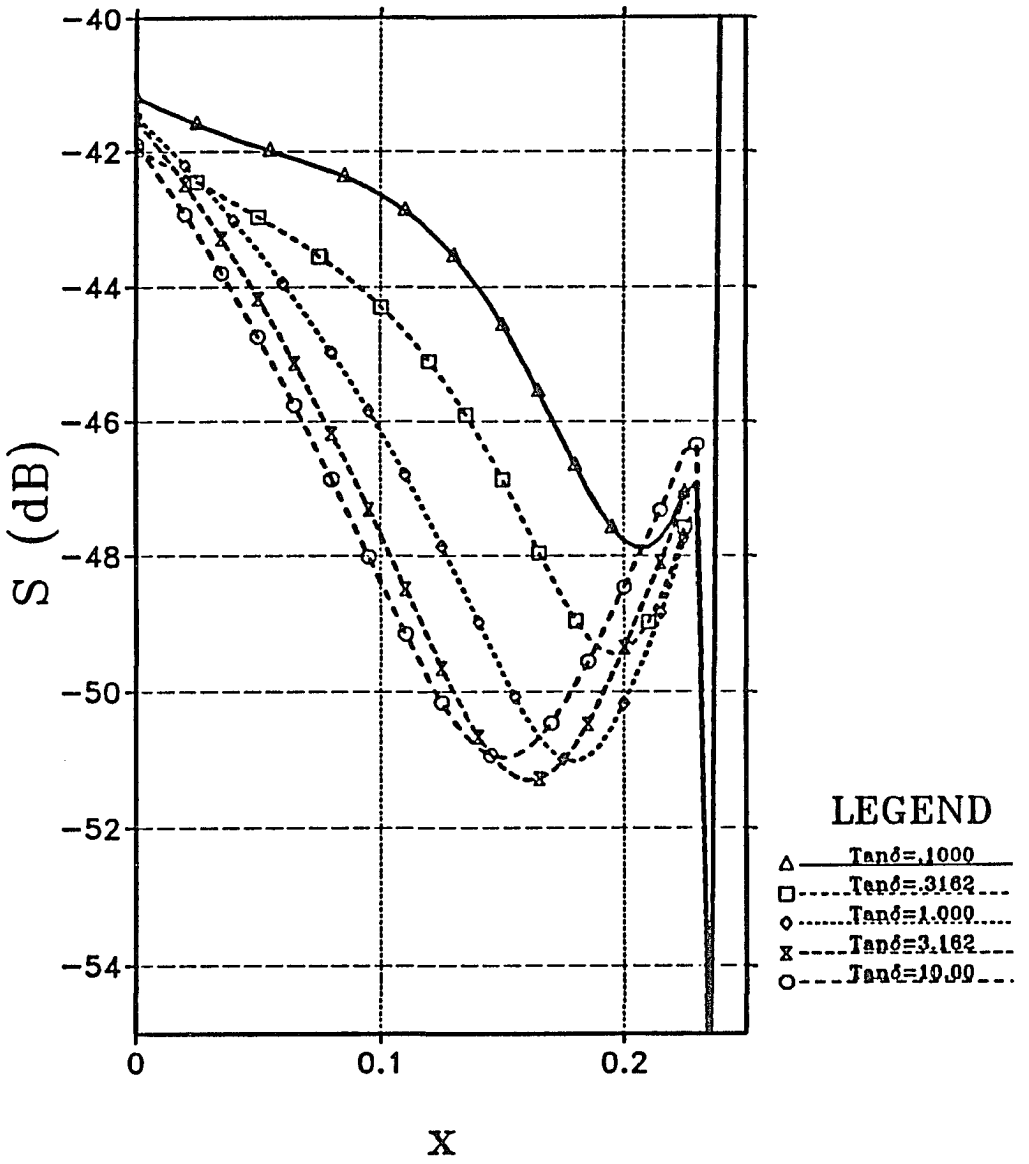

Figure 3-29 A plot of the shielding efficiency, S, as a function of x when varying $\tan\delta_2$ for the semi-circular cage. The shielding effectiveness is measured along a horizontal cut at a height of $0.1\lambda_1$ above the half space; x is measured in wavelengths. The relevant parameters are $h = .02\lambda_1$, $b = .25\lambda_1$, $E_0 = 1$ V/m, $k_1 a = 0.01$, $\theta_0 = 45^\circ$ and $\phi_0 = 0$.

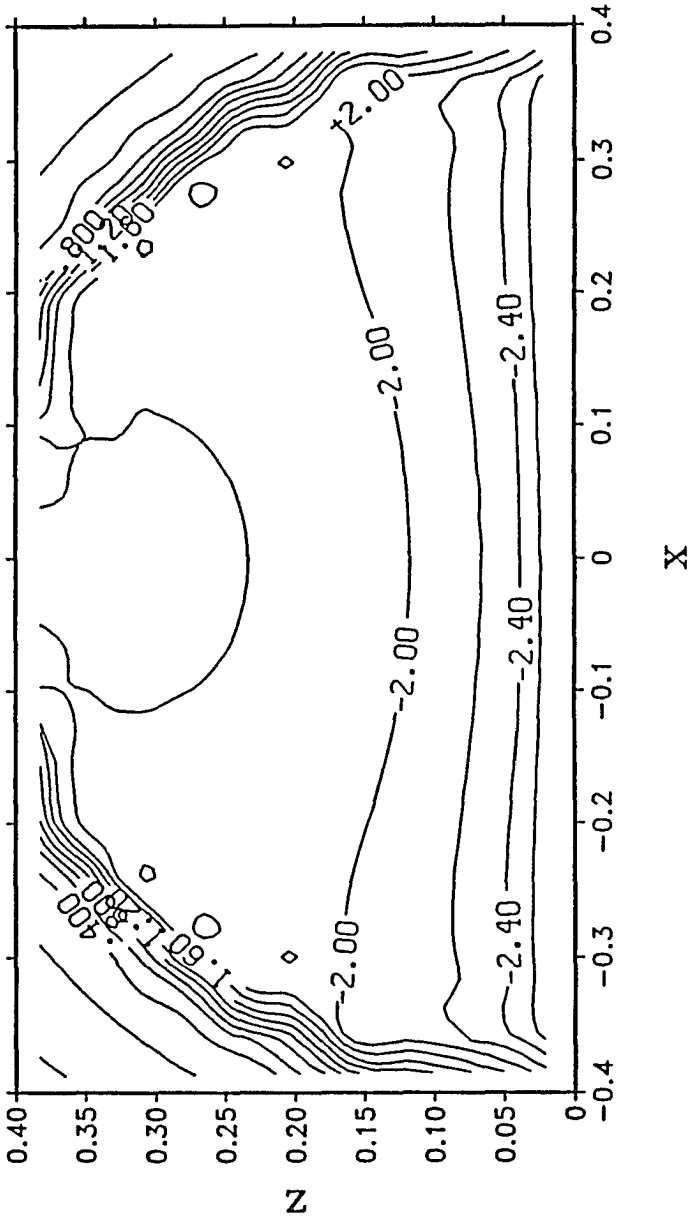

Figure 3-30 A contour plot of the logarithm of the E-field (i.e. $\log_{10}|E_y^{tot}|$) on the xz-plane for the semi-circular cage; x and z are measured in wavelengths. The relevant parameters are $h = .02\lambda_1$, $b = .3827\lambda_1$, $E_0 = 1$ V/m, $N = 77$ (i.e. 66 wires/λ_1), $K^2 = 8.00 - i179.8$, $k_1 a = 0.01$, $\theta_0 = 0$ and $\phi_0 = 0$.

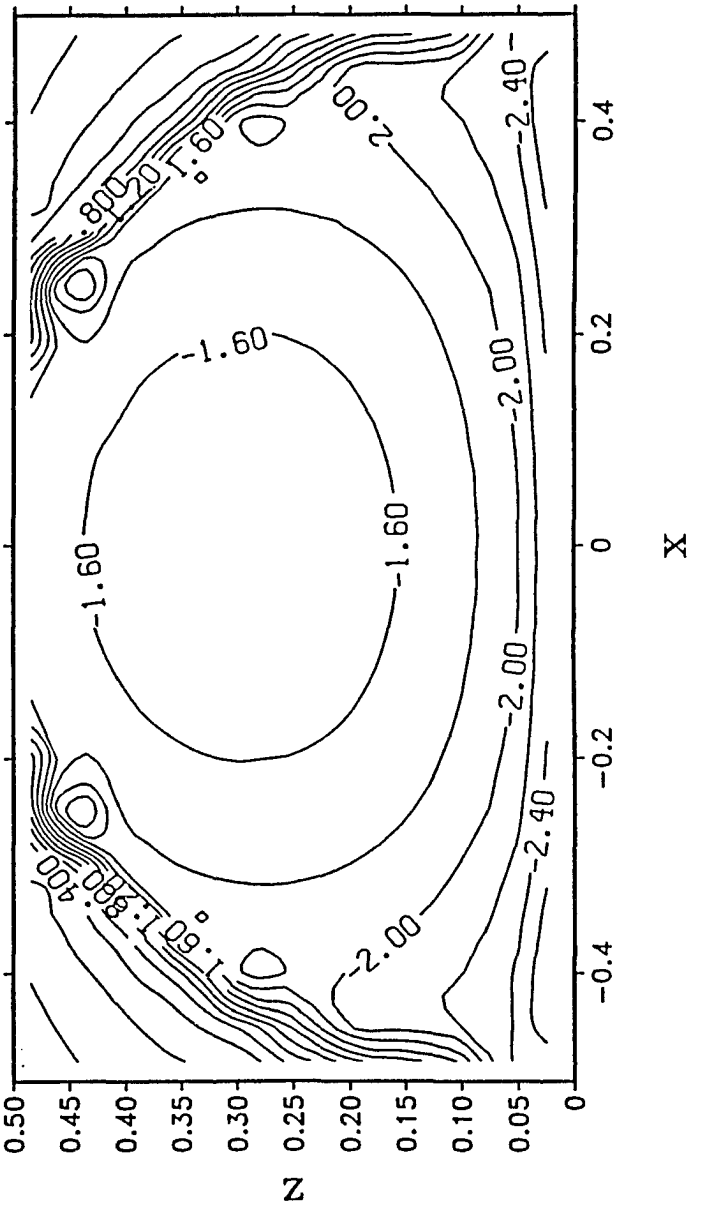

Figure 3-31 A contour plot of the logarithm of the E-field (i.e. $\log_{10}|E_y^{tot}|$) on the xz-plane for the semi-circular cage; x and z are measured in wavelengths. The relevant parameters are $h = .02\lambda_1$, $b = .5\lambda_1$, $E_0 = 1$ V/m, $N = 100$ (i.e. 66 wires/λ_1), $K^2 = 8.00 - i179.8$, $k_1 a = 0.01$, $\theta_0 = 0$ and $\phi_0 = 0$.

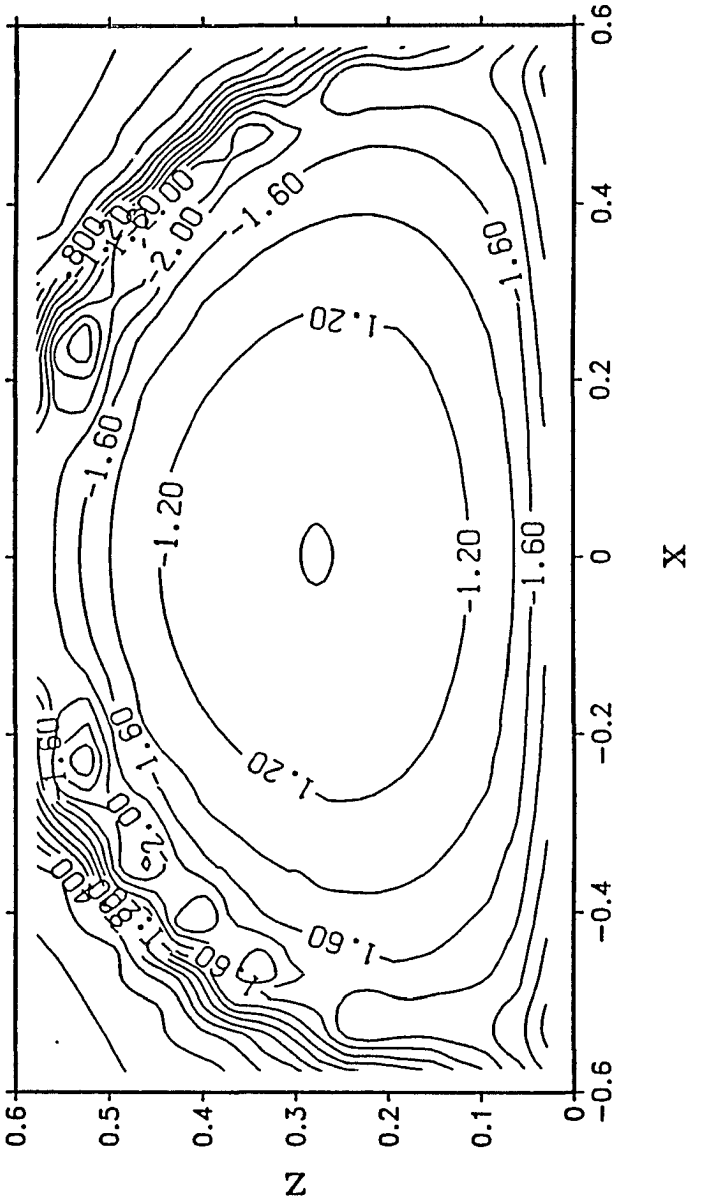

Figure 3-32 A contour plot of the logarithm of the E–field (i.e. $\log_{10}|E_y^{tot}|$) on the xz–plane for the semi–circular cage; x and z are measured in wavelengths. The relevant parameters are $h = .02\lambda_1$, $b = .6089\lambda_1$, $E_0 = 1$ V/m, $N = 122$ (i.e. 66 wires/λ_1), $K^2 = 8.00 - i179.8$, $k_1 a = 0.01$, $\theta_0 = 0$ and $\phi_0 = 0$.

numerical probe moves toward the interface, and consequently, the structure is not expected to support any $TE_{0,k}$ resonances; Figure 3–30 confirms this assertion. As the dimension b is increased, the resonant effects become more pronounced, as shown in Figure 3–31. If b is set such that the structure supports the TE_{11} resonance, the fields become greatly enhanced at the center of the cage. The E–field distribution is predicted to compare closely to the perfectly conducting continuous case; that is to say, $E_y \sim J_1(k_1\rho_{xz})\cos\phi$. ($\rho_{xz}$ and ϕ are the polar coordinates for the xz–plane.) Except for a slight shift in the peaking point, Figure 3–32 shows that the structure is resonating as predicted by this equation. Quantitatively, the field peaks to about 0.1 volt/meter, which implies that the shielding effectiveness has been degraded to about 20 dB.

A rectangular structure is now investigated as depicted in Figure 3–33. The studies associated with Figures 3–18 and 3–20 are repeated for Figures 3–34 and 3–35 when $\theta_0 = 0$ and $\theta_0 = 45^o$, respectively; the wire density remains invariant. In general, it appears that the structural configuration has little overall effect on the shielding performance.

Finally, the results obtained from the wire grid model are compared with a Method of Moments (MOM) solution for the perfectly conducting, continuous shell. Using a rectangular shell, as shown in Figure 3–33 (the continuous shell has the same geometry), we compare the results of Figure 3–34 with those furnished by Baertlein [1988] as shown in Figure 3–36. His method used pulse expansion functions with delta function weights to solve for the surface current in his integral equation. Figure 3–36 shows that the wire grid model, for a particular choice of N, will shield as well as the perfectly conducting continuous shell.

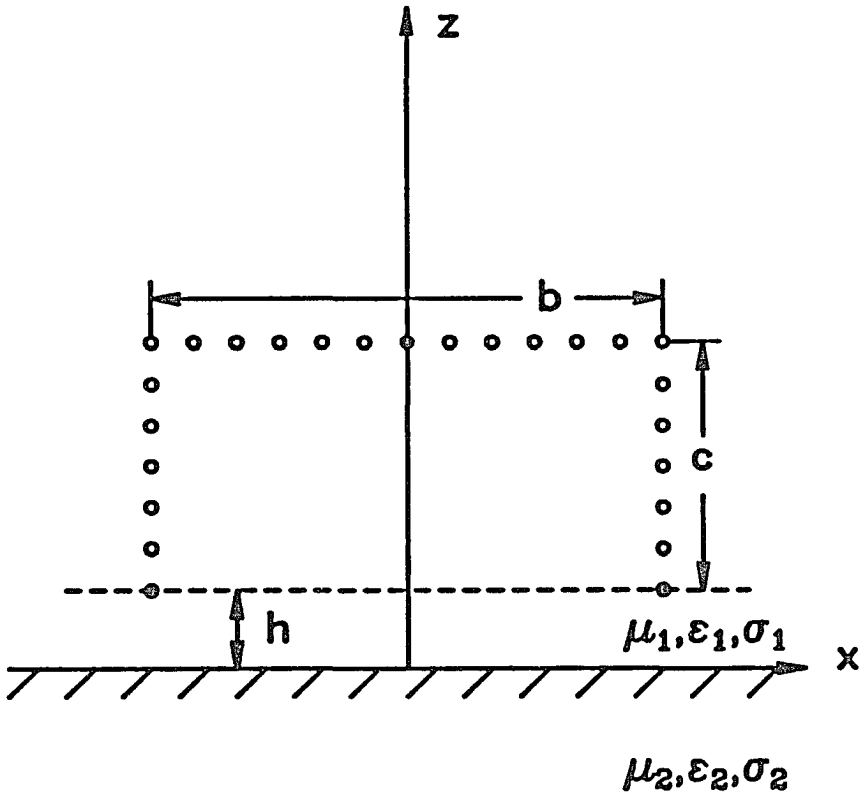

Figure 3-33 A rectangular cage of width b and height c displaced at a height h from the interface.

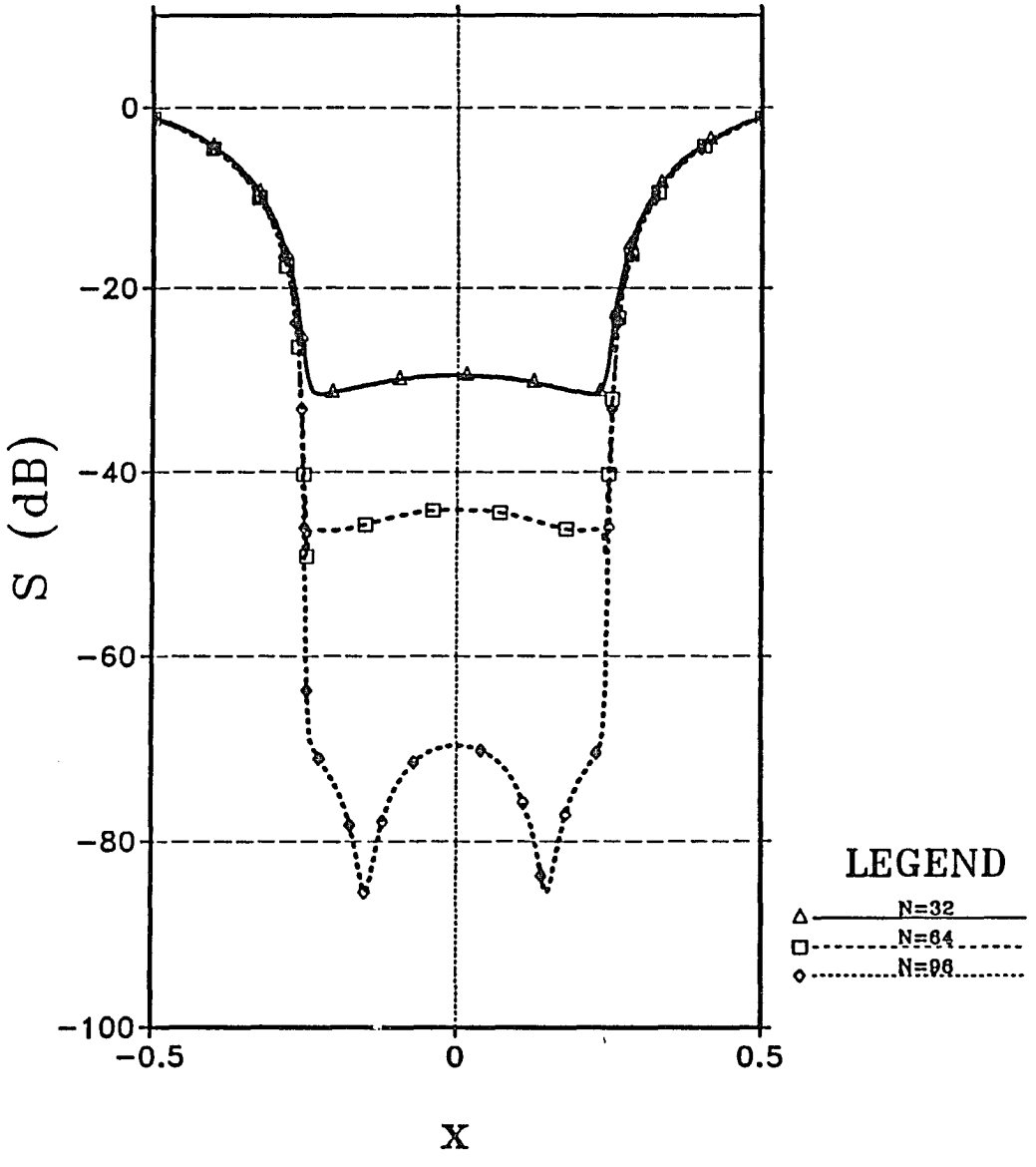

Figure 3-34 A plot of the shielding efficiency, S, as a function of x when varying N for the rectangular cage. The shielding effectiveness is measured along a horizontal cut at a height of $0.1\lambda_1$ above the half space; x is measured in wavelengths. The relevant parameters are $h = .02\lambda_1$, $c = .25\lambda_1$, $d = .5\lambda_1$, $E_0 = 1$ V/m, $K^2 = 8.00 - i17.98$, $k_1 a = 0.01$, $\theta_0 = 0$ and $\phi_0 = 0$.

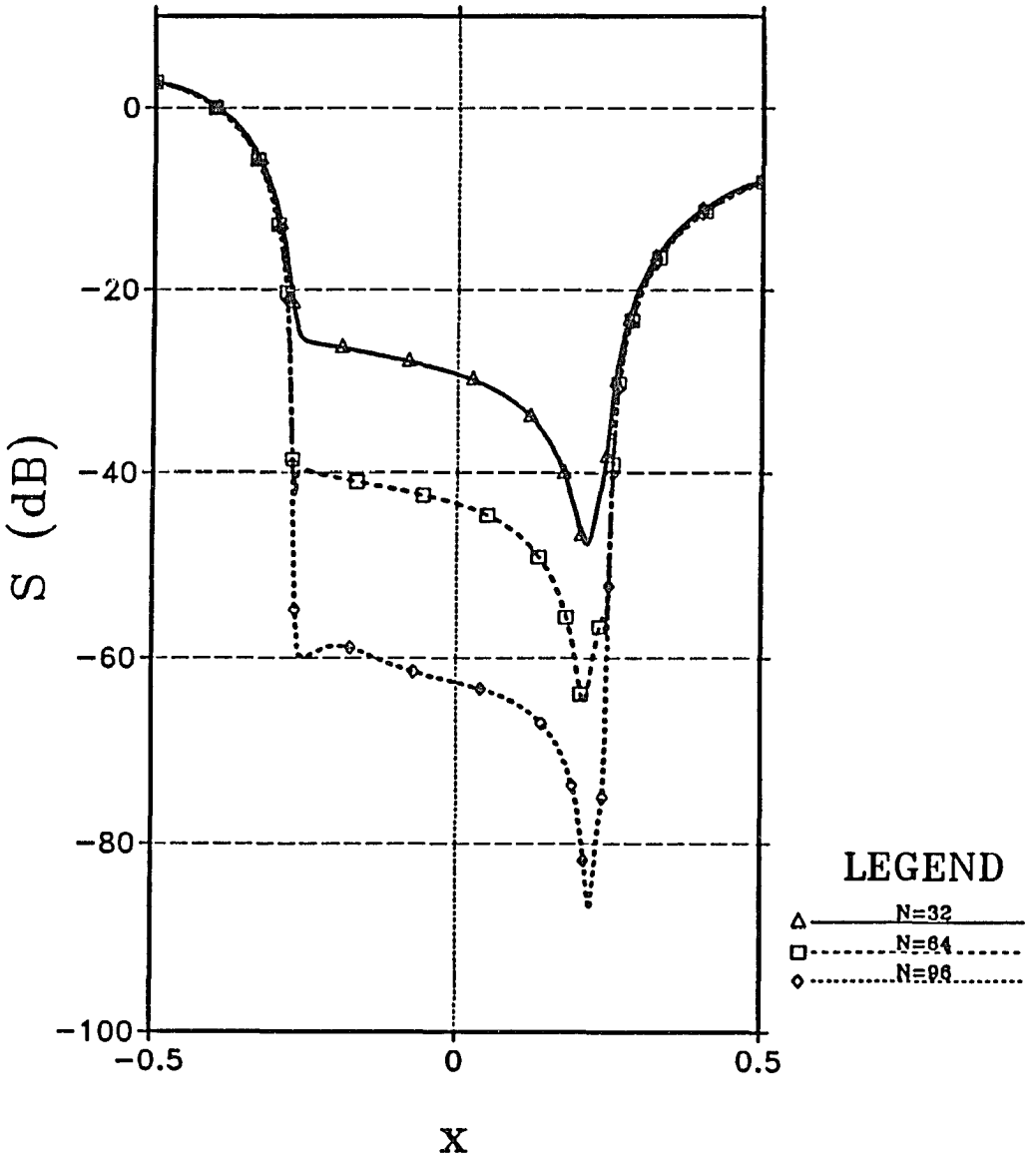

Figure 3-35 A plot of the shielding efficiency, S, as a function of x when varying N for the rectangular cage. The shielding effectiveness is measured along a horizontal cut at a height of 0.1λ above the half space; x is measured in wavelengths. The relevant parameters are $h = .02\lambda_1$, $c = .25\lambda_1$, $d = .5\lambda_1$, $E_0 = 1$ V/m, $K^2 = 8.00 - i17.98$, $k_1 a = 0.01$, $\theta_0 = 45^\circ$ and $\phi_0 = 0$.

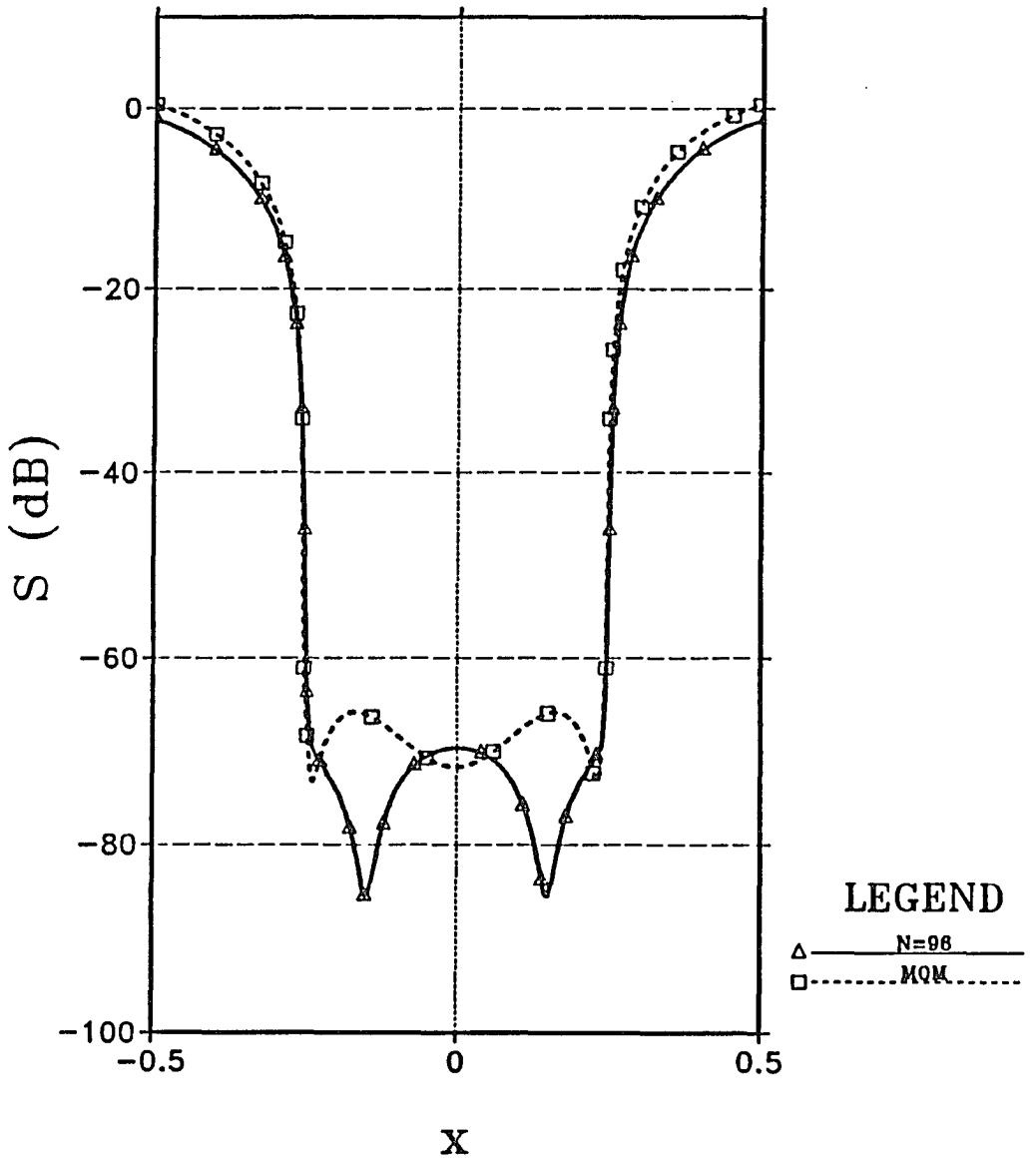

Figure 3-36 A comparison of the wire grid model with the continuous shell model (i.e. MOM solution) for the rectangular cage. The shielding effectiveness is measured along a horizontal cut at a height of 0.1λ above the half space; x is measured in wavelengths. The relevant parameters are $h = .02\lambda_1$, $c = .25\lambda_1$, $d = .5\lambda_1$, $E_0 = 1$ V/m, $K^2 = 8.00 - i17.98$, $k_1 a = 0.01$, $\theta_0 = 0$ and $\phi_0 = 0$.

3.3.4 Shielding Studies: Parallel Polarization

Some of the results given for the perpendicular polarization case will now be repeated for the parallel case. Since vertical polarization yields symmetrical results with respect to the x–axis, only the interval $x \in [0, .5\lambda_1]$ is presented.

Again, the semi–circular structure shown in Figure 3–17 is considered and the same parameters associated with Figure 3–18 will be used (i.e $K^2 = 8.00 - i17.98$). Figures 3–37, 3–38 and 3–39 show the shielding response when $\theta_0 = 30$, $\theta_0 = 45$ and $\theta_0 = 60$ degrees, respectively. The shielding distribution is affected by the zenith angle, but more importantly, the shielding response converges as N is increased. Unfortunately, increasing θ_0 degradates the shielding effectiveness.

Figure 3–40 shows the shielding response for the rectangular cage when $\theta_0 = 45^o$. The same parameters associated with Figure 3–31 are used here. Once again, the shielding configuration has little affect on the shielding performance.

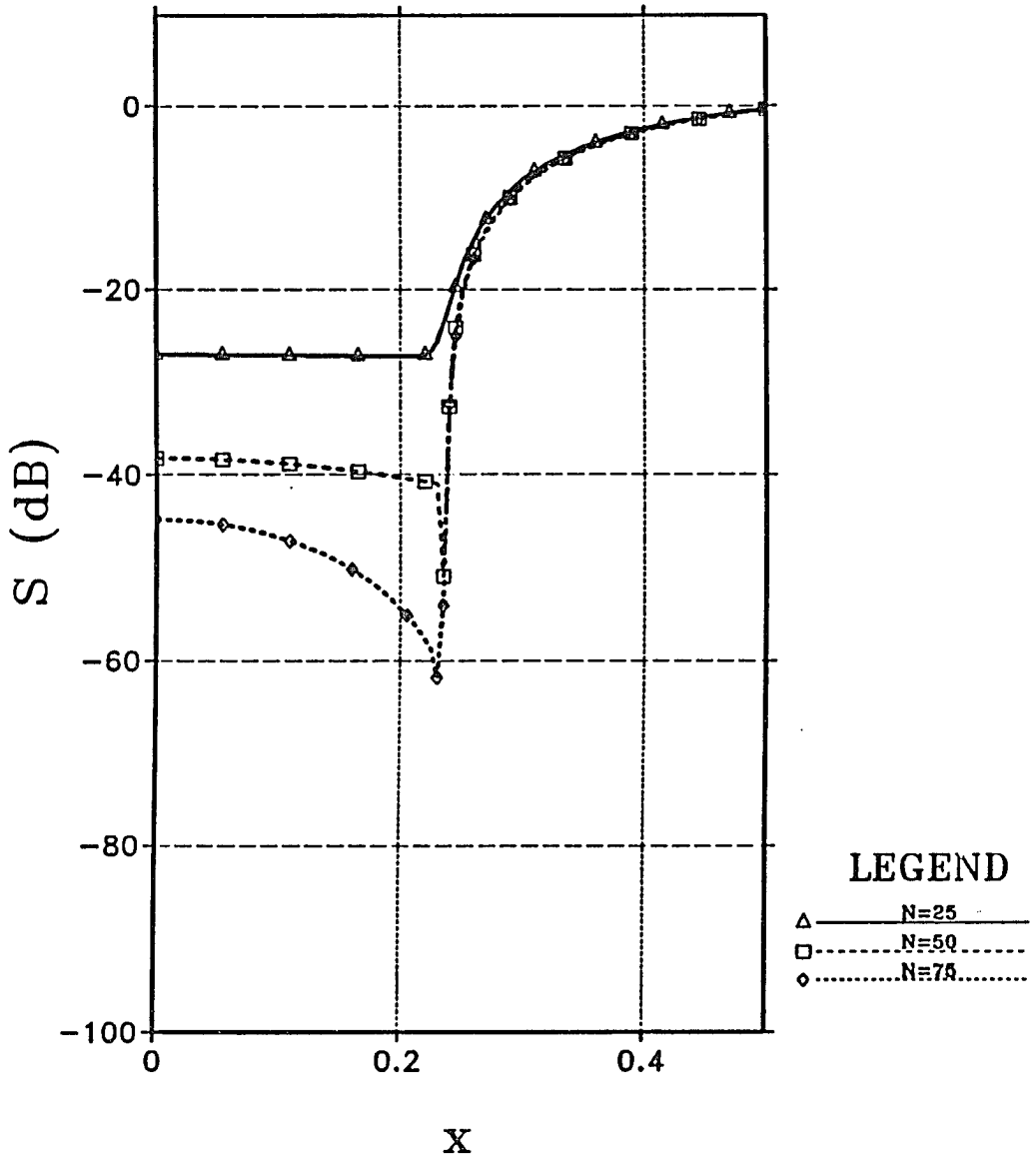

Figure 3-37 A plot of the shielding efficiency, S, as a function of x when varying N for the semi-circular cage. The shielding effectiveness is measured along a horizontal cut at a height of $0.1\lambda_1$ above the half space; x is measured in wavelengths. The relevant parameters are $h = .02\lambda_1$, $b = .25\lambda_1$, $E_0 = 1$ V/m, $K^2 = 8.00 - i17.98$, $k_1 a = 0.01$, $\theta_0 = 30^\circ$ and $\phi_0 = 90^\circ$.

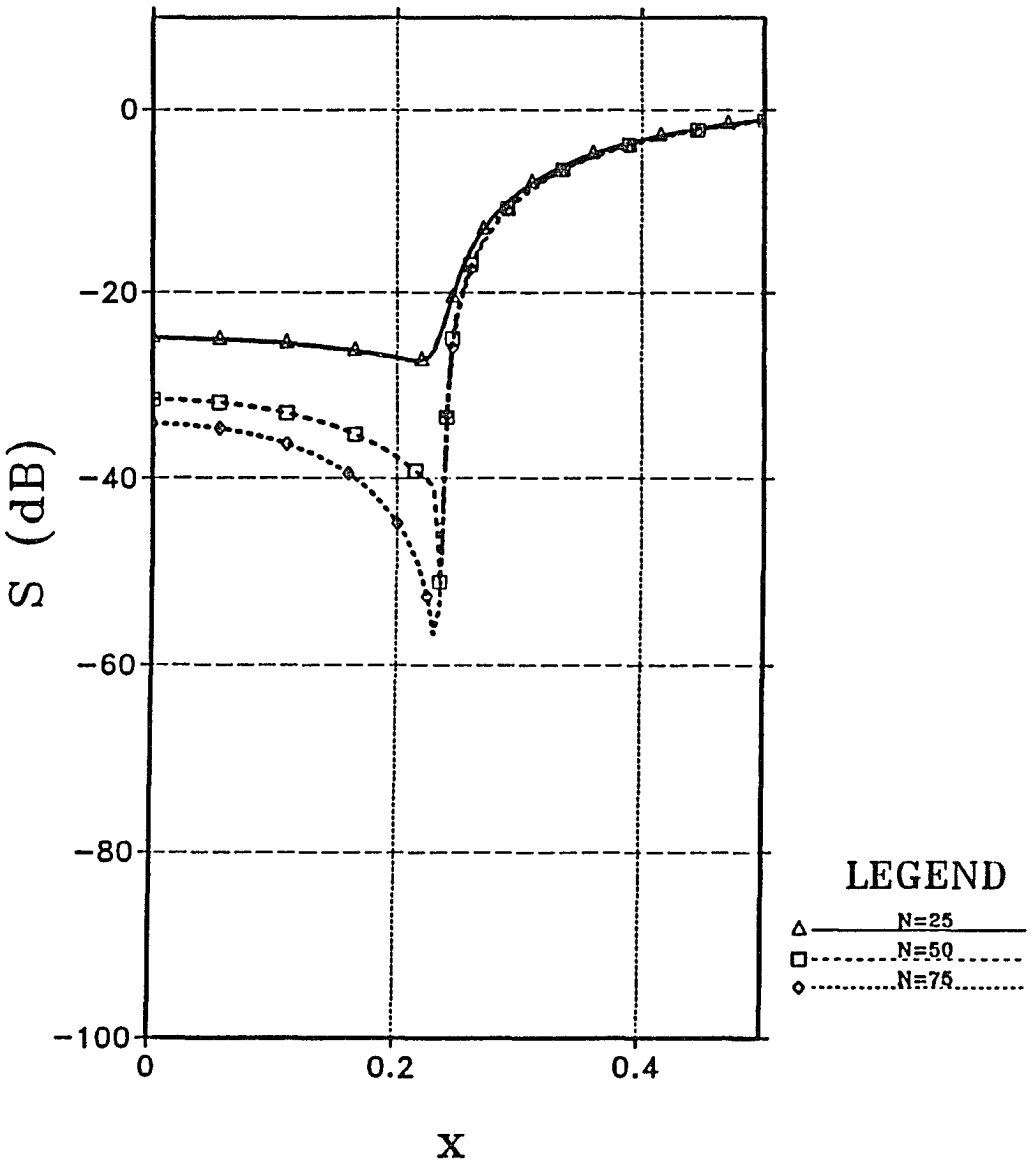

Figure 3-38 A plot of the shielding efficiency, S, as a function of x when varying N for the semi-circular cage. The shielding effectiveness is measured along a horizontal cut at a height of $0.1\lambda_1$ above the half space; x is measured in wavelengths. The relevant parameters are $h = .02\lambda_1$, $b = .25\lambda_1$, $E_0 = 1$ V/m, $K^2 = 8.00 - i17.98$, $k_1 a = 0.01$, $\theta_0 = 45^o$ and $\phi_0 = 90^o$.

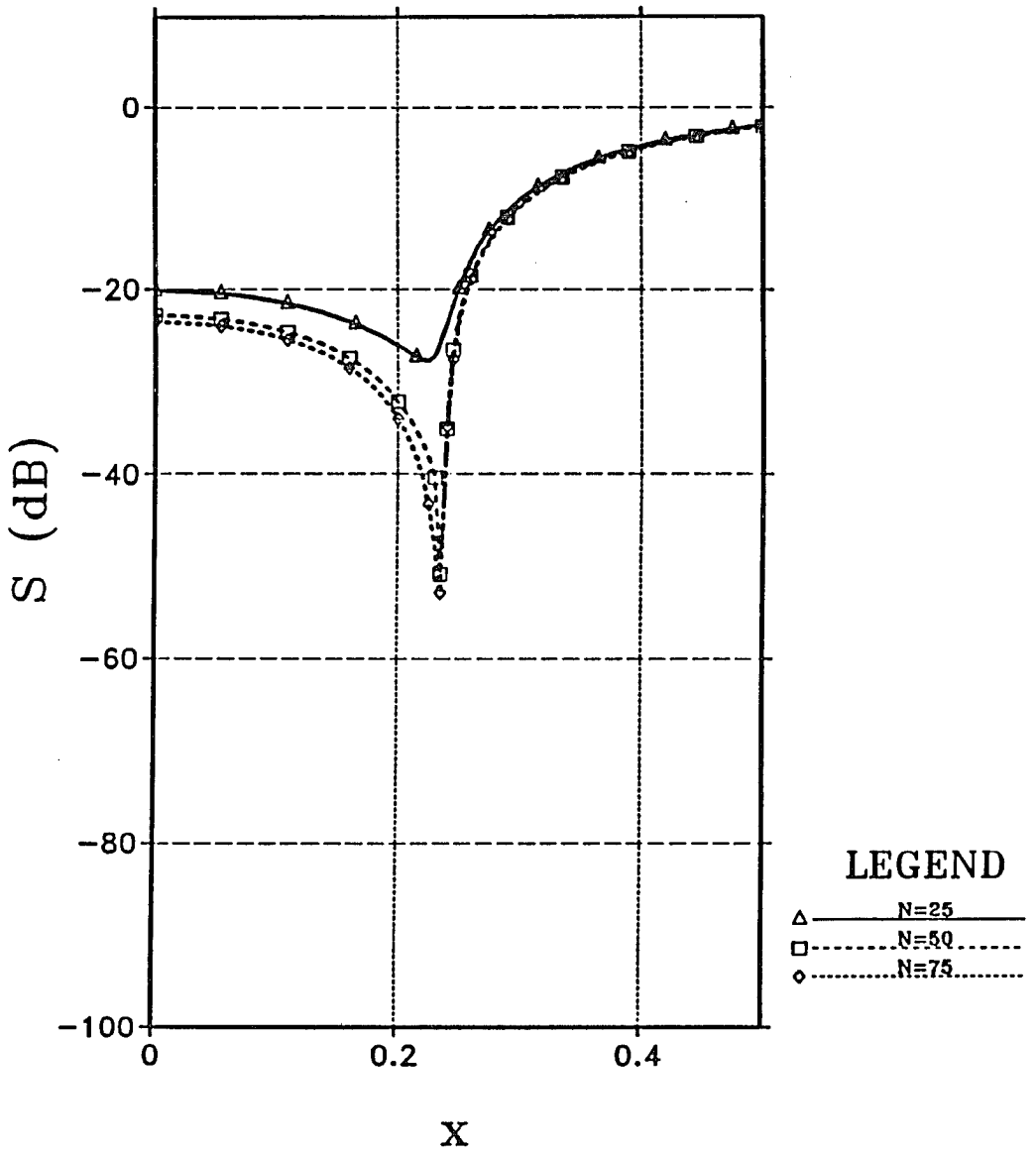

Figure 3-39 A plot of the shielding efficiency, S, as a function of x when varying N for the semi-circular cage. The shielding effectiveness is measured along a horizontal cut at a height of $0.1\lambda_1$ above the half space; x is measured in wavelengths. The relevant parameters are $h = .02\lambda_1$, $b = .25\lambda_1$, $E_0 = 1$ V/m, $K^2 = 8.00 - i17.98$, $k_1 a = 0.01$, $\theta_0 = 60^\circ$ and $\phi_0 = 90^\circ$.

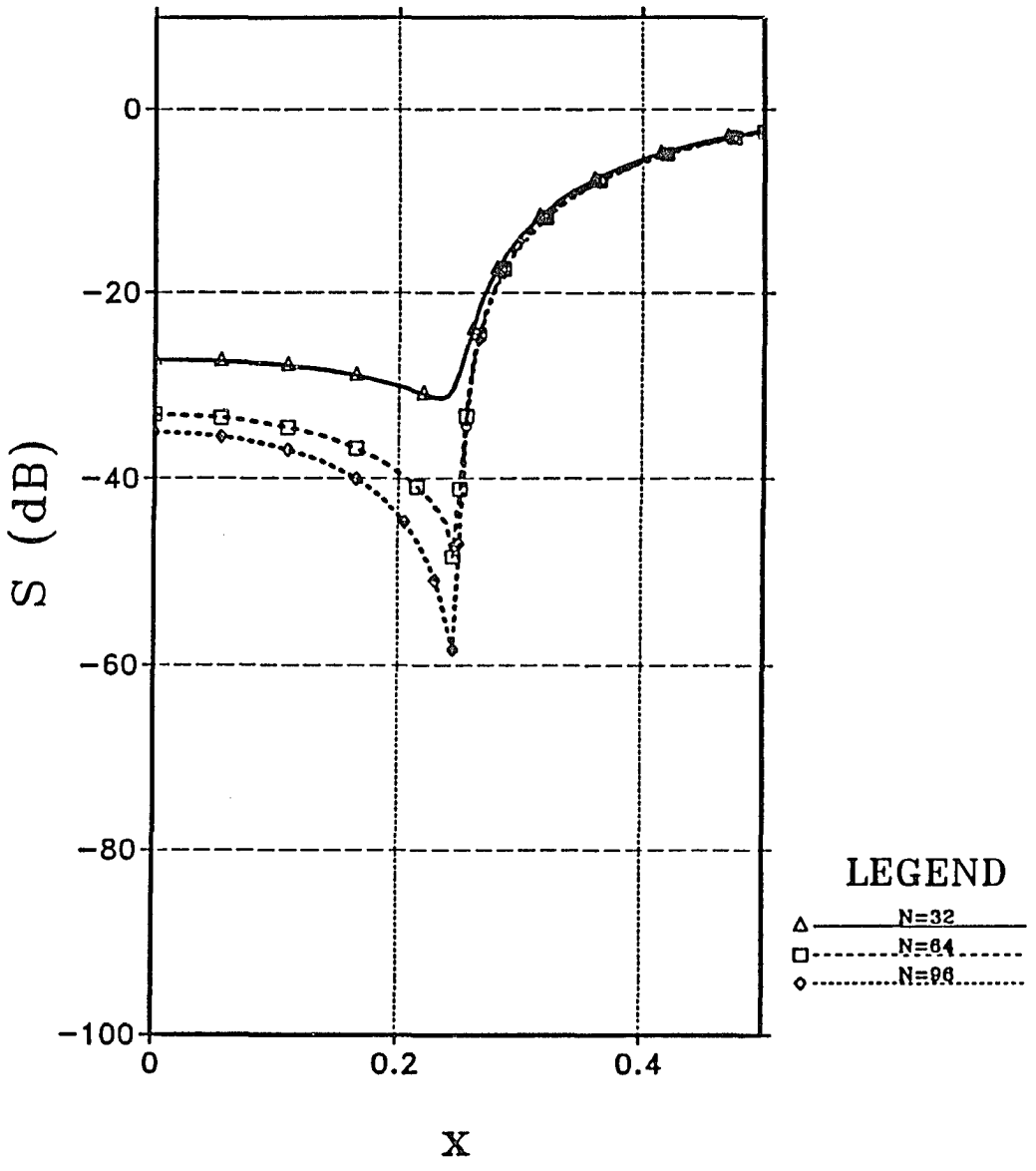

Figure 3-40 A plot of the shielding efficiency, S, as a function of x when varying N for the rectangular cage. The shielding effectiveness is measured along a horizontal cut at a height of $0.1\lambda_1$ above the half space; x is measured in wavelengths. The relevant parameters are $h = .02\lambda_1$, $c = .25\lambda_1$, $d = .5\lambda_1$, $E_0 = 1$ V/m, $K^2 = 8.00 - i17.98$, $k_1 a = 0.01$, $\theta_0 = 45^o$ and $\phi_0 = 90^o$.

CHAPTER 4

EM RESPONSE OF CROSSING WIRES

The electromagnetic response of a crossed wire configuration will be addressed in this chapter. We begin with the formulation of the general equations for two perpendicular wires over a lossy half space. These give rise to two coupled integral equations whose unknowns are the spectral currents flowing on each wire. The equations are given in terms of self and mutual impedance functions and generalized source functions in order to maintain analytic generality.

Two methods, both numerical, are used to solve for the spectral currents. The first relies on collocation moment method techniques; the second employs the iterative method of multiple scatterers such that the zeroth order, first order and higher order terms are considered sequentially. Both cases are shown to yield the same results for the leading terms. In either case, upon numerical implementation, the width of the sampling interval is determined from the Nyquist sampling theorem. Numerically computed curves are provided in order to compare the two solutions. Once the spectral currents are known, a fast Fourier transform (FFT) will be applied in order to obtain the spatial currents flowing on each wire.

Our results will focus on the detection of buried wires in an homogeneous medium when excited by a vertical magnetic dipole. The application of these results leads to further understanding of buried wire detection and cross coupling of buried communication lines [Wait, 1972b, 1978b].

4.1 Integral Equation Formulation

Two orthogonal, infinitely long, thin wires over a lossy half space, as shown in Figure 4–1, are considered. The wires are parallel to the xy–plane, and the surrounding medium is assumed to have the electrical parameters, ϵ_1 and μ_1 for $z > 0$, and ϵ_2 and μ_2 for $z < 0$. In general, ϵ and μ may be complex to account for dissipative losses. The y–directed wire is located at coordinates $x = 0$ and $z = h$ and the x–directed wire is positioned at $y = 0$ and $z = h + d$; the only restrictions are that $h > 0$, $h + d > 0$ and that the wires are non–touching. Again, the wires are assumed to be identical such that the radius, a, and the axial impedance, Z_w, are the same. The source will remain unspecified until a particular problem is addressed. The primary objective is to determine the induced currents in both the x–directed and y–directed wires.

As in Chapter 2, this problem is solved by Fourier transform methods. The transform pair for the y–directed wire is given by (2.11) and (2.12). A new transform pair is introduced for the x–directed wire. Defining $i_x(x)$ as the spatial current distribution on the x–directed wire, and $I_x(\lambda)$ as its spectral transform, we may state that

$$i_x(x) = \int_{-\infty}^{\infty} I_x(\lambda) e^{-i\lambda x} d\lambda \tag{4.1}$$

and

$$I_x(\lambda) = \frac{1}{2\pi} \int_{-\infty}^{\infty} i_x(x) e^{i\lambda x} dx \tag{4.2}$$

The single wire over a half space has already been considered in Chapter Two, so that the derivation of the Hertz potentials is not needed here. Recall from (2.24) and (2.25) that the y–component of the electric Hertz vector in region one,

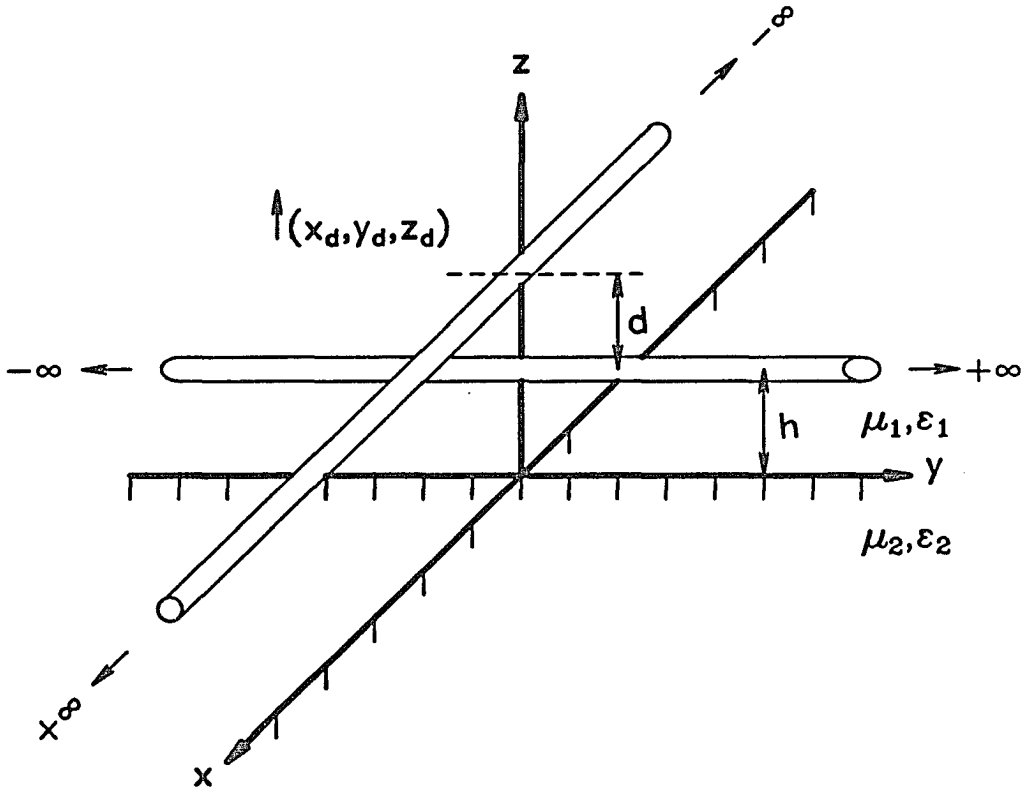

Figure 4-1 Two perpendicular wires over a half–space excited by a dipole.

related to the y–directed wire, was the combination of a primary component and a secondary component. The primary part has two equivalent forms:

$$\Pi_y^p = \frac{1}{2\pi i\omega\epsilon_1}\int_{-\infty}^{\infty} I_y(\beta)K_0(v_1\hat{\rho}_{xz})e^{-i\beta y}d\beta \tag{4.3}$$

or using the Fourier integral relationship for the MacDonald function,

$$\Pi_y^p = \frac{1}{4\pi i\omega\epsilon_1}\int_{-\infty}^{\infty} I_y(\beta)e^{-i\beta y}\int_{-\infty}^{\infty}\frac{e^{-u_1|z-h|}}{u_1}e^{-i\lambda x}d\lambda d\beta \tag{4.4}$$

where $v_1 = \sqrt{\beta^2 - k_1^2}$, $u_1 = \sqrt{\lambda^2 + v_1^2}$ and $\hat{\rho}_{xz} = \sqrt{x^2 + (z-h)^2}$. The unknown, $I_y(\beta)$ is to be determined. (Note that in the double transform expressions, the order of integration is arbitrary, and thus may be interchanged.) The secondary part was shown in Chapter Two to involve both electric and magnetic Hertz vectors. For the electric Hertz potential,

$$\Pi_y^s = \frac{1}{4\pi i\omega\epsilon_1}\int_{-\infty}^{\infty} I_y(\beta)e^{-i\beta y}\int_{-\infty}^{\infty} R_y(\lambda,\beta)\frac{e^{-u_1(z+h)}}{u_1}e^{-i\lambda x}d\lambda d\beta \tag{4.5}$$

where R_y is given by (2.37). The magnetic Hertz potential, as given in (2.27), is

$$\Pi_y^* = \frac{1}{4\pi i\omega\epsilon_1}\int_{-\infty}^{\infty} I_y(\beta)e^{-i\beta y}\int_{-\infty}^{\infty} M_y(\lambda,\beta)\frac{e^{-u_1(z+h)}}{u_1}e^{-i\lambda x}d\lambda d\beta \tag{4.6}$$

where M_y is given by (2.38).

The corresponding Hertz potentials for the x–directed wire are analogous to those for the y–directed wire. Particularly, the electric Hertz component, in region one, is a sum of a primary part and a secondary part:

$$\Pi_x^p = \frac{1}{2\pi i\omega\epsilon_1}\int_{-\infty}^{\infty} I_x(\lambda)K_0(w_1\hat{\rho}_{yz})e^{-i\lambda x}d\lambda \tag{4.7}$$

or

$$\Pi_x^p = \frac{1}{4\pi i\omega\epsilon_1}\int_{-\infty}^{\infty} I_x(\lambda)e^{-i\lambda x}\int_{-\infty}^{\infty}\frac{e^{-u_1|z-h-d|}}{u_1}e^{-i\beta y}d\beta d\lambda \tag{4.8}$$

where $I_x(\lambda)$ is to be determined. Here $w_1 = \sqrt{\lambda^2 - k_1^2}$ ($\mathrm{Re}[w_1] > 0$) and $\hat{\rho}_{yz} = \sqrt{y^2 + (z-h-d)^2}$. For the secondary part,

$$\Pi_x^s = \frac{1}{4\pi i\omega\epsilon_1}\int_{-\infty}^{\infty} I_x(\lambda)e^{-i\lambda x}\int_{-\infty}^{\infty} R_x(\lambda,\beta)\frac{e^{-u_1(z+h+d)}}{u_1}e^{-i\beta y}d\beta d\lambda \tag{4.9}$$

and

$$\Pi_x^* = \frac{1}{4\pi i\omega\epsilon_1}\int_{-\infty}^{\infty} I_x(\lambda)e^{-i\lambda x}\int_{-\infty}^{\infty} M_x(\lambda,\beta)\frac{e^{-u_1(z+h+d)}}{u_1}e^{-i\beta y}d\beta d\lambda \tag{4.10}$$

In (4.9) and (4.10), R_x and M_x can be determined from (2.37) and (2.38) (see also [Wait, 1972a]), but with y replaced with x and β replaced with λ. That is,

$$R_x = \frac{\lambda^2\beta^2(1-K_x)^2 + \omega^2(\epsilon_1 u_1 - \epsilon_2 u_2 K_x)(\mu_1 u_1 + \mu_2 u_2 K_x)}{-\lambda^2\beta^2(1-K_x)^2 + \omega^2(\epsilon_1 u_1 + \epsilon_2 u_2 K_x)(\mu_1 u_2 + \mu_2 u_2 K_x)} \tag{4.11}$$

and

$$M_x = \frac{2i\omega\lambda\beta(1-K_x)\epsilon_1 u_1}{-\lambda^2\beta^2(1-K_x)^2 + \omega^2(\epsilon_1 u_1 + \epsilon_2 u_2 K_x)(\mu_1 u_1 + \mu_2 u_2 K_x)} \tag{4.12}$$

where

$$K_x = \frac{k_1^2 - \lambda^2}{k_2^2 - \lambda^2} \tag{4.13}$$

and where $u_2 = \sqrt{\lambda^2 + \beta^2 - k_2^2}$ with $\mathrm{Re}[u_2] > 0$.

From (2.9) the total horizontal electric fields produced by the wires, for $z > 0$, can be explicitly determined from

$$E_x^w = \left(k_1^2 + \frac{\partial^2}{\partial x^2}\right)\Pi_x + \frac{\partial^2}{\partial x \partial y}\Pi_y + i\omega\mu_1 \frac{\partial}{\partial z}\Pi_y^* \tag{4.14}$$

and

$$E_y^w = \left(k_1^2 + \frac{\partial^2}{\partial y^2}\right)\Pi_y + \frac{\partial^2}{\partial x \partial y}\Pi_x - i\omega\mu_1 \frac{\partial}{\partial z}\Pi_x^* \tag{4.15}$$

The electric field components, produced by the currents in the wires, for $z > 0$ are then

$$\begin{aligned} E_x^w =& \frac{-1}{2\pi i\omega\epsilon_1}\int_{-\infty}^{\infty} w_1^2 I_x(\lambda) e^{-i\lambda x}\left[K_0(w_1\hat{\rho}_{yz}) + \frac{1}{2}\int_{-\infty}^{\infty} R_x(\lambda,\beta) e^{-u_1(z+h+d)}\frac{e^{-i\beta y}}{u_1} d\beta\right] d\lambda \\ &- \frac{1}{4\pi i\omega\epsilon_1}\int_{-\infty}^{\infty}\beta I_y(\beta) e^{-i\beta y}\int_{-\infty}^{\infty}\lambda\left[e^{-u_1|z-h|} + R_y(\lambda,\beta)e^{-u_1(z+h)}\right]\frac{e^{-i\lambda x}}{u_1} d\lambda d\beta \\ &- \frac{\eta_1^2}{4\pi}\int_{-\infty}^{\infty} I_y(\beta) e^{-i\beta y}\int_{-\infty}^{\infty} M_y(\lambda,\beta) e^{-u_1(z+h)} e^{-i\lambda x} d\lambda d\beta \end{aligned} \tag{4.16}$$

and

$$\begin{aligned} E_y^w =& \frac{-1}{2\pi i\omega\epsilon_1}\int_{-\infty}^{\infty} v_1^2 I_y(\beta) e^{-i\beta y}\left[K_0(v_1\hat{\rho}_{xz}) + \frac{1}{2}\int_{-\infty}^{\infty} R_y(\lambda,\beta) e^{-u_1(z+h)}\frac{e^{-i\lambda x}}{u_1} d\lambda\right] d\beta \\ &- \frac{1}{4\pi i\omega\epsilon_1}\int_{-\infty}^{\infty}\lambda I_x(\lambda) e^{-i\lambda x}\int_{-\infty}^{\infty}\beta\left[e^{-u_1|z-h-d|} + R_x(\lambda,\beta)e^{-u_1(z+h+d)}\right]\frac{e^{-i\beta y}}{u_1} d\beta d\lambda \\ &+ \frac{\eta_1^2}{4\pi}\int_{-\infty}^{\infty} I_x(\lambda) e^{-i\lambda x}\int_{-\infty}^{\infty} M_x(\lambda,\beta) e^{-u_1(z+h+d)} e^{-i\beta y} d\beta d\lambda \end{aligned} \tag{4.17}$$

where $\eta_1 = \sqrt{\mu_1/\epsilon_1}$.

The matching points for the thin wire operators of the x–directed wire are chosen, per our definition given in (2.52) to be $y = 0$ and $z = h + d + a$; for the y–directed wire, $x = 0$ and $z = h + a$. Consequently, the thin wire operators are then

$$\int_{-\infty}^{\infty} I_x(\lambda) Z_a(\lambda) e^{-i\lambda x} d\lambda = E_x^w(x, 0, h + d + a) + E_x^s(x, 0, h + d + a) \tag{4.18}$$

and

$$\int_{-\infty}^{\infty} I_y(\beta) Z_b(\beta) e^{-i\beta y} d\beta = E_y^w(0, y, h + a) + E_y^s(0, y, h + a) \tag{4.19}$$

Here E_x^s and E_y^s are the spatial representations (still unspecified) for the source distribution for the x and y components, respectively. Implicit in this procedure is that E_x^s and E_y^s must satisfy the continuity conditions at the interface. Also, in (4.18) and (4.19), Z_a and Z_b are the spatially dispersive axial impedances for the x–directed and y–directed wires (see Equation 2.53). In the present context,

$$Z_a(\lambda) = \frac{w_w}{2\pi a(\sigma_w + i\omega\epsilon_w)} \frac{I_0(w_w a)}{I_1(w_w a)} \tag{4.20}$$

and

$$Z_b(\beta) = \frac{v_w}{2\pi a(\sigma_w + i\omega\epsilon_w)} \frac{I_0(v_w a)}{I_1(v_w a)} \tag{4.21}$$

where $w_w = \sqrt{\gamma_w^2 + \lambda^2}$, $v_w = \sqrt{\gamma_w^2 + \beta^2}$ and $\gamma_w = \sqrt{i\omega\mu_w(\sigma_w + i\omega\epsilon_w)}$ ($\mathrm{Re}[w_w, v_w] > 0$ and $\mathrm{Re}[\gamma_w] > 0$).

Another cable structure that will be needed in future numerical results is the coated wire. For a metalic conductor of radius b coated with an insulating region of radius a, the spatially dispersive axial impedances are [Wait, 1986b],

$$Z_a^c(\lambda) = Z_a(\lambda) + \frac{(\lambda^2 - k_i^2)}{2\pi i\omega\epsilon_i} \ln(a/b) \tag{4.22}$$

and

$$Z_b^c(\beta) = Z_b(\beta) + \frac{(\beta^2 - k_i^2)}{2\pi i\omega\epsilon_i} \ln(a/b) \tag{4.23}$$

where ϵ_i is the insulator's permittivity and $k_i = \omega\sqrt{\mu_0\epsilon_i}$. When $a = b$, the axial impedance results degenerate to the case of a bare conductor.

By applying the axial impedance operators at the surface of each wire and equating integrands for all x of (4.18), we obtain the following coupled integral relationship between I_x and I_y:

$$I_x(\lambda)Z_{xx}(\lambda) + \int_{-\infty}^{\infty} I_y(\beta)Z_{xy}(\lambda,\beta)d\beta + E_x^s(\lambda) = I_x(\lambda)Z_a(\lambda) \tag{4.24}$$

where

$$Z_{xx}(\lambda) = \frac{-w_1^2}{2\pi i\omega\epsilon_1}\left[K_0(w_1 a) + \frac{1}{2}\int_{-\infty}^{\infty} R_x(\lambda,\beta)\frac{e^{-2u_1(h+d)}}{u_1}d\beta\right] \tag{4.25}$$

and

$$Z_{xy}(\lambda,\beta) = \frac{-\lambda\beta}{4\pi i\omega\epsilon_1}\left\{\frac{e^{-u_1|d|} + R_y(\lambda,\beta)e^{-u_1(2h+d)}}{u_1}\right\} - \frac{\eta_1^2}{4\pi}M_y(\lambda,\beta)e^{-u_1(2h+d)} \tag{4.26}$$

Here $E_x^s(\lambda)$ is the spectral representation for the source's x–component evaluated at the surface of the x–directed wire.

By similar construction, the y–directed electric field components are matched at the surface of each wire using (4.19) to obtain

$$I_y(\beta)Z_{yy}(\beta) + \int_{-\infty}^{\infty} I_x(\lambda)Z_{yx}(\lambda,\beta)d\lambda + E_y^s(\beta) = I_y(\beta)Z_b(\beta) \tag{4.27}$$

where

$$Z_{yy}(\beta) = \frac{-v_1^2}{2\pi i\omega\epsilon_1}\left[K_0(v_1 a) + \frac{1}{2}\int_{-\infty}^{\infty} R_y(\lambda,\beta)\frac{e^{-2u_1 h}}{u_1}d\lambda\right] \tag{4.28}$$

and

$$Z_{yx}(\lambda,\beta) = \frac{-\lambda\beta}{4\pi i\omega\epsilon_1}\left\{\frac{e^{-u_1|d|} + R_x(\lambda,\beta)e^{-u_1(2h+d)}}{u_1}\right\} + \frac{\eta_1^2}{4\pi}M_x(\lambda,\beta)e^{-u_1(2h+d)} \tag{4.29}$$

Here, $E_y^s(\beta)$ is the spectral representation for the y–component of the source field evaluated at the surface of the y–directed wire.

Clearly, (4.24) and (4.27) represent a coupled set of integral equations. The quantities Z_{xx} and Z_{yy} are the spectral self impedance terms for the x–directed and y–directed wires, respectively; they correspond to a single wire as derived in Chapter Two. The impedances Z_{xy} and Z_{yx} are the spectral mutual coupling impedances between wires which are integrated over the entire spectral space. The mutual coupling impedances are odd functions of the spectral variables. Hence, from (4.24) and (4.27), the inter–wire coupling is a function of the odd components of the spectral currents.

When the ground is perfectly conducting, $R_{x,y} = -1$ and $M_{x,y} = 0$ so that the impedance functions reduce to

$$Z_{xx}(\lambda) = \frac{-w_1^2}{2\pi i\omega\epsilon_1}\left[K_0(w_1 a) - K_0[2w_1(h+d)]\right] \tag{4.30}$$

$$Z_{xy}(\lambda,\beta) = \frac{-1}{4\pi i\omega\epsilon_1}\lambda\beta\left[\frac{e^{-u_1|d|} - e^{-u_1(2h+d)}}{u_1}\right] \tag{4.31}$$

$$Z_{yy}(\beta) = \frac{-v_1^2}{2\pi i\omega\epsilon_1}\Big[K_0(v_1 a) - K_0(2v_1 h)\Big] \tag{4.32}$$

and

$$Z_{yx}(\lambda,\beta) = \frac{-1}{4\pi i\omega\epsilon_1}\lambda\beta\left[\frac{e^{-u_1|d|} - e^{-u_1(2h+d)}}{u_1}\right] \tag{4.33}$$

For this special case, the mutual impedance functions are symmetric in β and λ; that is, $Z_{xy} = Z_{yx}$.

When no interface is present, $R_{x,y} = 0$ and $M_{x,y} = 0$, and consequently,

$$Z_{xx}(\lambda) = \frac{-w_1^2}{2\pi i\omega\epsilon_1}K_0(w_1 a) \tag{4.34}$$

$$Z_{xy}(\lambda,\beta) = \frac{-1}{4\pi i\omega\epsilon_1}\lambda\beta\frac{e^{-u_1|d|}}{u_1} \tag{4.35}$$

$$Z_{yy}(\beta) = \frac{-v_1^2}{2\pi i\omega\epsilon_1}K_0(v_1 a) \tag{4.36}$$

and

$$Z_{yx}(\lambda,\beta) = \frac{-1}{4\pi i\omega\epsilon_1}\lambda\beta\frac{e^{-u_1|d|}}{u_1} \tag{4.37}$$

Again, the mutual impedance functions are symmetric in β and λ.

Provided that the integral equations can be solved for the spectral currents, the electric field components can then be determined from (4.14) and (4.15) (a similar expression for the z–component can be computed from (2.9)). For the case where the conductors are buried in a lossy earth, the resulting magnetic fields are

of more interest. When the medium is entirely homogeneous (i.e $R_{x,y} = M_{x,y} = 0$), (2.10) shows that $\mathbf{H} = i\omega\epsilon_1 \nabla \times \mathbf{\Pi}$ or

$$H_x^w = \frac{(z-h)}{\hat{\rho}_{xz}} \Lambda_y \tag{4.38}$$

$$H_y^w = -\frac{(z-h-d)}{\hat{\rho}_{yz}} \Lambda_x \tag{4.39}$$

and

$$H_z^w = \frac{y}{\hat{\rho}_{yz}} \Lambda_x - \frac{x}{\hat{\rho}_{xz}} \Lambda_y \tag{4.40}$$

where

$$\Lambda_x = \frac{1}{2\pi} \int_{-\infty}^{\infty} I_x(\lambda) w_1 K_1(w_1 \hat{\rho}_{yz}) e^{-i\lambda x} d\lambda \tag{4.41}$$

and

$$\Lambda_y = \frac{1}{2\pi} \int_{-\infty}^{\infty} I_y(\beta) v_1 K_1(v_1 \hat{\rho}_{xz}) e^{-i\beta y} d\beta \tag{4.42}$$

4.2 Source Term: Dipole Excitation

Hitherto, the source terms have been left unspecified. For sake of generality, the spectral electric field source terms, $E_x^s(\lambda)$ and $E_y^s(\beta)$, for the vertical electric dipole (VED) and the vertical magnetic dipole (VMD) are presented. Horizontal and tilted dipoles can also be used; the derivations are similar to those given below.

4.2.1 Vertical Electric Dipole

From Wait [1985, §6.2], the electric Hertz potential for a VED, of moment Idl, located at x_d, y_d, z_d, in an homogeneous medium is

$$\Pi_z^d = \frac{Idl}{4\pi i\omega\epsilon_1}\frac{e^{-ik_1R_d}}{R_d} \tag{4.43}$$

where $R_d = \sqrt{\rho_d^2 + (z-z_d)^2}$ and $\rho_d = \sqrt{(x-x_d)^2 + (y-y_d)^2}$. By employing the Sommerfeld identity [Wait, 1959], we find that the Hertz potential can be expanded in a Fourier integral in either λ or β. That is,

$$\Pi_z^d = \frac{Idl}{4\pi^2 i\omega\epsilon_1}\int_{-\infty}^{\infty} K_0(v_1 r_{xz}) e^{-i\beta(y-y_d)} d\beta \tag{4.44}$$

or equivalently,

$$\Pi_z^d = \frac{Idl}{4\pi^2 i\omega\epsilon_1}\int_{-\infty}^{\infty} K_0(w_1 r_{yz}) e^{-i\lambda(x-x_d)} d\lambda \tag{4.45}$$

where $r_{xz} = \sqrt{(x-x_d)^2 + (z-z_d)^2}$ and $r_{yz} = \sqrt{(y-y_d)^2 + (z-z_d)^2}$. The electric field, for the x and y components, can be computed using (2.9):

$$E_x^d = \frac{\partial^2}{\partial x \partial z}\Pi_z^d \tag{4.46}$$

and

$$E_y^d = \frac{\partial^2}{\partial y \partial z}\Pi_z^d \tag{4.47}$$

so that

$$E_x^d = \frac{Idl}{4\pi^2 i\omega\epsilon_1}\frac{(z-z_d)}{r_{yz}}\int_{-\infty}^{\infty} i\lambda w_1 K_1(w_1 r_{yz}) e^{-i\lambda(x-x_d)} d\lambda \tag{4.48}$$

and

$$E_y^d = \frac{Idl}{4\pi^2 i\omega\epsilon_1}\frac{(z-z_d)}{r_{xz}}\int_{-\infty}^{\infty} i\beta v_1 K_1(v_1 r_{xz}) e^{-i\beta(y-y_d)} d\beta \tag{4.49}$$

The above forms are consistent with previously derived formulas [Hill and Wait, 1977]. Therefore, from (4.48) and (4.49), $E_x^s(\lambda)$ and $E_y^s(\beta)$ in (4.24) and (4.27), at the surface of their respective wires, are then

$$E_x^s(\lambda) = \frac{Idl}{4\pi^2 i\omega\epsilon_1}\frac{(h+d-z_d)}{\hat{r}_{yz}} i\lambda w_1 K_1(w_1\hat{r}_{yz}) e^{i\lambda x_d} \tag{4.50}$$

and

$$E_y^s(\beta) = \frac{Idl}{4\pi^2 i\omega\epsilon_1}\frac{(h-z_d)}{\hat{r}_{xz}} i\beta v_1 K_1(v_1\hat{r}_{xz}) e^{i\beta y_d} \tag{4.51}$$

where $\hat{r}_{xz} = \sqrt{x_d^2 + (h-z_d)^2}$ and $\hat{r}_{yz} = \sqrt{y_d^2 + (h+d-z_d)^2}$.

The above field representations were necessary in order to match the boundary conditions at the surface of each wire. To determine the fields at any other location, the conventional approach [Wait, 1986a, §5.3] may be used. Starting with (2.9) and (2.10), and converting the Cartesian system into a spherical system referenced at the origin of the dipole, we obtain the following:

$$H_\phi^d = \frac{Idl}{4\pi R_d^2}(1+ik_1R_d)e^{-ik_1R_d}\sin\theta_d \tag{4.52}$$

$$E_R^d = \frac{Idl}{2\pi i\omega\epsilon_1 R_d^3}(1+ik_1R_d)e^{-ik_1R_d}\cos\theta_d \tag{4.53}$$

and

$$E_\theta^d = \frac{Idl}{4\pi i\omega\epsilon_1 R_d^3}(1+ik_1R_d-k_1^2R_d^2)e^{-ik_1R_d}\sin\theta_d \tag{4.54}$$

where, from geometrical considerations, $\sin\theta_d = \rho_d/R_d$ and $\cos\theta_d = (z-z_d)/R_d$. That is, θ_d is measured from the vertical axis of the dipole.

4.2.2 Vertical Magnetic Dipole

Again, from Wait [1985, §6.2], the magnetic Hertz potential for a VMD, of strength IdA, located at x_d, y_d, z_d in an homogeneous medium is

$$\Pi_z^{*d} = \frac{IdA}{4\pi} \frac{e^{-ik_1 R_d}}{R_d} \tag{4.55}$$

When the Sommerfeld identity is applied, the spectral representations for (4.55) are

$$\Pi_z^{*d} = \frac{IdA}{4\pi^2} \int_{-\infty}^{\infty} K_0(v_1 r_{xz}) e^{-i\beta(y-y_d)} d\beta \tag{4.56}$$

or

$$\Pi_z^{*d} = \frac{IdA}{4\pi^2} \int_{-\infty}^{\infty} K_0(w_1 r_{yz}) e^{-i\lambda(x-x_d)} d\lambda \tag{4.57}$$

The electric field vector is computable from (2.9). Particularly, $\mathbf{E} = -i\omega\mu_1 \nabla \times \mathbf{\Pi}^*$, or

$$E_x^d = -i\omega\mu_1 \frac{\partial}{\partial y} \Pi_z^{*d} \tag{4.58}$$

and

$$E_y^d = i\omega\mu_1 \frac{\partial}{\partial x} \Pi_z^{*d} \tag{4.59}$$

Therefore,

$$E_x^d = i\omega\mu_1 \frac{IdA}{4\pi^2} \frac{(y-y_d)}{r_{yz}} \int_{-\infty}^{\infty} w_1 K_1(w_1 r_{yz}) e^{-i\lambda(x-x_d)} d\lambda \tag{4.60}$$

and

$$E_y^d = -i\omega\mu_1 \frac{IdA}{4\pi^2} \frac{(x-x_d)}{r_{xz}} \int_{-\infty}^{\infty} v_1 K_1(v_1 r_{xz}) e^{-i\beta(y-y_d)} d\beta \tag{4.61}$$

At the surface of each of the wires, $E_x^s(\lambda)$ and $E_y^s(\beta)$ in (4.24) and (4.27) are

$$E_x^s(\lambda) = -i\omega\mu_1 \frac{IdA}{4\pi^2} \frac{y_d}{\hat{r}_{yz}} w_1 K_1(w_1 \hat{r}_{yz}) e^{i\lambda x_d} \tag{4.62}$$

and

$$E_y^s(\beta) = i\omega\mu_1 \frac{IdA}{4\pi^2} \frac{x_d}{\hat{r}_{xz}} v_1 K_1(v_1 \hat{r}_{xz}) e^{i\beta y_d} \tag{4.63}$$

Alternate field representations will again be needed for later results. Adapting Wait's analysis [1986a, §5.8] to our coordinate system yields

$$E_\phi^d = -i\omega\mu_1 \frac{IdA}{4\pi R_d^2}(1 + ik_1 R_d) e^{-ik_1 R_d} \sin\theta_d \tag{4.64}$$

$$H_R^d = \frac{IdA}{2\pi R_d^3}(1 + ik_1 R_d) e^{-ik_1 R_d} \cos\theta_d \tag{4.65}$$

and

$$H_\theta^d = \frac{IdA}{4\pi R_d^3}(1 + ik_1 R_d - k_1^2 R_d^2) e^{-ik_1 R_d} \sin\theta_d \tag{4.66}$$

The trignometric functions are the same as defined in the previous section.

In later results, when using the VMD, the magnetic field Cartesian components will be of more interest. Applying standard geometrical identities, we find

$$\begin{aligned} H_x^d &= H_R^d \sin\theta\cos\phi + H_\theta^d \cos\theta\cos\phi \\ H_y^d &= H_R^d \sin\theta\sin\phi + H_\theta^d \cos\theta\sin\phi \\ H_z^d &= H_R^d \cos\theta - H_\theta^d \sin\theta \end{aligned} \tag{4.67}$$

where $\sin\theta = \rho/R$, $\cos\theta = z/R$, $\sin\phi = y/\rho$ and $\cos\phi = x/\rho$ with $R = \sqrt{\rho^2 + z^2}$ and $\rho = \sqrt{x^2 + y^2}$.

4.3 Matrix Solution: Moment Method

To solve for the current functions in (4.24) and (4.27), the even and odd properties of the current and field functions will be exploited. Let

$$I_x(\lambda) = I_x^{even}(\lambda) + I_x^{odd}(\lambda) \tag{4.68}$$

where

$$I_x^{even}(\lambda) = \frac{1}{2}[I_x(\lambda) + I_x(-\lambda)] \tag{4.69}$$

and

$$I_x^{odd}(\lambda) = \frac{1}{2}[I_x(\lambda) - I_x(-\lambda)] \tag{4.70}$$

In a similar fashion let

$$I_y(\beta) = I_y^{even}(\beta) + I_y^{odd}(\beta) \tag{4.71}$$

$$E_x^s(\lambda) = E_x^{even}(\lambda) + E_x^{odd}(\lambda) \tag{4.72}$$

and

$$E_y^s(\beta) = E_y^{even}(\beta) + E_y^{odd}(\beta) \tag{4.73}$$

By matching the even and odd parts in (4.24) and (4.27), we now have a system of four equations and four unknowns; two of which are immediately solvable:

$$I_x^{even}(\lambda) = \frac{E_x^{even}(\lambda)}{Z_a(\lambda) - Z_{xx}(\lambda)} \tag{4.74}$$

and

$$I_y^{even}(\beta) = \frac{E_y^{even}(\beta)}{Z_b(\beta) - Z_{yy}(\beta)} \tag{4.75}$$

with

$$I_x^{odd}(\lambda) - \frac{2}{Z_a(\lambda) - Z_{xx}(\lambda)} \int_0^\infty I_y^{odd}(\beta) Z_{xy}(\lambda, \beta) d\beta = \frac{E_x^{odd}(\lambda)}{Z_a(\lambda) - Z_{xx}(\lambda)} \qquad (4.76)$$

and

$$I_y^{odd}(\beta) - \frac{2}{Z_b(\beta) - Z_{yy}(\beta)} \int_0^\infty I_x^{odd}(\lambda) Z_{yx}(\lambda, \beta) d\lambda = \frac{E_y^{odd}(\beta)}{Z_b(\beta) - Z_{yy}(\beta)} \qquad (4.77)$$

Note that only the odd portion of the current functions provide the electromagnetic coupling between wires; the even portions are not affected by the presence of another wire.

Since no analytical solution is known for (4.76) and (4.77), the solution is to be given in terms of numerical approximations, viz. the method of moments. Although the integral operator is bounded for $\mathrm{Im}[k_1] < 0$ (see Appendix B), the numerical approximation is not mathematically established as a solution unless 1) the expansion functions and the weighting functions are identical, 2) the expansion sequence is complete in the Hilbert space of the operator and 3) the operator is positive [Dudley, 1985]; these conditions cannot be demonstrated for our situation. However, as Dudley points out, *self* and *comparative* checks can be devised that will numerically validate the results. This validation process will be addressed when a specific example is under consideration.

For our purposes, collocation, a subset of moment theory, will be employed. For this method, the following staircase approximation is sufficient (for $\lambda, \beta > 0$):

$$I_x^{odd}(\lambda) = \lim_{N \to \infty} \sum_{n=1}^{N} a_n P_n(\lambda) \qquad (4.78)$$

and

$$I_y^{odd}(\beta) = \lim_{N\to\infty} \sum_{n=1}^{N} b_n P_n(\beta) \tag{4.79}$$

where $P_n(\alpha) = 1$ if $\alpha \in [(n-1/2)\Delta, (n+1/2)\Delta]$ and $P_n(\alpha) = 0$ otherwise; the situation is depicted in Figure 4–2. Here Δ has been defined as the spectral sampling interval and a_n and b_n are the sampled current values. Also, when dealing with odd functions, $a_0 = b_0 = 0$. For subsequent analysis, the limit operator will be suppressed and implied. Of course, for numerical purposes some finite number (i.e. N) of expansion functions must be assumed for the spectral representations, but this choice will be addressed in a later section.

By inserting the forms of (4.78) and (4.79) into the coupled integral equations of (4.76) and (4.77), we find that the integrals can be easily evaluated in close–form such that (4.76) and (4.77) reduce to

$$\sum_{n=1}^{N} a_n P_n(\lambda) + \frac{\lambda}{2\pi i\omega\epsilon_1 |d|[Z_a(\lambda) - Z_{xx}(\lambda)]} \sum_{n=1}^{N} b_n \left[e^{-\Delta_1|d|} - e^{-\Delta_2|d|}\right] = \frac{E_x^{odd}(\lambda)}{Z_a(\lambda) - Z_{xx}(\lambda)} \tag{4.80}$$

and

$$\sum_{n=1}^{N} b_n P_n(\beta) + \frac{\beta}{2\pi i\omega\epsilon_1 |d|[Z_b(\beta) - Z_{yy}(\beta)]} \sum_{n=1}^{N} a_n \left[e^{-\Delta_3|d|} - e^{-\Delta_4|d|}\right] = \frac{E_y^{odd}(\beta)}{Z_b(\beta) - Z_{yy}(\beta)} \tag{4.81}$$

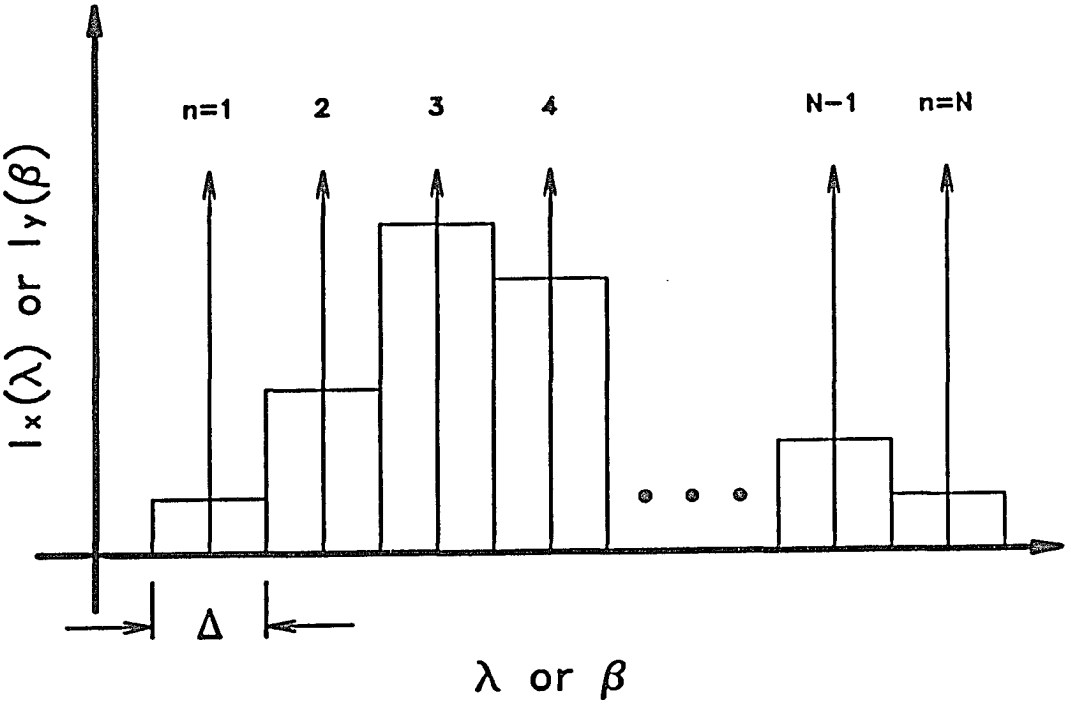

Figure 4-2 Pictorial description of the staircase expansion functions and the delta function weights used in the method of moment analysis.

where

$$\begin{aligned}\Delta_1 &= \sqrt{(n-1/2)^2\Delta^2 + \lambda^2 - k_1^2} \\ \Delta_2 &= \sqrt{(n+1/2)^2\Delta^2 + \lambda^2 - k_1^2} \\ \Delta_3 &= \sqrt{(n-1/2)^2\Delta^2 + \beta^2 - k_1^2} \\ \Delta_4 &= \sqrt{(n+1/2)^2\Delta^2 + \beta^2 - k_1^2}\end{aligned} \tag{4.82}$$

The simple identity $\int \lambda \frac{e^{-u_1 d}}{u_1} d\lambda = -\frac{e^{-u_1 d}}{d}$ was used in the previous analysis. The above equations are now sampled at the points $m\Delta$. In effect, this is implemented by taking the inner product of equation (4.80) with $\delta(\lambda - m\Delta)$ and (4.81) with $\delta(\beta - m\Delta)$, for $m = 1, 2, \ldots, N$. Doing thus, we obtain the following coupled matrix equations:

$$\mathbf{a} + \mathbf{R}\mathbf{b} = \mathbf{s} \tag{4.83}$$

and

$$\mathbf{b} + \mathbf{T}\mathbf{a} = \mathbf{q} \tag{4.84}$$

where the matrix elements of $\mathbf{R}$ and $\mathbf{T}$ are given by

$$R_{m,n} = \frac{m\Delta}{2\pi i\omega\epsilon_1 |d| [Z_a(m\Delta) - Z_{xx}(m\Delta)]} \Omega_{m,n} \tag{4.85}$$

and

$$T_{m,n} = \frac{m\Delta}{2\pi i\omega\epsilon_1 |d| [Z_b(m\Delta) - Z_{yy}(m\Delta)]} \Omega_{m,n} \tag{4.86}$$

where

$$\begin{aligned}\Omega_{m,n} = &\exp\left\{-[(n-1/2)^2\Delta^2 + (m\Delta)^2 - k_1^2]^{\frac{1}{2}}|d|\right\} \\ &- \exp\left\{-[(n+1/2)^2\Delta^2 + (m\Delta)^2 - k_1^2]^{\frac{1}{2}}|d|\right\}\end{aligned} \tag{4.87}$$

Since the wires are identical, $\mathbf{R} = \mathbf{T}$. The elements of source vectors $\mathbf{q}$ and $\mathbf{s}$ are also found to be

$$s_m = \frac{E_x^{odd}(m\Delta)}{Z_a(m\Delta) - Z_{xx}(m\Delta)} \tag{4.88}$$

and

$$q_m = \frac{E_y^{odd}(m\Delta)}{Z_b(m\Delta) - Z_{yy}(m\Delta)} \tag{4.89}$$

By applying standard matrix manipulations to (4.83) and (4.84), we find that the vectors $\mathbf{a}$ and $\mathbf{b}$ are given explicitly by

$$\mathbf{a} = [\mathbf{1} - \mathbf{R}^2]^{-1}[\mathbf{s} - \mathbf{R}\mathbf{q}] \tag{4.90}$$

and

$$\mathbf{b} = [\mathbf{1} - \mathbf{R}^2]^{-1}[\mathbf{q} - \mathbf{R}\mathbf{s}] \tag{4.91}$$

Here $\mathbf{1}$ represents the identity matrix.

At this juncture we make a few key observations. First, the matrix $\mathbf{R}$ and the vectors $\mathbf{s}$ and $\mathbf{q}$ can be loaded numerically without much difficulty. Second, the system of equations can be easily solved using standard numerical matrix techniques. Third, for $m\Delta >> |k_1|$, s_m and q_m rapidly tend toward zero.

Our attention is now returned to the even parts of the spectral current functions. Again, from the sampling theorem, the functions may be represented using a similar staircase approximation as before. Let, (for $\lambda, \beta > 0$)

$$I_x^{even}(\lambda) = \sum_{n=0}^{N} c_n P_n(\lambda) \tag{4.92}$$

and

$$I_y^{even}(\beta) = \sum_{n=0}^{N} d_n P_n(\beta) \tag{4.93}$$

Substituting these forms into (4.74) and (4.75) and taking the inner product of the resulting equations with the delta function, we easily deduce that

$$c_n = \frac{E_x^{even}(n\Delta)}{Z_a(n\Delta) - Z_{xx}(n\Delta)} \tag{4.94}$$

and

$$d_n = \frac{E_y^{even}(n\Delta)}{Z_b(n\Delta) - Z_{yy}(n\Delta)} \tag{4.95}$$

Now that the even and odd coefficients are known, the sample current expressions may be written using (4.68) and (4.71). For $\lambda, \beta \geq 0$,

$$I_x(\lambda) = c_0 P_0(\lambda) + \sum_{n=1}^{N} (c_n + a_n) P_n(\lambda) \tag{4.96}$$

and

$$I_y(\beta) = d_0 P_0(\beta) + \sum_{n=1}^{N} (d_n + b_n) P_n(\beta) \tag{4.97}$$

Similarly, for $\lambda, \beta \leq 0$,

$$I_x(\lambda) = c_0 P_0(\lambda) + \sum_{n=1}^{N} (c_n - a_n) P_n(\lambda) \tag{4.98}$$

and

$$I_y(\beta) = d_0 P_0(\beta) + \sum_{n=1}^{N} (d_n - b_n) P_n(\beta) \tag{4.99}$$

Since Hill and Wait [1977] have already dealt with the question of the dipole coupling to a single wire, our attention will be focused on the effect of the crossing wire on the current distribution. That is, if the current spectrum is decomposed into two components in the form $I_x(\lambda) = I_x^d(\lambda) + I_x^w(\lambda)$, where $I_x^d(\lambda)$ is the spectral current induced by the dipole and $I_x^w(\lambda)$ is the spectral current induced by the y–directed wire, then $I_x^w(\lambda) = I_x(\lambda) - I_x^d(\lambda)$, or

$$I_x^w(\lambda) = \sum_{n=1}^{N} e_n P_n(\lambda); \qquad \lambda > 0 \tag{4.100}$$

and

$$I_y^w(\beta) = \sum_{n=1}^{N} f_n P_n(\lambda) \qquad \beta > 0 \tag{4.101}$$

where $e_n = a_n - s_n$ and $f_n = b_n - q_n$. (Recall, the coupling between wires is a function of only the odd components.)

The coefficients of (4.100) and (4.101) are computed by taking a difference of two known coefficients. Unfortunately, from a numerical perspective these equations can lead to errors when $e_n \approx 0$ and $f_n \approx 0$. That is, the difference may yield only numerical noise. To circumvent this difficulty, an alternative definition for I_x^w and I_y^w is given from the original integral equations, as follows:

$$I_x^w(\lambda) = \frac{2}{Z_a(\lambda) - Z_{xx}(\lambda)} \int_0^\infty I_y^{odd}(\beta) Z_{xy}(\lambda, \beta) d\beta \tag{4.102}$$

and

$$I_y^w(\beta) = \frac{2}{Z_b(\beta) - Z_{yy}(\beta)} \int_0^\infty I_x^{odd}(\lambda) Z_{xy}(\lambda, \beta) d\lambda \tag{4.103}$$

Inserting (4.78) into (4.103) and (4.79) into (4.102), integrating the resultant equation, sampling the equation at $m\Delta$ and performing a few algebraic steps, we obtain the following matrix equation for the coefficients e_n and f_n:

$$\begin{aligned} \mathbf{e} &= -\mathbf{R}\mathbf{b} \\ &= \mathbf{R}[\mathbf{1} - \mathbf{R}^2]^{-1}[\mathbf{R}\mathbf{s} - \mathbf{q}] \end{aligned} \tag{4.104}$$

and

$$\begin{aligned} \mathbf{f} &= -\mathbf{R}\mathbf{a} \\ &= \mathbf{R}[\mathbf{1} - \mathbf{R}^2]^{-1}[\mathbf{R}\mathbf{q} - \mathbf{s}] \end{aligned} \tag{4.105}$$

Equations (4.104) and (4.105) can be used to calculate the coefficients e_n and f_n. However, for reasons that will become obvious in the next section, recall that $\mathbf{a} = \mathbf{s} + \mathbf{e}$ and $\mathbf{b} = \mathbf{q} + \mathbf{f}$. Hence, a new definition may be established for $\mathbf{a}$ and $\mathbf{b}$ using (4.104) and (4.105):

$$\mathbf{a} = \mathbf{s} + \mathbf{R}[\mathbf{1} - \mathbf{R}^2]^{-1}[\mathbf{R}\mathbf{s} - \mathbf{q}] \tag{4.106}$$

and

$$\mathbf{b} = \mathbf{q} + \mathbf{R}[\mathbf{1} - \mathbf{R}^2]^{-1}[\mathbf{R}\mathbf{q} - \mathbf{s}] \tag{4.107}$$

The beginnings of a geometrical matrix sequence are observed by examining (4.106) and (4.107). This leads us to consider a new $N \times N$ matrix, say $\mathbf{A}$, formed by the following powers of $\mathbf{R}$:

$$\mathbf{A} = \mathbf{1} + \mathbf{R}^2 + \mathbf{R}^4 + \ldots + \mathbf{R}^{2P} \tag{4.108}$$

A new matrix, $\mathbf{A}\mathbf{R}^2$, may also be formed:

$$\mathbf{A}\mathbf{R}^2 = \mathbf{R}^2 + \mathbf{R}^4 + \ldots + \mathbf{R}^{2P} + \mathbf{R}^{2(P+1)} \tag{4.109}$$

A closed form expression may be obtained, after a few matrix manipulations, by subtracting the two former equations. This yields,

$$\begin{aligned}\mathbf{A} &= [\mathbf{1} - \mathbf{R}^{2(P+1)}][\mathbf{1} - \mathbf{R}^2]^{-1} \\ &= [\mathbf{1} - \mathbf{R}^2]^{-1} - \mathbf{R}^{2(P+1)}[\mathbf{1} - \mathbf{R}^2]^{-1}\end{aligned} \tag{4.110}$$

Consequently, inserting the definition of $\mathbf{A}$ into (4.110), we obtain the following identity:

$$[\mathbf{1} - \mathbf{R}^2]^{-1} = \mathbf{1} + \sum_{p=1}^{P} \mathbf{R}^{2p} + \mathbf{R}^{2(P+1)}[\mathbf{1} - \mathbf{R}^2]^{-1} \tag{4.111}$$

We may state a new definition for $\mathbf{a}$ and $\mathbf{b}$ by using (4.90) and (4.91) along with (4.111):

$$\mathbf{a} = \left[\mathbf{1} + \sum_{p=1}^{P} \mathbf{R}^{2p}\right]\left[\mathbf{s} - \mathbf{R}\mathbf{q}\right] + \mathbf{a}' \tag{4.112}$$

and

$$\mathbf{b} = \left[\mathbf{1} + \sum_{p=1}^{P} \mathbf{R}^{2p}\right]\left[\mathbf{q} - \mathbf{R}\mathbf{s}\right] + \mathbf{b}' \tag{4.113}$$

where the remainders are given by

$$\mathbf{a}' = \mathbf{R}^{2(P+1)}[\mathbf{1} - \mathbf{R}^2]^{-1}[\mathbf{s} - \mathbf{R}\mathbf{q}] \tag{4.114}$$

and

$$\mathbf{b}' = \mathbf{R}^{2(P+1)}[\mathbf{1} - \mathbf{R}^2]^{-1}[\mathbf{q} - \mathbf{R}\mathbf{s}] \tag{4.115}$$

The above matrix series may be interpreted from the perspective of multiple scatterer theory. This discussion will be postponed until the close of the following section.

4.4 Multiple Scatterer Theory

The method of multiple scatterers is an iterative approach to decouple the integral equations of (4.76) and (4.77). The zeroth order approximation assumes that no coupling exists between the crossing wires, which in effect considers the integral terms negligible. That is,

$$I_x^{(0)}(\lambda) = \frac{E_x(\lambda)}{Z_a(\lambda) - Z_{xx}(\lambda)} \tag{4.116}$$

and

$$I_y^{(0)}(\beta) = \frac{E_y(\beta)}{Z_b(\beta) - Z_{yy}(\beta)} \tag{4.117}$$

The first order results are then obtained by inserting the zeroth order equations back into the integrals of (4.76) and (4.77). Doing so, we get

$$I_x^{(1)}(\lambda) - \frac{2}{Z_a(\lambda) - Z_{xx}(\lambda)} \int_0^\infty I_y^{(0)}(\beta) Z_{xy}(\lambda, \beta) d\beta = I_x^{(0)}(\lambda) \tag{4.118}$$

and

$$I_y^{(1)}(\beta) - \frac{2}{Z_b(\beta) - Z_{yy}(\beta)} \int_0^\infty I_x^{(0)}(\lambda) Z_{yx}(\lambda, \beta) d\lambda = I_y^{(0)}(\beta) \tag{4.119}$$

The above integral equations are decoupled and hence, an expression exists for the first order forms, providing the integrals can be evaluated. The second order results are obtained by inserting the first order forms back into the integrals of (4.76) and (4.77):

$$I_x^{(2)}(\lambda) - \frac{2}{Z_a(\lambda) - Z_{xx}(\lambda)} \int_0^\infty I_y^{(1)}(\beta) Z_{xy}(\lambda, \beta) d\beta = I_x^{(0)}(\lambda) \tag{4.120}$$

and

$$I_y^{(2)}(\beta) - \frac{2}{Z_b(\beta) - Z_{yy}(\beta)} \int_0^\infty I_x^{(1)}(\lambda) Z_{yx}(\lambda, \beta) d\lambda = I_y^{(0)}(\beta) \tag{4.121}$$

Higher order approximations may be obtained by continuing this iterative process.

Unfortunately, the integrals of (4.118) and (4.119) cannot be evaluated in close form. However, the first order forms may approximated using the following staircase expansion:

$$I_x^{(0)}(\lambda) = \sum_{n=1}^{N} s_n P_n(\lambda) \tag{4.122}$$

and

$$I_y^{(0)}(\beta) = \sum_{n=1}^{N} q_n P_n(\beta) \tag{4.123}$$

where the pulse function is defined as before and the leading coefficients are given by (4.88) and (4.89). Recalling the expansion approximation for I_x^{odd} and I_y^{odd}, inserting (4.122) and (4.123) back into (4.119) and (4.118), respectively, evaluating the integrals, and sampling at every $m\Delta$, we obtain the following decoupled set of matrix equations:

$$\mathbf{a} = \mathbf{s} - \mathbf{R}\mathbf{q} \tag{4.124}$$

and

$$\mathbf{b} = \mathbf{q} - \mathbf{R}\mathbf{s} \tag{4.125}$$

Equations (4.124) and (4.125) are the first order sampled approximations. The second order approximations are obtained by inserting the first order forms back

into the original integral equations. This leads to a new matrix equation for the second order forms:

$$\mathbf{a} = \mathbf{s} - \mathbf{Rq} + \mathbf{R}^2\mathbf{s} \tag{4.126}$$

and

$$\mathbf{b} = \mathbf{q} - \mathbf{Rs} + \mathbf{R}^2\mathbf{q} \tag{4.127}$$

As this process is continued, the third order forms are

$$\mathbf{a} = \mathbf{s} - \mathbf{Rq} + \mathbf{R}^2\mathbf{s} - \mathbf{R}^3\mathbf{q} \tag{4.128}$$

and

$$\mathbf{b} = \mathbf{q} - \mathbf{Rs} + \mathbf{R}^2\mathbf{q} - \mathbf{R}^3\mathbf{s} \tag{4.129}$$

A striking similarity exists between (4.128) and (4.129) with (4.112) and (4.113). That is, the multiple scatterer results may be calculated from the moment method solution with the added bonus of knowing the higher order terms contained in the remainders. The moment method will yield the closed form result for any wire spacing at the numerical sacrifice of squaring and inverting larger matrices. If the wire spacing is *large* such that the remainder term may be neglected for scattering orders of two or more, then the leading coeficients are obtainable from simple operation of matrix multiplication and addition via (4.124) and (4.125).

The multiple scatterer forms derived herein are very similar to those derived by Wait [1986a §7.9] for the parallel wire case. Each term in the series of (4.112) and (4.113) represents one round trip of the scatter wave between wires. That is, the source wave impinges against, say the x–directed wire, which then produces a scattered wave, which in turn interacts with the y–directed wire. The y–directed

wire will act as a secondary source and will scatter this wave back onto the x–directed wire. However, there is one basic and crucial dissimilarity between the two cases. For the parallel wire case, the multiple scatterer series converges like $1/d$. In contrast with the perpendicular wire case, the squaring of the **R** matrix produces series convergence like $1/d^2$. Hence, as expected, higher order interactions effects may have negligible affect such that the first order forms might be sufficient.

4.5 Numerical Considerations

With either the moment method or the method of multiple scatterers, the sample values of the spectral currents can be determined. The spatial quantities are easily obtained through the use of an FFT package [Press, et al.,1986, §12.1]. However, before applying the FFT alogrithm, we must first consider the sampling range, $N\Delta$, and second, the samplng interval Δ.

The sampling range must be chosen such that for all numerical purposes the functions $I_x(\lambda)$ and $I_y(\beta)$ are effectively band limited. That is, for all $\lambda > N\Delta$ and $\beta > N\Delta$

$$\frac{|I_x(\lambda)|}{\max_{\lambda\in[0,\infty)}|I_x(\lambda)|} < 10^{-l} \tag{4.130}$$

and

$$\frac{|I_y(\beta)|}{\max_{\beta\in[0,\infty)}|I_y(\beta)|} < 10^{-l} \tag{4.131}$$

where l specifies the numerical dynamic range ($l \geq 3$ usually sufficies). Unfortunately, there is no *a priori* knowledge that can be invoked to determine $N\Delta$.

However, an adequate estimation can be obtained for $N\Delta$ by removing the coupling between wires. Then, by choosing some value for Δ, we can find an N such that for all $n > N$,

$$\frac{|c_n + s_n|}{\max_{n=1,2,\ldots} |c_n + s_n|} < 10^{-l} \tag{4.132}$$

and

$$\frac{|d_n + q_n|}{\max_{n=1,2,\ldots} |d_n + q_n|} < 10^{-l} \tag{4.133}$$

The sampling interval in the spectral domain and the numerical support of $i_x(x)$ and $i_y(y)$ in the spatial domain, where $x \in [-x_{max}, x_{max}]$ and $y \in [-y_{max}, y_{max}]$, are related through the rule $x_{max} = y_{max} = \pi/\Delta$. Hence, for proper numerical representation of the spatial currents we must find an x_{max} and y_{max} such that for all $x > x_{max}$ and $y > y_{max}$

$$\frac{|i_x(x)|}{\max_{x\in(-\infty,\infty)} |i_x(x)|} < 10^{-l} \tag{4.134}$$

and

$$\frac{|i_y(y)|}{\max_{y\in(-\infty,\infty)} |i_y(y)|} < 10^{-l} \tag{4.135}$$

If x_{max} and y_{max} were known, which they are not, then $\Delta = \pi/x_{max}$ or $\Delta = \pi/y_{max}$, depending on which result is smaller. Now, if Δ has been incorrectly chosen too coarse, all the spatial current "density which lies outside the range $-x_{max} < x < x_{max}$ is spuriously mapped into that range" [Press et al., 1986, §12.1]. This is known as aliasing. Unfortunately, for the case of the bare wire, numerical experimentation is required.

The general spatial behavior of the current on the coated wire can be effectively postulated by considering its surface wave properties. For a single coated wire in an homogeneous medium the general exponential behavior for $i_x(x)$ is of the form [Hill, 1988],

$$i_x(x) = C(\lambda_p)e^{-i\lambda_p x} \tag{4.136}$$

where C is some function of λ_p and

$$\lambda_p \approx k_i\sqrt{1+\kappa} \tag{4.137}$$

with

$$\kappa = \frac{K_0(ik_1a)}{\ln(a/b)} \tag{4.138}$$

An implicit assumption for the previous forms is that the inner conductor is lossless. These formulas agree well with the curves given by Wait [1978b].

The imaginary part of λ_p corresponds to the attenuation rate of the current function. By desiring the current function to be less than some small value, we may roughly determine x_{max}, and consequently Δ, through the simple relationship

$$\Delta = \frac{\pi Im[\lambda_p]}{2.3l} \tag{4.139}$$

Again, $l \geq 3$ should be sufficient.

4.6 Numerical Results

As mentioned earlier, we wish to address the coupling and the geophysical detection of buried conductors which are either bare or coated [Hill, 1988]. For this case, magnetic dipole excitation is a common source for borehole detection. However, there is no fundamental difficulty in extending these results for the VED.

In both the bare and coated wire, the electromagnetic parameters, except for the dielectric coating, will be the same. A moist, nonmagnetic rock earth is assumed, such that $\sigma_1 = 0.005$ S/m, $\epsilon_1 = 10\epsilon_0$ and $\mu_1 = \mu_0$. The metallic wire will be copper, so that $\sigma_w = 5.8 \times 10^7$ S/m, $\epsilon_1 = \epsilon_0$ and $\mu_1 = \mu_0$, with a radius, $a = 0.5$ cm. The dipole will operate at $f = 100$ kHz and with a dipole moment, IdA, of 1 A-m^2. The geometrical settings are $h = 0$, $d = 1$ m, $x_d = -15$ m, $y_d = 15$ m, and $z_d = 0$.

In Figures 4–3 and 4–4 respectively, the calculated spectral currents flowing on the x–directed and y–directed wires are plotted. Each figure shows the total current, I (given by (4.96) – (4.99)); the odd–symetrical current, I^{odd} (given by (4.78) – (4.79)); the even-symmetrical current, I^{even} (given by (4.92) – (4.93)); and the induced current resulting from the presence of the other conductor, I^w (given by (4.100) – (4.101)). Through trial and error computations, we have found that $\Delta = .3/64$ and $N = 64$ are sufficient to characterize the currents. Increasing the value for N produces no significant change in the results (a self check proposed by Dudley [1985] for validating the moment method *solution*). As seen from the figures, for these two values of N, the total spectral dynamic range is roughly on the order of 10^3. The most striking characteristic of these two plots is that the induced current arising from the presence of the other wire is negligible. Although the

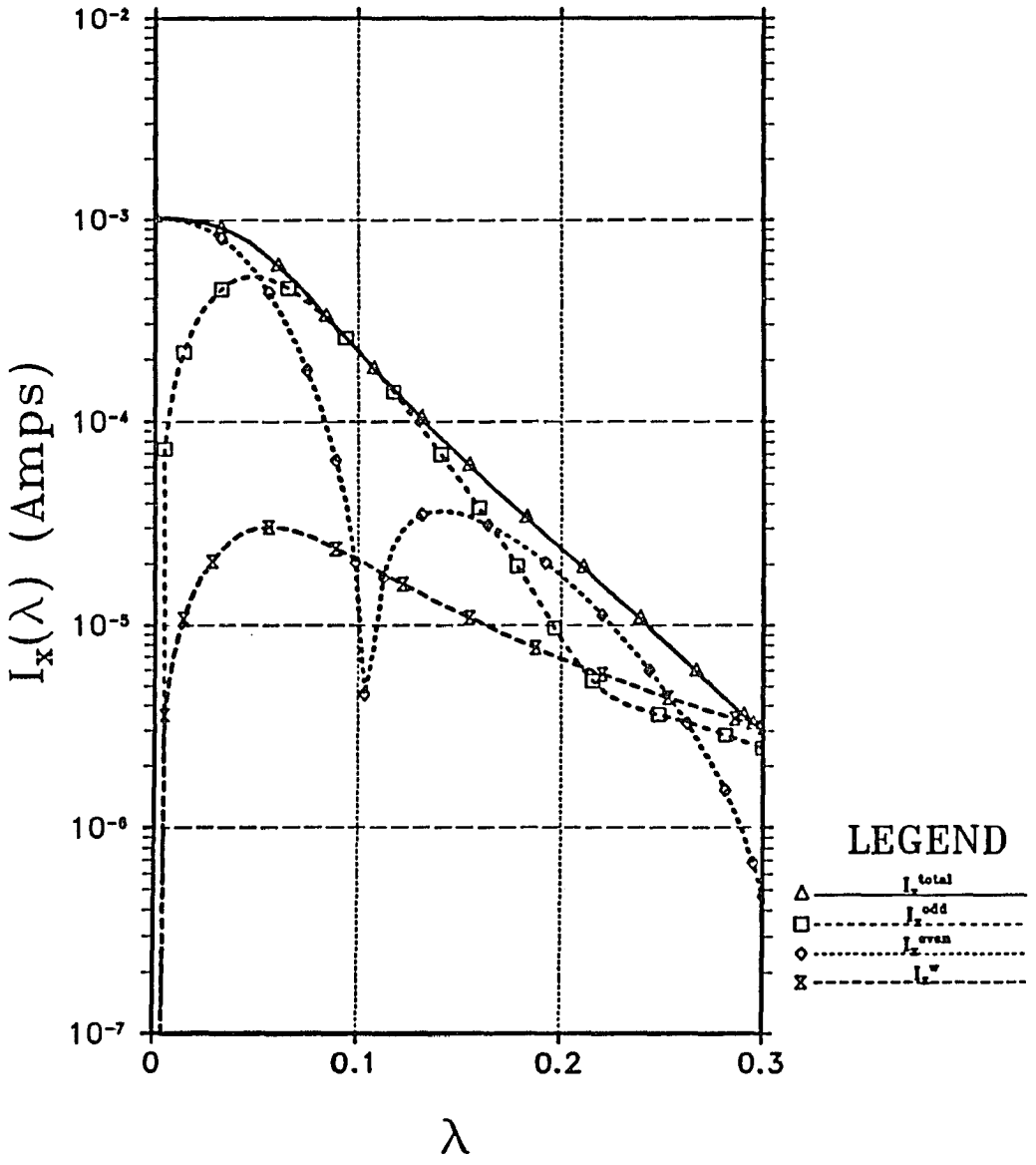

Figure 4-3 The spectral currents induced on the x-directed bare wire when excited by a magnetic dipole in a lossy homogeneous earth. The relevant parameters are: $f = 100$ kHz, $IdA = 1$ A-m^2, $\sigma_1 = 0.005$ S/m, $\epsilon_1 = 10\epsilon_0$, $\mu_1 = \mu_0$, $a = 0.5$ cm, $h = 0$, $d = 1$ m, $x_d = -15$ m, $y_d = 15$ m, and $z_d = 0$.

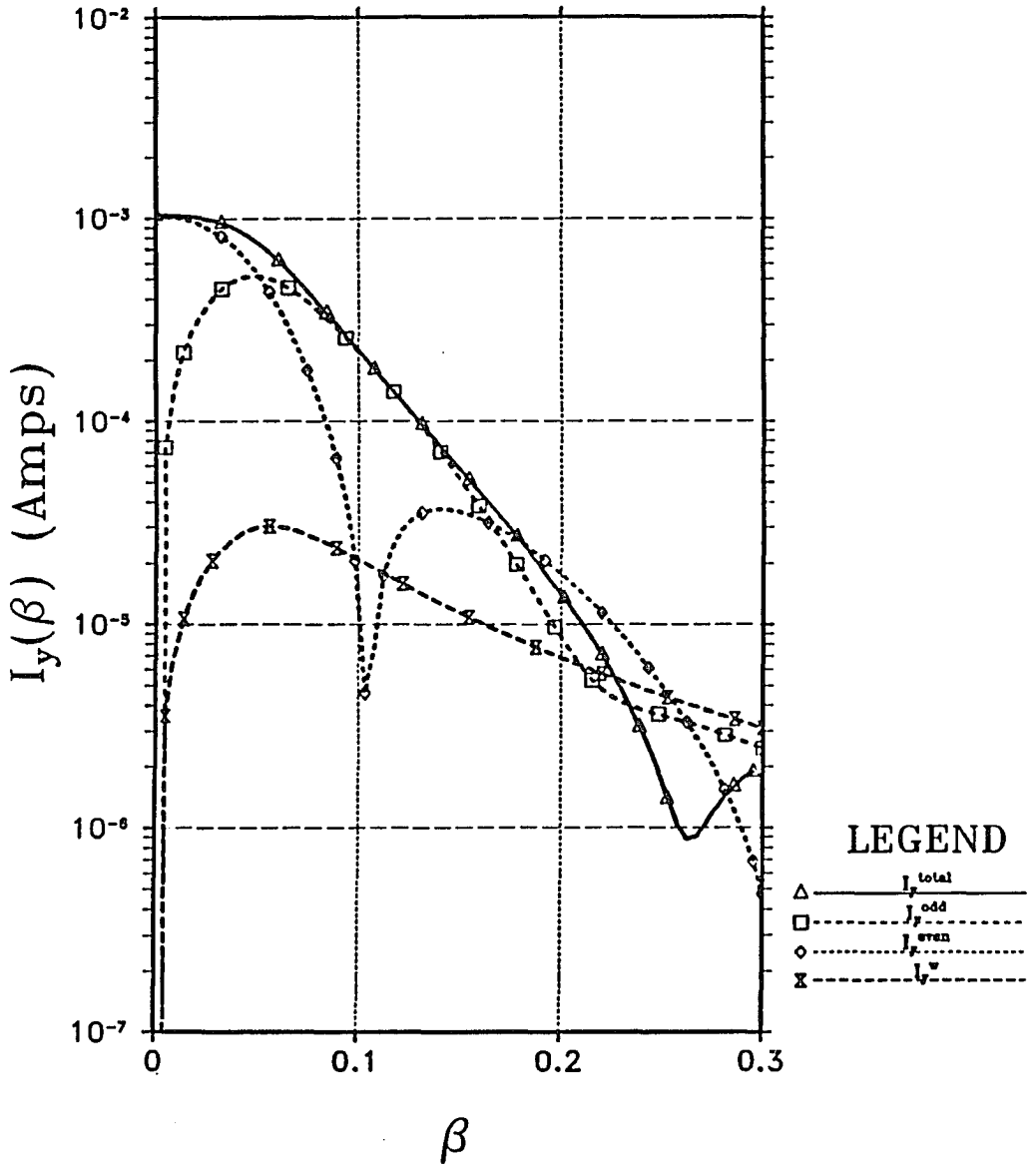

Figure 4-4 The spectral currents induced on the y-directed bare wire when excited by a magnetic dipole in a lossy homogeneous earth. The relevant parameters are: $f = 100$ kHz, $IdA = 1$ A-m^2, $\sigma_1 = 0.005$ S/m, $\epsilon_1 = 10\epsilon_0$, $\mu_1 = \mu_0$, $a = 0.5$ cm, $h = 0$, $d = 1$ m, $x_d = -15$ m, $y_d = 15$ m, and $z_d = 0$.

presence of the crossing wire affects higher spectral components, at these spectral frequencies, the over–all magnitude is down by several orders such that the crossing wire has little effect.

For the next set of figures, the MOM solution is plotted against the zero and first order approximations as given in (4.120), (4.121), (4.124) and (4.125), respectively. As seen in Figures 4–5 and 4–6, the zero order solution approximates the MOM solution (i.e. I_x^{odd} and I_y^{odd}) quite well for the lower spectral frequencies. However, by adding a first order correction term, which accounts for one wave bounce from the other wire, we see that this approximation yields very good results for all spectral frequencies.

The first order approximation is advantageous due to its numerical efficiency. The MOM solution requires the squaring and inverting of large matrices, whereas the first order approximation requires none. The computional savings is roughly a factor of N. That is, for this problem the first order approximation can be computed at least 64 times faster than the MOM solution.

Figure 4–7 shows a plot of the spatial currents determined by the application of an inverse FFT [Press et al., 1986, §12.1]. The general behavior and attenuation rate along the wires' axes is similar to that observed in earlier studies [Hill, 1988]. Such a rapid rate of decay is due to the *bleeding* of current from the wire into the conducting medium. The peaks correspond to the Cartesian coordinates of the dipole.

Our study of bare wire detection concludes with plots of the magnetic field, as a function of z, produced by both the wires and dipole. Figures 4–8 and 4–9 show the magnetic field strength for the x and y components, respectively. The

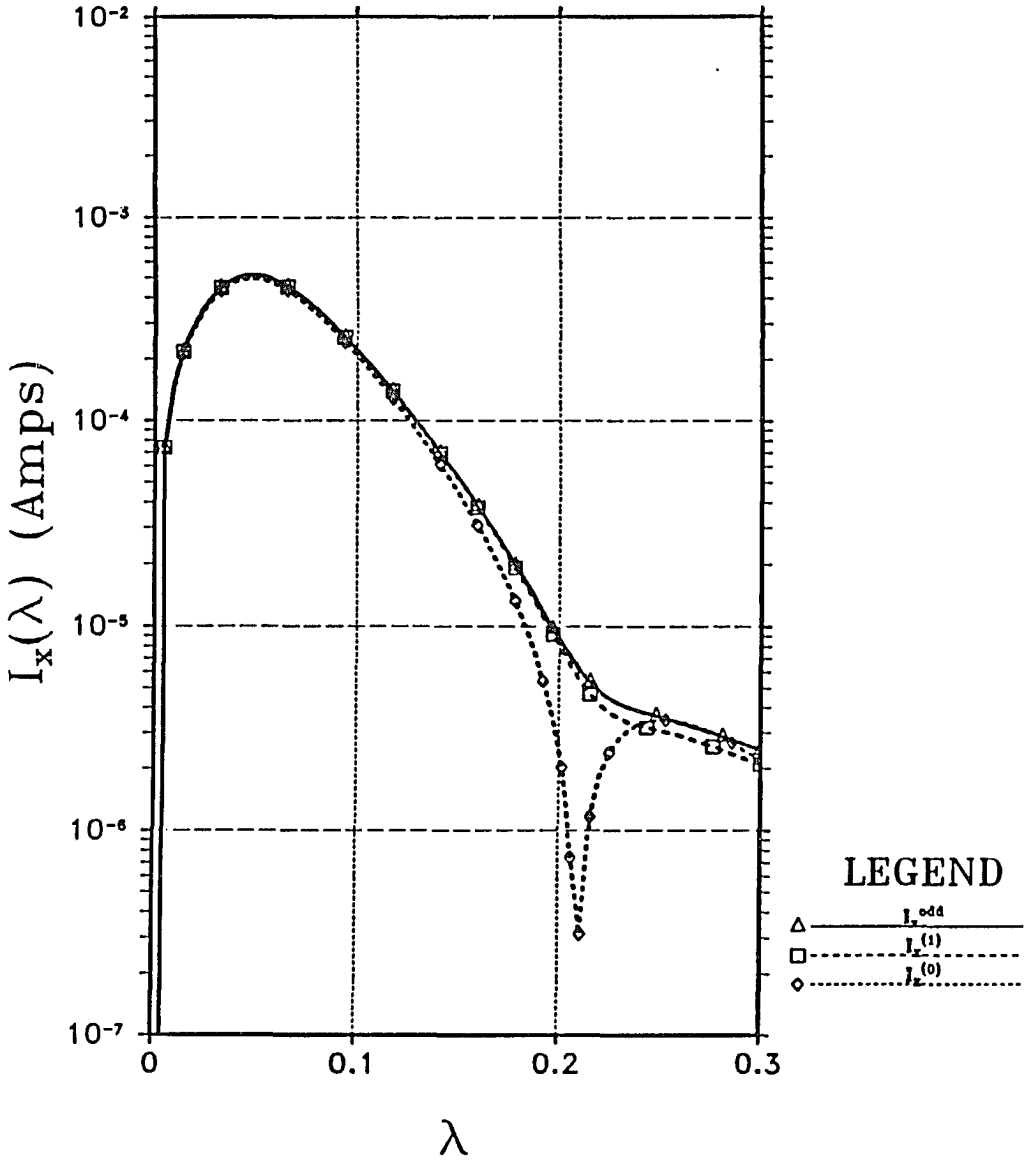

Figure 4-5 Comparison of the MOM solution to the zero and first order approximations for the bare wire excited by a VMD.

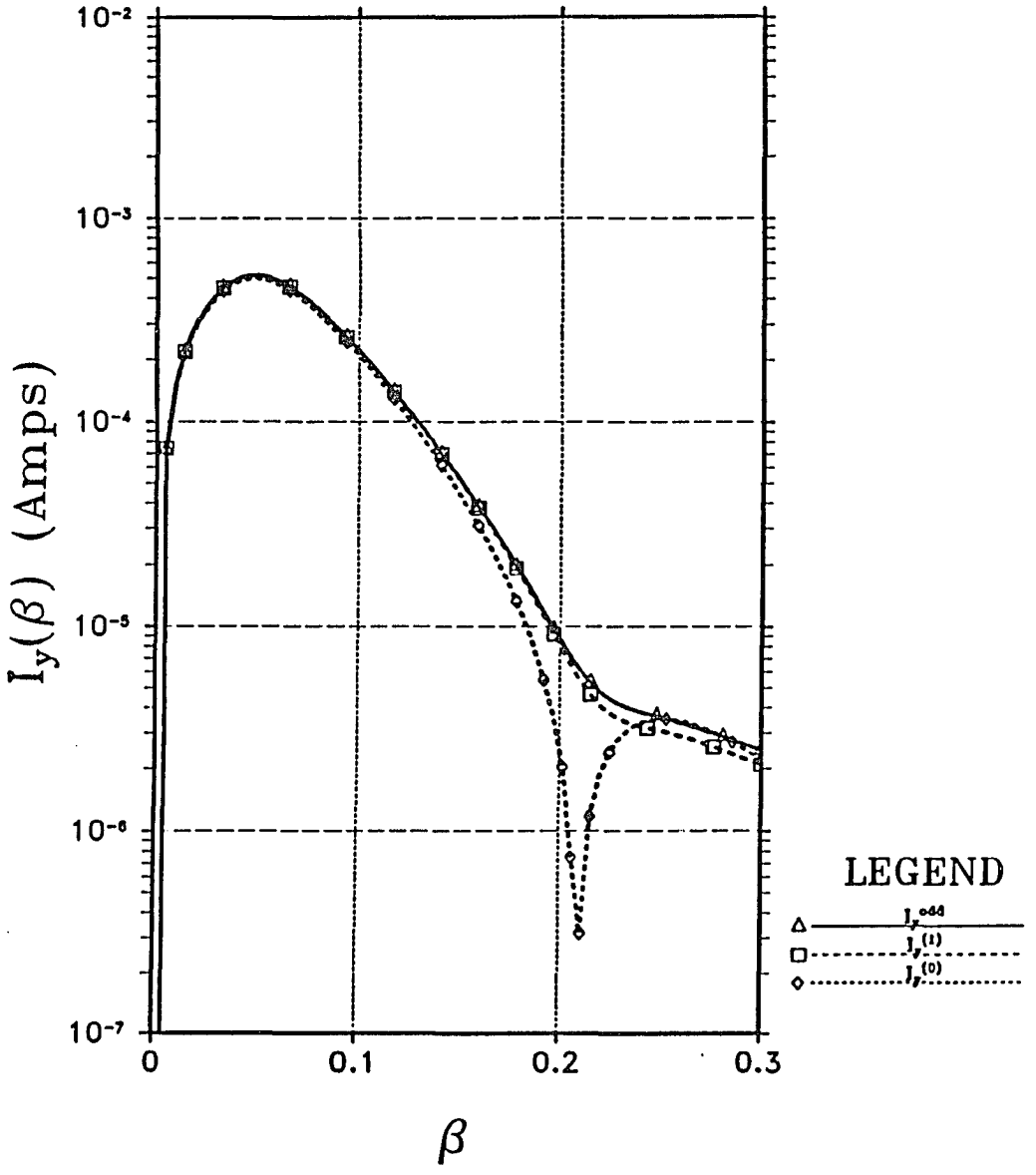

Figure 4-6 Comparison of the MOM solution to the zero and first order approximations for the bare wire excited by a VMD.

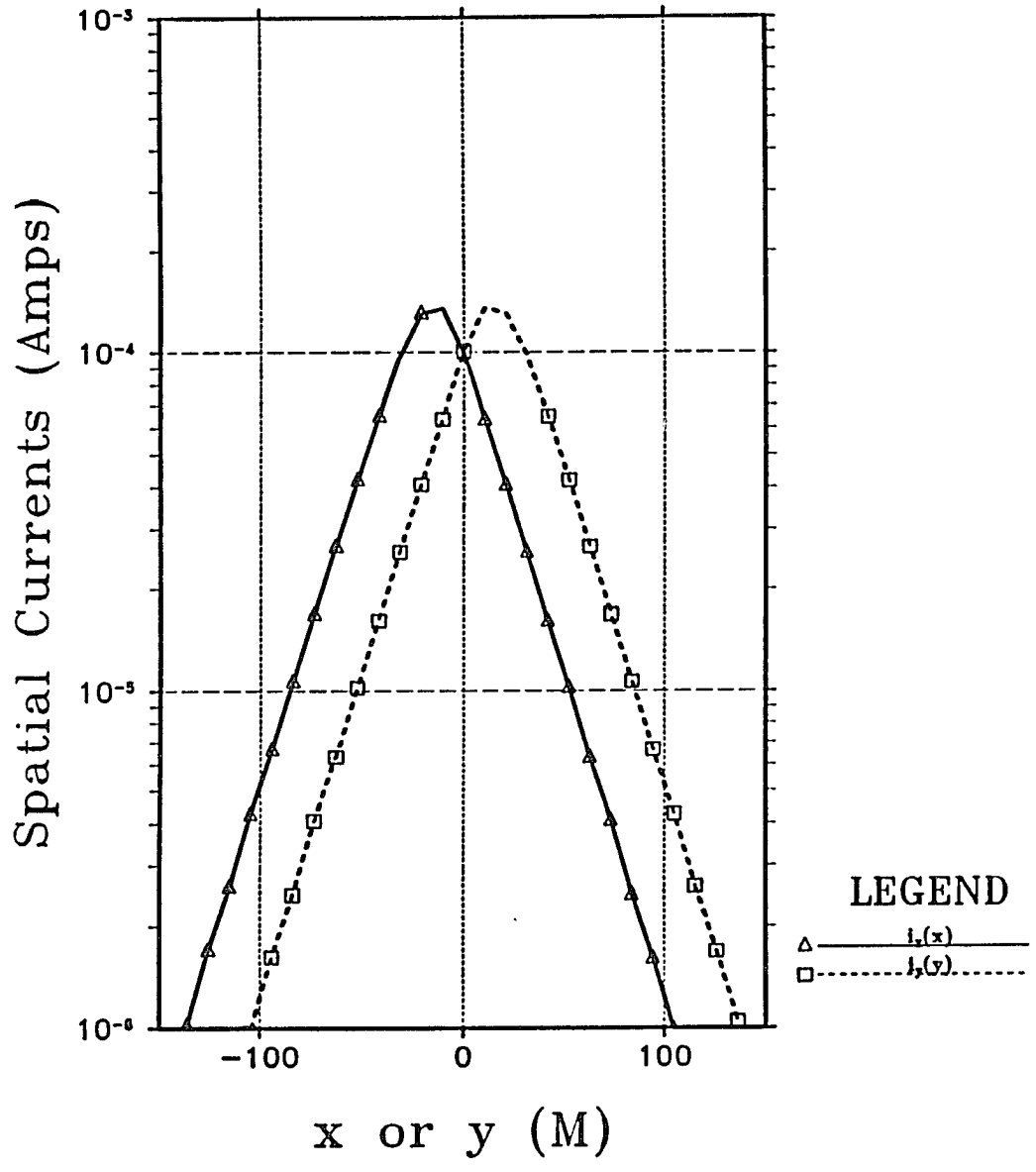

Figure 4-7 The spatial currents induced on the bare wires by a magnetic dipole in a lossy homogeneous earth.

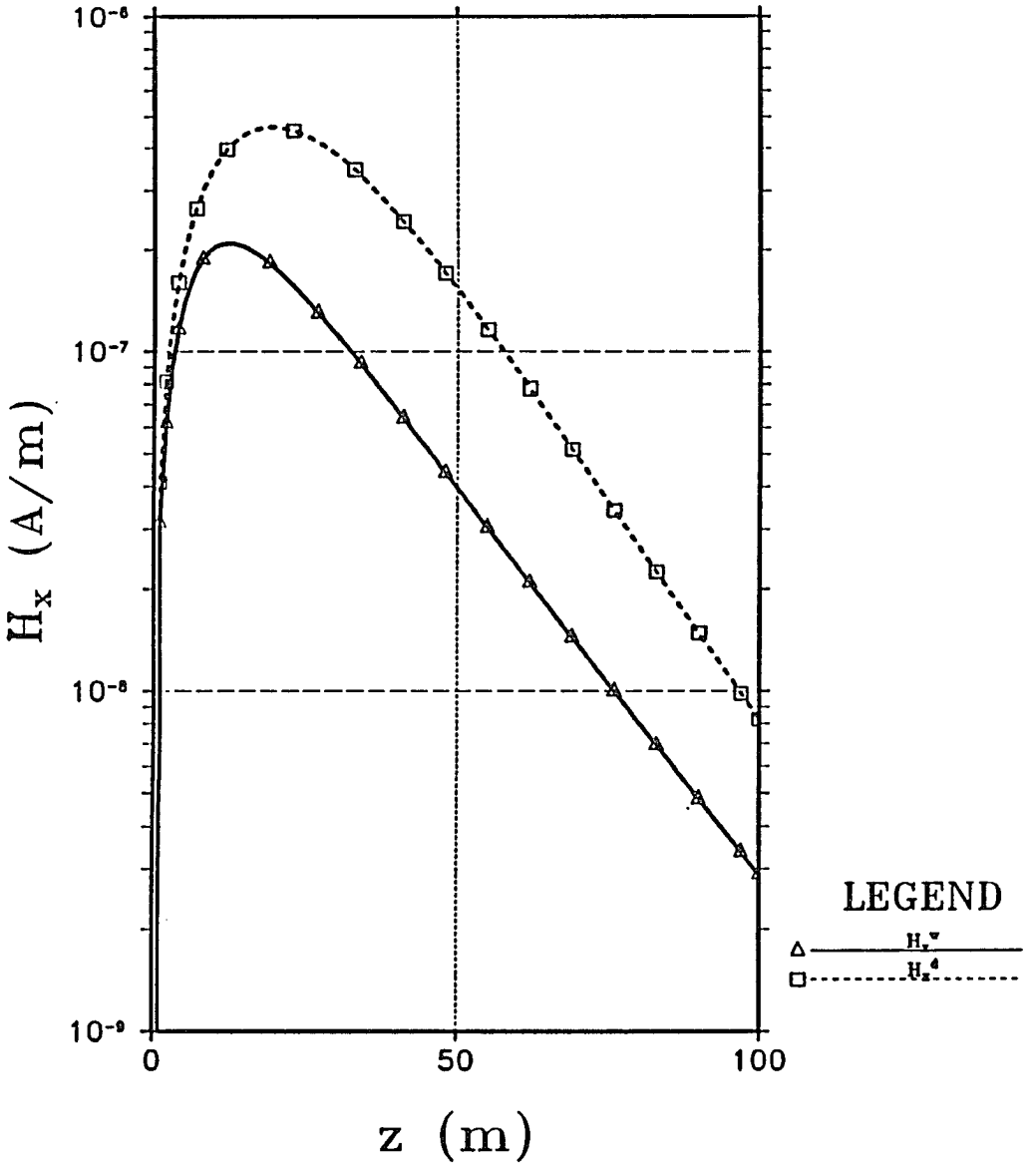

Figure 4-8 The x–component of the magnetic field as a function of z produced by the bare wires and the dipole. Here $x = 15$ m and $y = -15$ m.

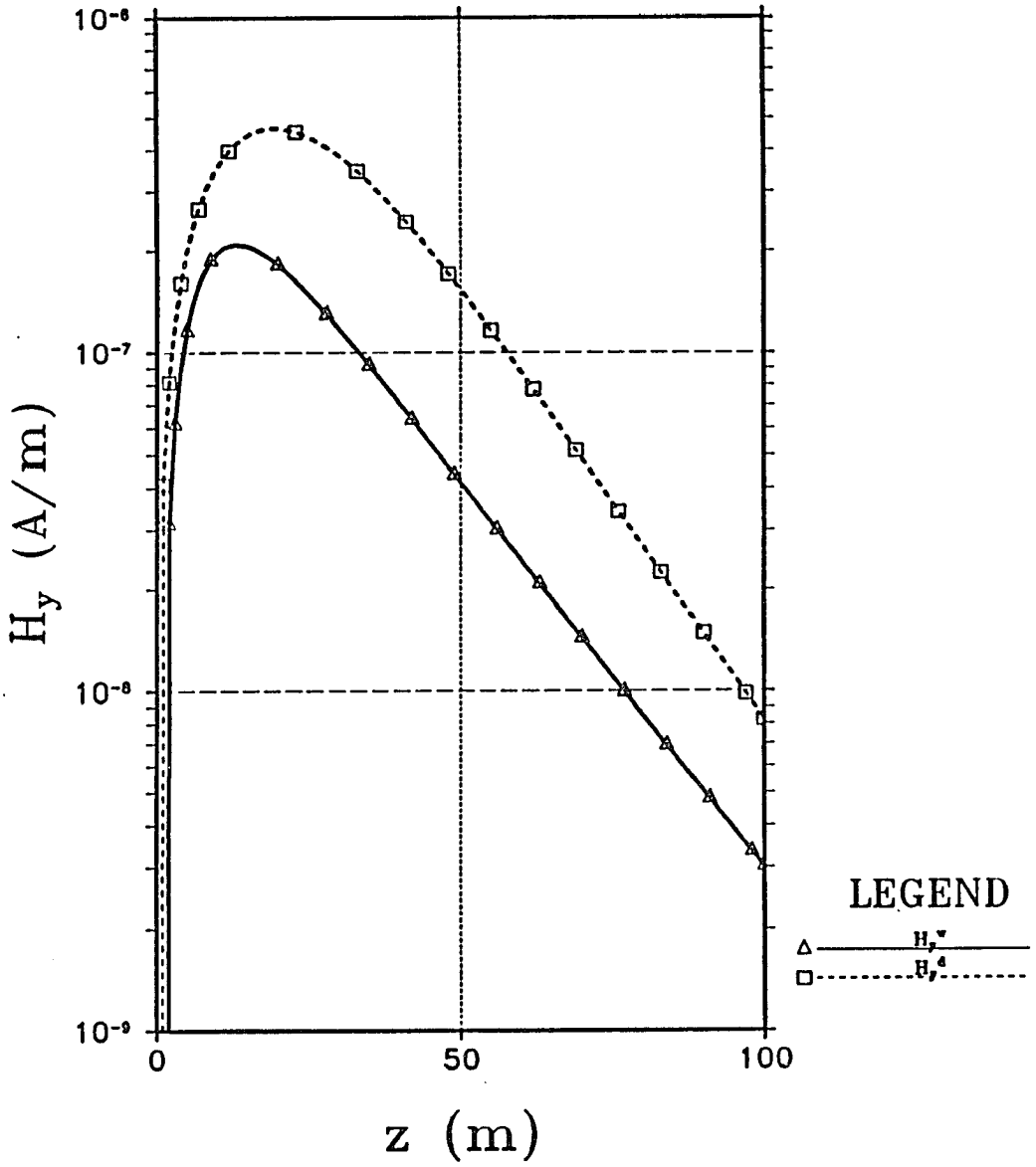

Figure 4-9 The y–component of the magnetic field, as a function of z, produced by the wires and the dipole. Here $x = 15$ m and $y = -15$ m.

x–component is solely a function of the current flowing on the y–directed wire; the y–component is a function of the current flowing on the x–directed wire; the z–component provides no unique information about either wire. The plots were calculated along the axis $x = 15$ and $y = -15$ for $z \in [0, 100]$; all distances are in meters. As seen from the plots, the magnetic strength of the dipole and the magnetic strength of the wires are large enough for detection. Thus, a two axis magnetic probe will detect the presence of two crossing conductors.

The foregoing computations for coated wires are repeated for our next set of figures. Here an inner wire radius of $b = 0.5$ cm and an outer wire radius of $a = 0.1$ cm are assumed. The insulating region is considered to be free–space so that the situation is analogous to two crossing tunnels with conductors in each. For this situation, we have found from (4.133) that $\Delta = .1/256$ and $N = 256$ would suffice.

Figures 4–10 and 4–11 show the total, the even and the odd spectral currents along with the spectral current induced by the crossing conductor. Note, the presence of the other conductor has little affect on the over–all current distribution. The induction effects from the other wire is on the order 10^3 less than the current induced by the dipole. The peaking behavior occurs in the vicinity of the real part of the surface wave pole as predicted by (4.137). Such little interaction between wires is to be expected for coated wires since the surface wave attached to the inner conductor is highly evanescent outside the insulation.

In the next two series of plots, Figures 4–12 and 4–13, the MOM, zero and first order solutions are presented. Not too surprisingly, all three solutions yield the same result. Again, this is primarily due to the negligible coupling that exists

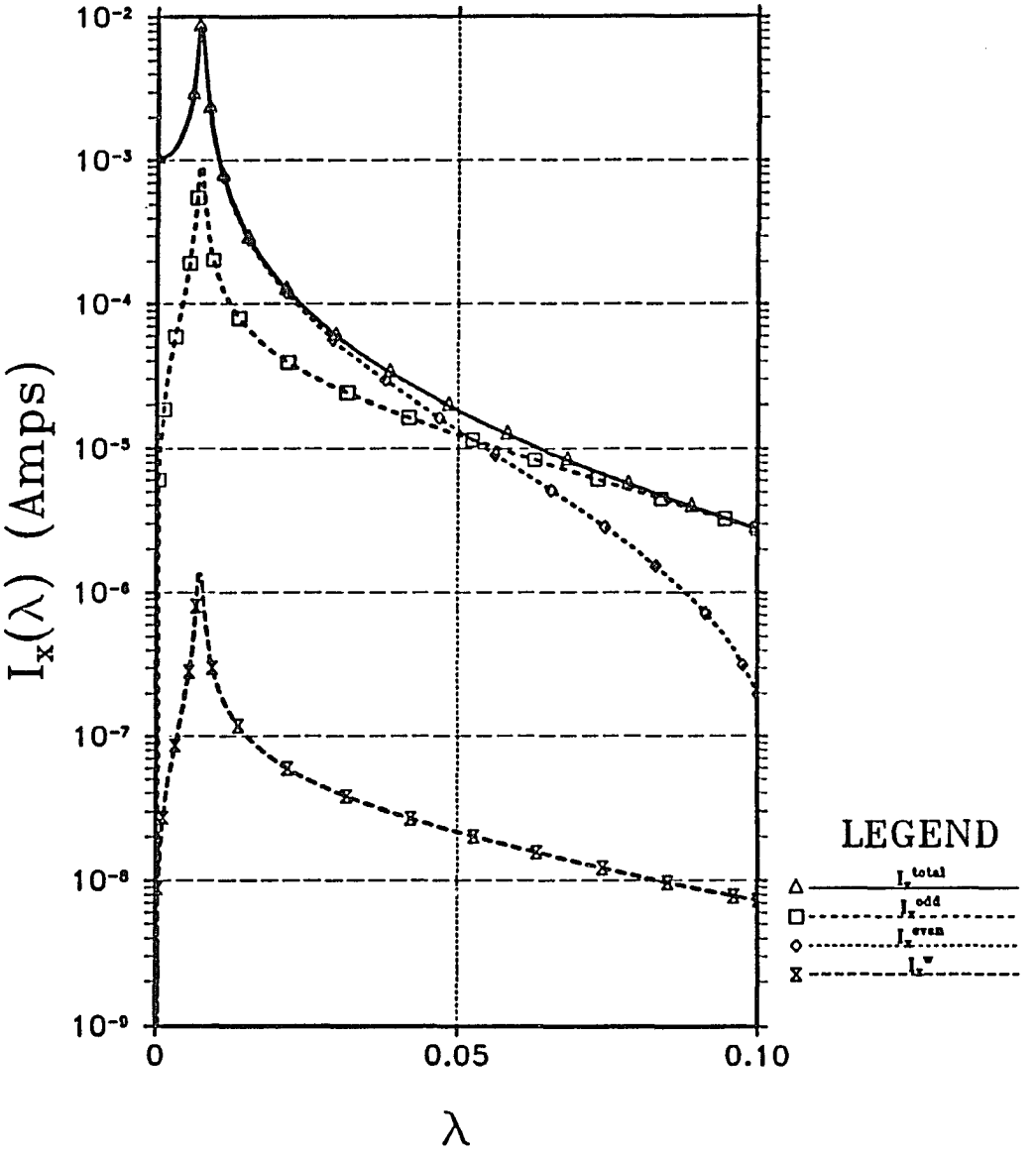

Figure 4-10 The spectral currents induced on the x–directed coated wire when excited by a magnetic dipole in a lossy homogeneous earth. The relevant parameters are: $f = 100$ kHz, $IdA = 1$ A-m^2, $\sigma_1 = 0.005$ S/m, $\epsilon_1 = 10\epsilon_0$, $\mu_1 = \mu_0$, $\epsilon_i = \epsilon_0$, $\mu_i = \mu_0$, $\sigma_i = 0$, $a = 1.0$ cm, $b = 0.5$ cm, $h = 0$, $d = 1$ m, $x_d = -15$ m, $y_d = 15$ m, and $z_d = 0$.

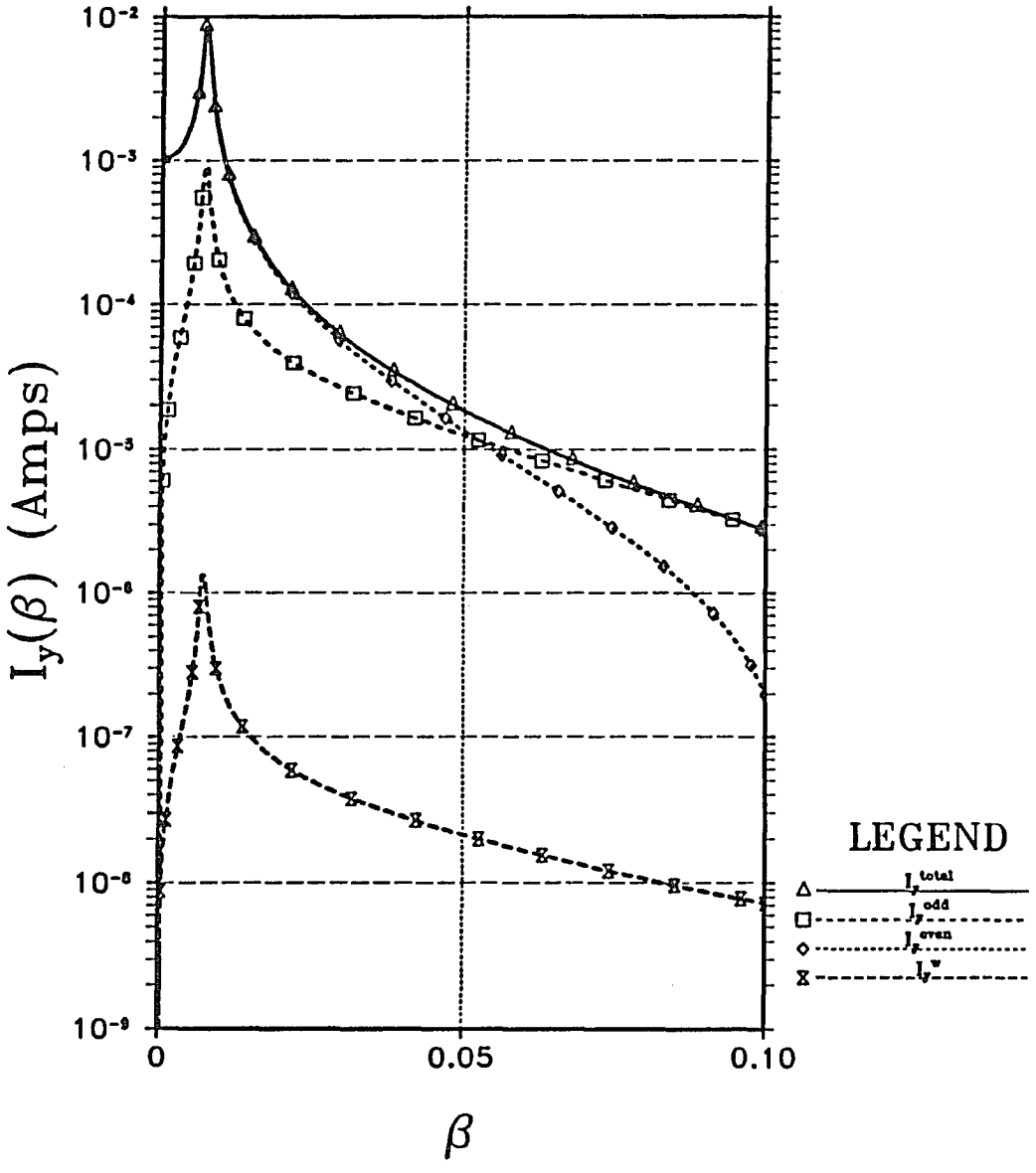

Figure 4-11 The spectral currents induced on the y–directed coated wire when excited by a magnetic dipole in a lossy homogeneous earth. The relevant parameters are: $f = 100$ kHz, $IdA = 1$ A-m^2, $\sigma_1 = 0.005$ S/m, $\epsilon_1 = 10\epsilon_0$, $\mu_1 = \mu_0$, $\epsilon_i = \epsilon_0$, $\mu_i = \mu_0$, $\sigma_i = 0$, $a = 1.0$ cm, $b = 0.5$ cm, $h = 0$, $d = 1$ m, $x_d = -15$ m, $y_d = 15$ m, and $z_d = 0$.

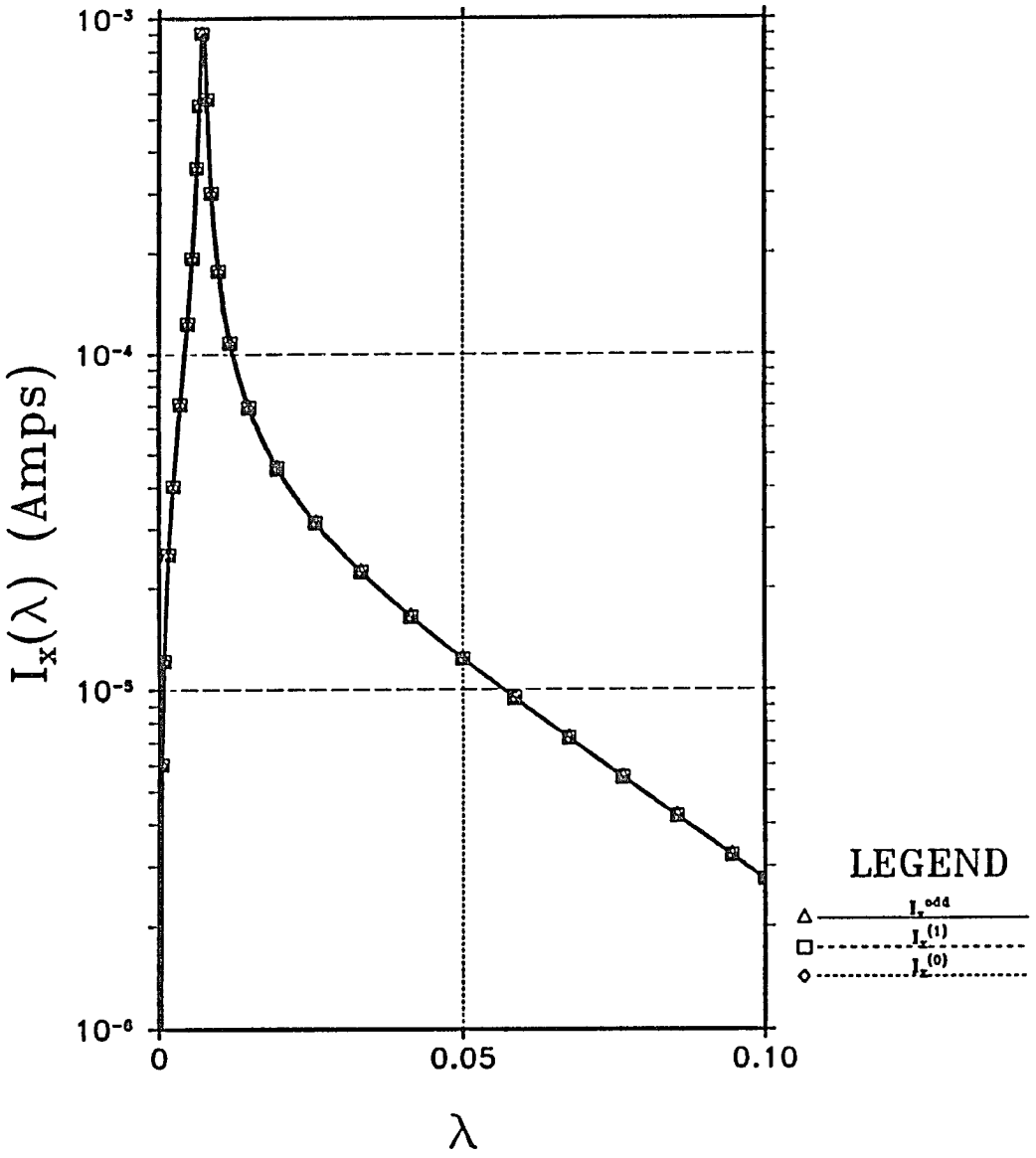

Figure 4-12 Comparison of the MOM solution to the zero and first order approximations for the coated wire excited by a VMD.

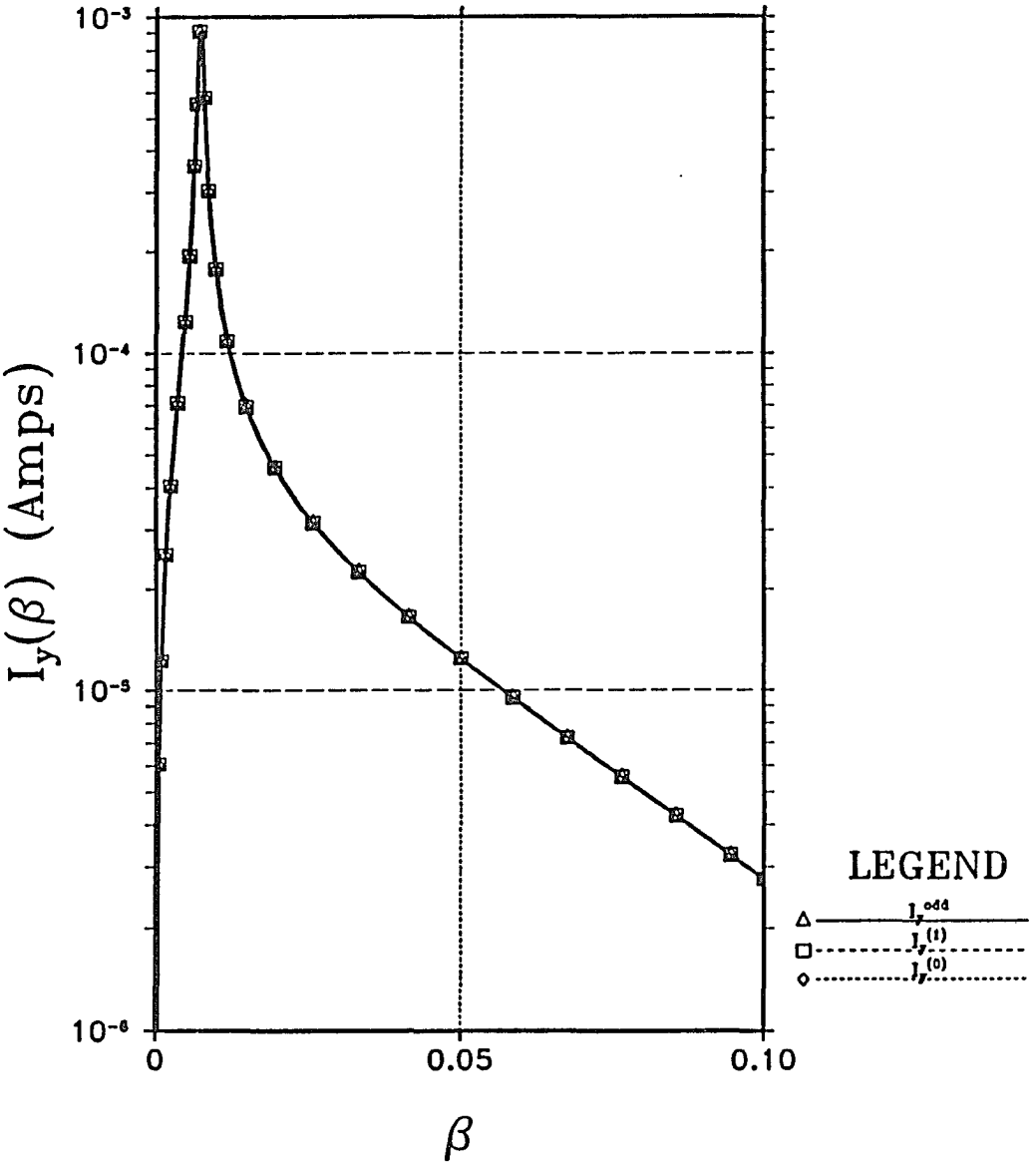

Figure 4-13 Comparison of the MOM solution to the zero and first order approximations for the coated wire excited by a VMD.

between coated conductors. Hence, to a very good approximation, the coupling integrals can be neglected and this problem can be solved by superpositioning the independent solutions of each wire.

Figure 4–14 shows the spatial behavior of the currents on each wire; a very slow decay exists for the spatial currents. Since no current can bleed off into the surrounding medium due to the presence of the insulator, the attenuation is a result of the wire re–radiating. Again, such phenonmena was observed by previous investigators [Hill, 1988].

To complete the buried wire investigation, the magnetic field results are shown for the coated wire, as seen in Figures 4–15 and 4–16. Computations are done along the same axis as before for the bare conductor. Nothing new is observed for this case and again, the detection of crossing buried conductors should be no problem.

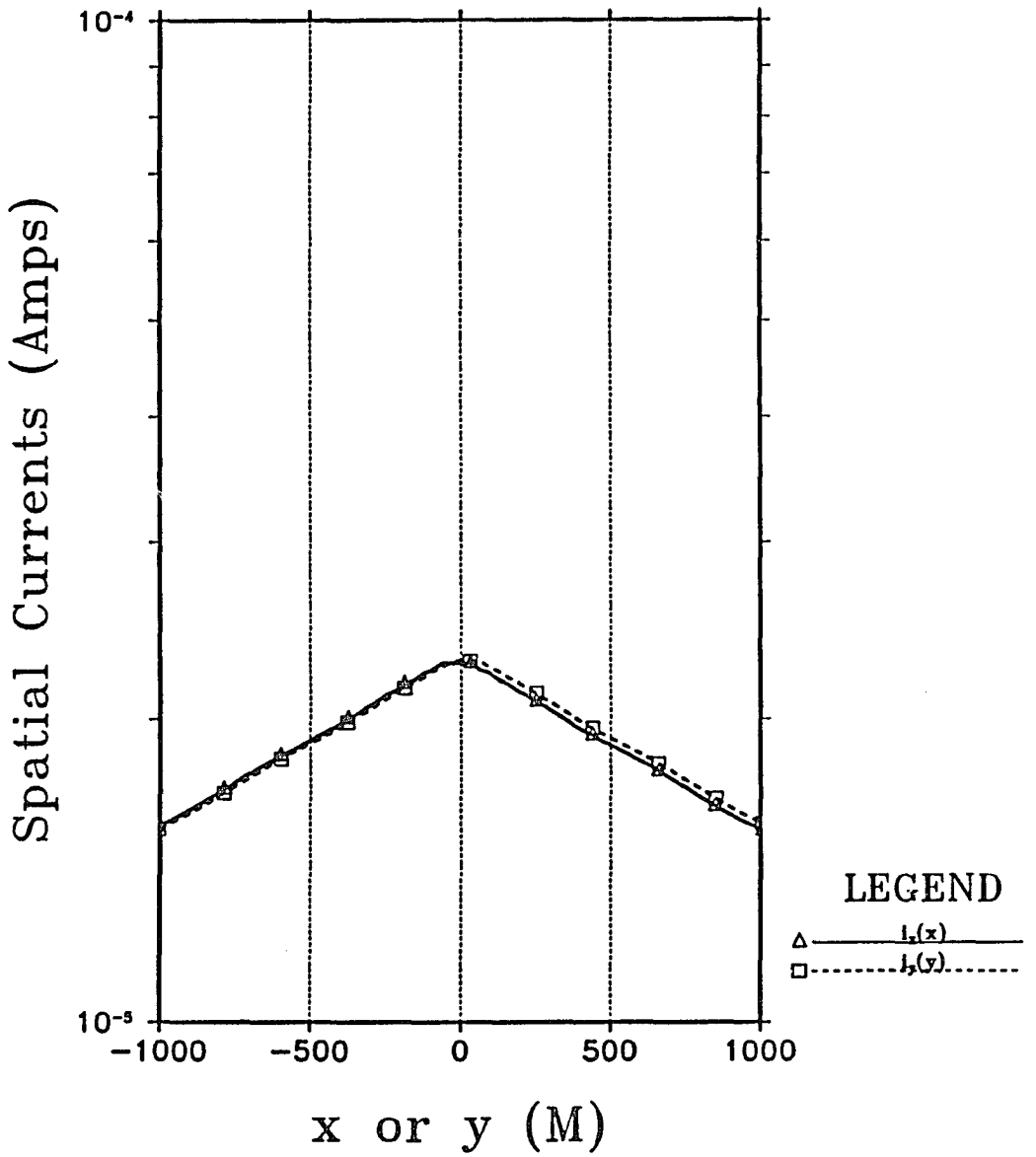

Figure 4-14 The spatial currents induced on the bare wires by a magnetic dipole in a lossy homogeneous earth.

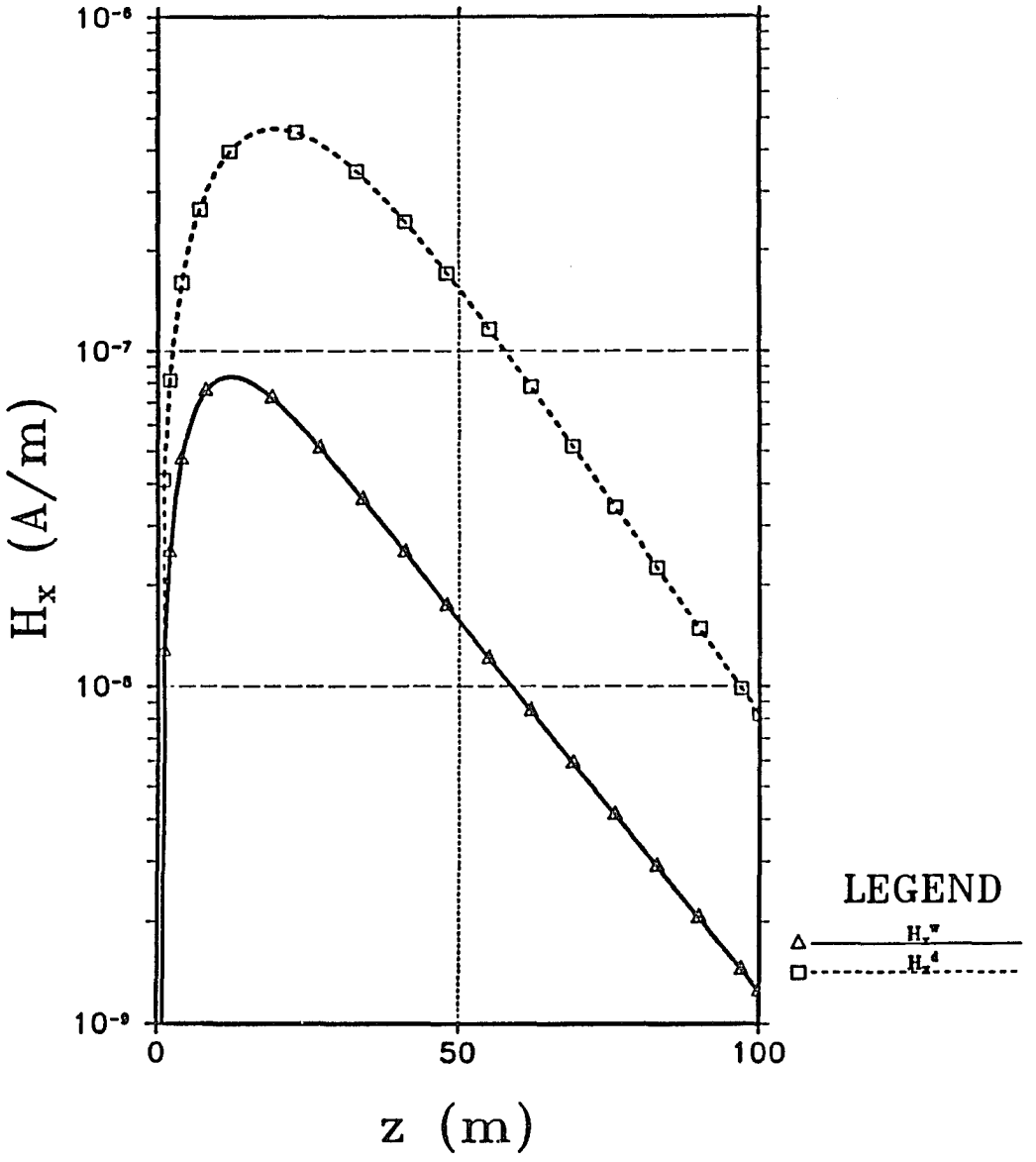

Figure 4-15 The x–component of the magnetic field as a function of z produced by the wires and the dipole. Here $x = 15$ m and $y = -15$ m.

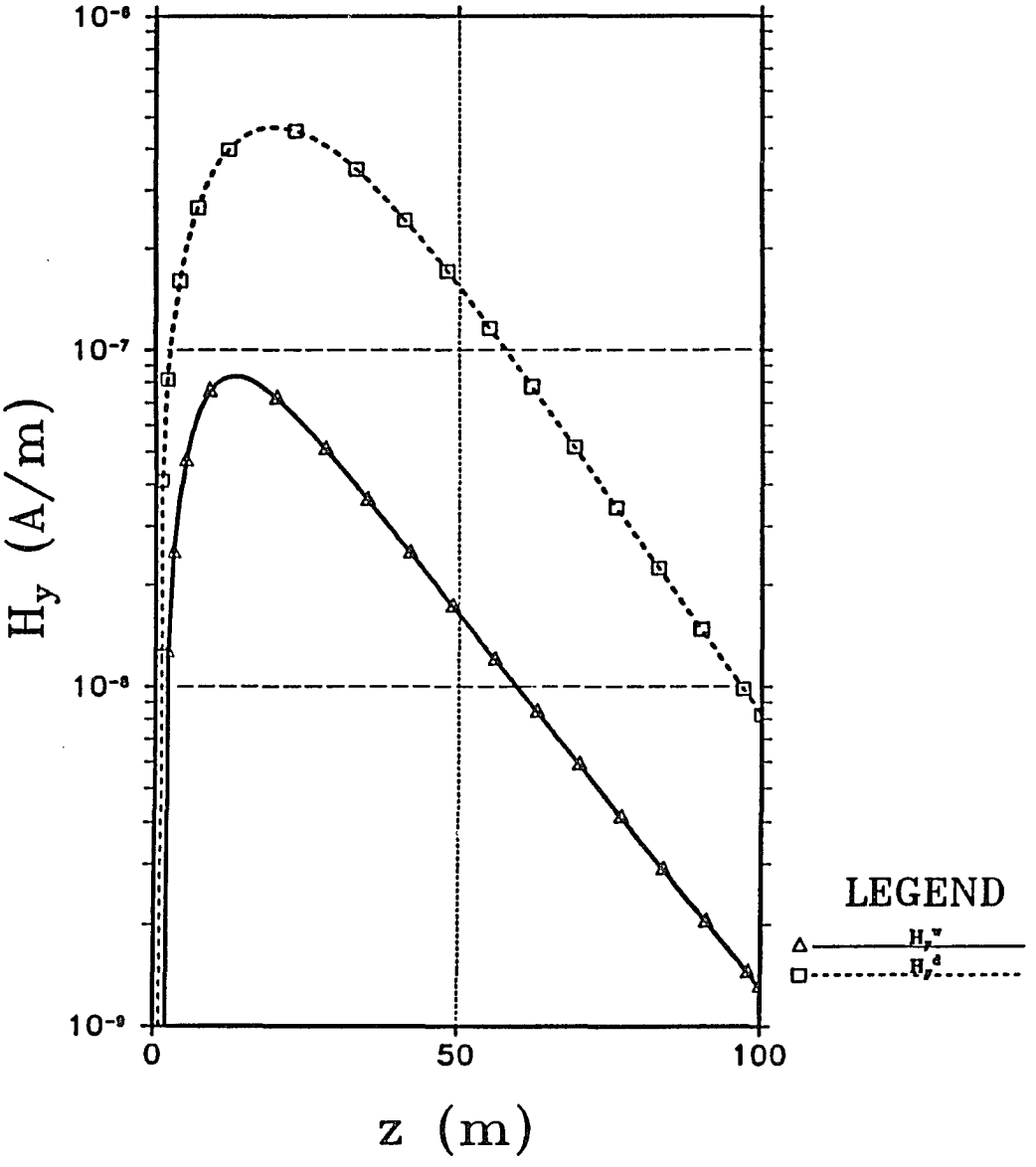

Figure 4-16 The y–component of the magnetic field as a function of z produced by the wires and the dipole. Here $x = 15$ m and $y = -15$ m.

CHAPTER 5

CONCLUSIONS AND RECOMMENDATIONS

In the previous chapters the electromagnetic response of thin, infinitely long wires was considered. Particularly, the geometrical configurations under investigation were the ensemble of parallel wires, the infinitely extended planar grid and the perpendicular crossing wires. In each instance the formal analytical development was given and the final solutions were obtained employing numerical techniques.

5.1 Shielding Studies

We have shown numerically that a wire ensemble over a lossy half space can be used to shield unwanted electromagnetic signals from entering a structure. Typical results range from -25 dB to -65 dB of shielding depending on such factors as angle of incidence, earth conductivity, over–all structure size, incident wave polarization and wire density. Obviously, shielding effectiveness will be heavily dependent on wire density. Doubling the number of wires will produce an additional 20 dB of shielding. Although not shown specifically (due to numerical precision limitations), we surmise that there should be an upper limit at which the increase in wire density will produce little effect on the shielding response.

With regard to the secondary factors, the results show that the earth plays the next most important role in achieving adequate shielding effectiveness. It seems that the actual values of the electrical parameters of the earth are not as important

as the existence of an air–earth interface with a dielectric contrast of at least eight (i.e. $|k_2/k_1|^2 = 8$). Polarization effects should also be considered in shielding design. For example, at grazing angles, the shielding effectiveness of the ensemble will degrade for an incident plane wave whose electric field vector is oblique to the wires. Most of the shielding results were obtained for objects of non–resonant dimensions. However, for structures of resonant, or near resonant dimensions, the shielding effectiveness can significantly diminish.

One result of interest was the comparison of the wire cage response to that of the perfectly conducting continuous shell of similar dimensions. For a particular choice of wire spacing, the shielding effectiveness was shown to be essentially the same. Such an observation is attractive to those who must construct a shield for an existing electromagnetic facility, since the wire cage is lighter, more flexible and more manageable than a metallic sheet. Also, the electromagnetic response of the finitely extended planar grid was compared with the infinitely extended planar grid. In the shadow region, the results were shown to be equivalent. Using an infinitely extended planar grid model to approximate a finitely extended planar grid allowed us to obtain quick results without the need to load large matrices.

Further work should primarily concentrate on two areas: source excitation and cross, non–planar meshes. We have considered only the shielding response of sources of infinite extent (i.e. plane waves). However, for practical situations, an electrical dipole may be more realistic. Even though the complete boundary value problem has been addressed in the literature [Wait, 1977b], no numerical results have been generated. The numerical algorithms would be significantly more difficult, since two–dimensional Fourier integrals must be numerically computed.

If semi–circular crossing wires were included with the cage shown in Figure 3–17, the structure would be virtually independent of polarization. The analytical solution would be an extension of the one presented in Chapter Three. In general the analysis would involve a Floquet expansion for each of the semi–circular wires, provided that the source was spatially periodic; otherwise, the procedure is the same as before, namely solving a system of N equations, where N is still the number of the straight parallel wires.

5.2 Crossed Wire Geometry

With respect to the crossed wire geometry, two methods were presented to solve for the spectral currents flowing on each wire. The first, a moment method technique, gave a numerical solution in terms of a linear combination of pulse functions. The second, based on the method of multiple scatterers, showed that the resulting matrix series is constructed of terms $1/d^{2n}$, where d is the interwire spacing and n represents the n^{th} wave bounce. Through various matrix manipulations, we showed that the moment method solution can be expressed in terms of zero and first order multiple scatterer solutions plus all higher order corrections.

In general, the coupling between wires is insignificant compared with the source–to–wire coupling, even for *small* wire spacing. Although the exact numerical solution can be obtained by moment method techniques, the first order multiple scatterer solution is an excellent approximation for bare wires. Furthermore, for coated wires, the zero order approximation is adequate for obtaining accurate results. Such approximations are advantageous in obtaining fast solutions (i.e. a

factor of N, where N is the number of pulse functions) compared with the MOM solution.

The cross–wire investigation given herein opens up numerous possibilities for further work. For instance, in our analysis we introduced the half–space at the outset, yet did not consider its effects numerically. In general, both the moment method and the multiple scatterer method may be implemented here by the techniques presented in Chapter Four. The coupling factor, Ω, for this case will no longer be an expression of exponentials but an integral relationship.

Touching or bonded wires is another possibility for future work. Although many of the same initial equations may result, a current junction condition must be introduced to account for the discontinuities in the current at such points. Also, the case of non–perpendicular wires is of practical interest, as might occur with power and communication lines which cross one another at an arbitrary angle. The resulting integral equations would couple both the even and odd current terms. Analogous studies of crossed periodic wire meshes suggest useful approaches [Wait, 1978a].

Finally, the analysis may be extended to the general case where there are M wires parallel to some interface but not necessarily parallel to each other. Such a configuration will produce M coupled integral equations, which in principle can be numerically solved using the methods presented herein.

APPENDIX A

FOURIER INTEGRALS

The following function of x and z is the focus of our numerical work:

$$I(x,z) = \int_0^\infty R_y(\lambda, k_y) \frac{e^{-u_a z}}{u_a} \cos \lambda x d\lambda \qquad (A.1)$$

where

$$R_y = \frac{\lambda^2 k_y^2 (1-K_a)^2 + \omega^2(\epsilon_1 u_a - \epsilon_2 u_b K_a)(\mu_1 u_a + \mu_2 u_b K_a)}{-\lambda^2 k_y^2 (1-K_a)^2 + \omega^2(\epsilon_1 u_a + \epsilon_2 u_b K_a)(\mu_1 u_a + \mu_2 u_b K_a)} \qquad (A.2)$$

with $k_y = k_1 \sin\theta_0 \sin\phi_0$, $u_a = \sqrt{\lambda^2 + v_a^2}$, $u_b = \sqrt{\lambda^2 + v_b^2}$, $K_a = v_a^2/v_b^2$, $v_a = \sqrt{k_y^2 - k_1^2}$, and $v_b = \sqrt{k_y^2 - k_2^2}$. All double-valued functions are chosen such that their real part is greater than zero.

Before considering (A.1), we find that it is desireable to decompose the integrand into two factors. For the special case where $\mu_1 = \mu_2$, the expression for R_y is decomposed into the form [Wait, 1972a]:

$$R_y = -1 - \frac{2k_1^2}{v_a^2}\left[\frac{1}{u_a + u_b} - \frac{k_y^2}{k_1^2 u_b + k_2^2 u_a}\right] u_a \qquad (A.3)$$

The insertion of (A.3) into (A.1) and the use of the integral representation for the MacDoanld function [Gradshteyn and Ryzhik, 1980, # 3.961.2], yields

$$I(x,z) = -K_0(v_a \rho_{xz}) - \frac{2k_1^2}{v_a^2}[P - k_y^2 Q] \qquad (A.4)$$

where $\rho_{xz} = \sqrt{x^2 + z^2}$ and the functions P and Q are defined by the relationships

$$P = \int_0^\infty \frac{e^{-u_a z}}{u_a + u_b} \cos(\lambda x) d\lambda \qquad (A.5)$$

and

$$Q = \int_0^\infty \frac{e^{-u_a z}}{k_2^2 u_a + k_1^2 u_b} \cos(\lambda x) d\lambda \qquad (A.6)$$

The real axis integration path of (A.5) and (A.6) must bypass the branch point singularities, $\lambda = \pm k_1$, when region one is lossless. For later analysis, we will need a new doubled–value function: $\kappa_a = \sqrt{k_1^2 - k_y^2}$ so that $u_a = \sqrt{\lambda^2 - \kappa_a^2}$

A.1 Numerical Implementation

The development of numerical methods associated with Fourier integrals that arise in electromagnetic diffraction type problems is an on going process. In general, there are two genre of methods that can be employed. The first involves real axis integration techniques along with various asymptotic extraction methods. The second involves various mapping functions that eventually transform a real axis integration into an integration along a steepest descent path (SDP). For large values of $v_a \rho_{xz}$, this method is superior due to its rapidly decaying exponential integrand. On the other hand, for observation distances *close* to the wire, real axis integration may lead to more accurate results [Baertlein, 1988]. Also, care must be exercised when applying SDP integration to Q. For various parametric values, Q has a pole singularity that may lie *near* the SDP, which requires more delicate evaluation during the contour deformation [Tamir and Oliner, 1963]. For

these reasons, the two methods that will be employed herein are based on real axis evaluations.

Before going into the numerical details and equations, we will discuss the convergence properties of P and Q. For large values of the integration variable λ, the integrands converge like $\cos(\lambda x)e^{-\lambda z}/\lambda$. Obviously, for small values of z and large values of x, the integrand is slowly convergent and highly oscillatory; therefore, some asymptotic extraction technique must be employed if any useful, accurate and expedient results are to be obtained. For the case where x is small and z is large, the integral is highly convergent, which poses no numerical problems.

Both techniques developed in subsequent sections are based on the method described by Johnson and Dudley [1983]. They observed that in a region close to the branch point, $\lambda = \kappa_a$, the oscillations in the integrand become tightly packed. The integrand peaks near the branch point which adds further complexity to the situation. By dividing the open interval into three sections, with various transformations applied to the first two intervals, we can space these oscillations more evenly so that numerical quadrature can be applied. The differences between the two methods used in this appendix lies in the technique of extracting the asymptotic behavior. For lack of a better notation, the names of the these two methods will be identified as Method A and Method B.

A.1.1 Method A

In general, the mathematics applied to one integral, say P, can be easily translated to Q and hence, only the developement for P will be given. Consider the following integrals:

$$P_1 = \int_0^{\kappa_a} \frac{e^{-u_a z}}{u_a + u_b} \cos \lambda x d\lambda \tag{A.7}$$

$$P_2 = \int_{\kappa_a}^{2\kappa_a} \frac{e^{-u_a z}}{u_a + u_b} \cos \lambda x d\lambda \tag{A.8}$$

$$P_3 = \int_{2\kappa_a}^{\infty} \frac{e^{-u_a z}}{u_a + u_b} \cos \lambda x d\lambda \tag{A.9}$$

where $P = P_1 + P_2 + P_3$.

For P_1, the transformation $\lambda = \kappa_a \sin\theta$ is applied. From this, the interval $[0, \kappa_a]$ is mapped into the interval $[0, \pi/2]$. Also, $d\lambda = \kappa_a \cos\theta d\theta$ and $u_a = i\kappa_a \cos\theta$. If $\varsigma = v_b^2/v_a^2$, then

$$P_1 = -i \int_0^{\pi/2} \frac{e^{-i\kappa_a z \cos\theta}}{\cos\theta + \sqrt{\varsigma^2 - \sin^2\theta}} \cos(\kappa_a x \sin\theta) \cos\theta d\theta \tag{A.10}$$

Quadrature is applied between successive nulls and peaks of the integrand which result from both the cosinusodial and exponential terms. The integration tracking points are defined by

$$\theta_n = \sin^{-1}\left[\frac{n\pi}{2\kappa_a x}\right] \tag{A.11}$$

and

$$\theta_m = \cos^{-1}\left[\frac{m\pi}{2\kappa_a z}\right] \tag{A.12}$$

where $n = 1,2,\ldots,n_{max}$ and $m = 1,2,\ldots,m_{max}$ with $n_{max} = INT[2\kappa_a x/\pi]$ and $m_{max} = INT[2\kappa_a z/\pi]$. Here the notation of the Fortran integer function is used to indicate that an integer value is obtain from a real value by truncating all remaining figures after the decimal point. The corresponding expresion for Q is

$$Q_1 = -i\int_0^{\pi/2} \frac{e^{-i\kappa_a z\cos\theta}}{k_2^2\cos\theta + k_1^2\sqrt{\varsigma^2 - \sin^2\theta}} \cos(\kappa_a x\sin\theta)\cos\theta d\theta \qquad (A.13)$$

For the integral P_2, the transformation $\lambda = \kappa_a \sec\theta$ is applied. This maps the interval $[\kappa_a, 2\kappa_a]$ into the interval $[0,\pi/3]$. Hence, $u_a = \kappa_a\tan\theta$, $d\lambda = \kappa_a\sec\theta\tan\theta d\theta$ and

$$P_2 = \int_0^{\pi/3} \frac{e^{-\kappa_a z\tan\theta}}{\tan\theta + \sqrt{\sec^2\theta - \varsigma^2}} \cos(\kappa_a x\sec\theta)\sec\theta\tan\theta d\theta \qquad (A.14)$$

The quadrature tracking points are specified by the peaks and nulls of the cosine term. That is,

$$\theta_n = \cos^{-1}\left[\frac{2\kappa_a x}{n\pi}\right] \qquad (A.15)$$

where $n = n_{min},\ldots,n_{max}$ with $n_{min} = INT[2\kappa_a x/\pi+1]$ and $n_{max} = INT[4\kappa_a x/\pi]$. The exponential term does not oscillate in this interval, but can rapidly decay for large $\kappa_a z$; this decay will also be tracked. It has been recommended [Johnson and Dudley, 1983] that the interval $\lambda = [\kappa_a, 2\kappa_a]$ be subdivided as follows:

$$\lambda \in \left[\kappa_a, \kappa_a + \Delta, \kappa_a + 2\Delta, \ldots, \kappa_a + m\Delta, \ldots, 2\kappa_a\right]$$

where $\Delta = \min[.4\pi/\kappa_a z, \kappa_a]$. In θ–space this corresponds to

$$\theta \in \left[0, \cos^{-1}\left(\frac{\kappa_a}{\kappa_a+\Delta}\right), \ldots, \cos^{-1}\left(\frac{\kappa_a}{\kappa_a+m\Delta}\right), \ldots, \frac{\pi}{3}\right] \qquad (A.16)$$

for $m = 1, 2, \ldots, m_{max}$ with $m_{max} = INT[\kappa_a/\Delta]$. These tracking points given in (A.15) and (A.16) are sorted and quadrature is applied between successive points. For Q it is found that

$$Q_2 = \int_0^{\pi/3} \frac{e^{-\kappa_a z \tan\theta}}{k_2^2 \tan\theta + k_1^2 \sqrt{\sec^2\theta - \varsigma^2}} \cos(\kappa_a x \sec\theta) \sec\theta \tan\theta d\theta \qquad (A.17)$$

For the last interval we consider an asymptotic extraction and apply the change of variable $\lambda = \kappa_a t$:

$$P_3 = \int_2^{\infty} \frac{e^{-\kappa_a z \sqrt{t^2-1}}}{\sqrt{t^2-\varsigma^2} + \sqrt{t^2-1}} \cos(\kappa_a x t) dt \qquad (A.18)$$

As discussed earlier, for large $\kappa_a x$ and small $\kappa_a z$ the above integral is poorly convergent. For $t >> |\varsigma|$ and $t >> 1$, the following approximations can be made:

$$\begin{aligned} \sqrt{t^2-1} &\sim t\left[1 - \frac{1}{2t^2}\right] \\ \sqrt{t^2-\varsigma^2} &\sim t\left[1 - \frac{\varsigma^2}{2t^2}\right] \\ e^{-\kappa_a z\sqrt{t^2-1}} &\sim e^{-\kappa_a z t}\left(1 + \frac{\kappa_a z}{2t}\right) \end{aligned} \qquad (A.19)$$

Using the approximation that $1/(z-1) \approx 1+z$ for $|z| << 1$, retaining terms of no greater order than $1/t^2$, and applying (A.19) we obtain the following approximation for large t:

$$\frac{e^{-\kappa_a z\sqrt{t^2-1}}}{\sqrt{t^2-\varsigma^2} + \sqrt{t^2-1}} \approx \frac{e^{-\kappa_a z t}}{2}\left(\frac{\alpha_1}{t} + \frac{\alpha_2}{t^2}\right) \qquad (A.20)$$

where $\alpha_1 = 1$ and $\alpha_2 = \kappa_a z/2$. The addition and subtraction of this approximation in the integrand of (A.18) gives

$$P_3 = \int_2^\infty \left[\frac{e^{-\kappa_a z\sqrt{t^2-1}}}{\sqrt{t^2-1}+\sqrt{t^2-\varsigma^2}} - \frac{e^{-\kappa_a zt}}{2}\left(\frac{\alpha_1}{t}+\frac{\alpha_2}{t^2}\right)\right]\cos(\kappa_a xt)dt \qquad (A.21)$$
$$+ASYM_1$$

where

$$ASYM_1 = \sum_{n=1}^{2}\frac{\alpha_n}{2}\int_2^\infty \frac{e^{-\kappa_a zt}}{t^n}cos(\kappa_a xt)dt \qquad (A.22)$$

The exponential function of argument z, $E_n(z)$, is defined by the relationship [Abramowitz and Stegun, 1970 §5.1],

$$E_n(z) = \int_1^\infty \frac{e^{-zt}}{t^n}dt \qquad (A.23)$$

Thus, the asymptotic extraction term is

$$ASYM_1 = \sum_{n=1}^{2}\frac{\alpha_n}{2^n}Re\{E_n[2\kappa_a(z-ix)]\} \qquad (A.24)$$

where the property $E_n(z^*) = E_n^*(z)$ [Abramowitz and Stegun 1970 §5.1] was applied in (A.24). Higher order terms can be included but these terms can reduce the accuracy of the result for large ς [Baertlein, 1988].

As before, (A.21) is integrated by summing successive quadrature contributions between nulls and peaks. The truncation of the infinite interval is accomplished by dividing each quadrature contribution by the total quadrature sum. When this ratio is less than 10^{-6}, the integral is defined as numerically convergent.

Similar results can be obtain for Q, which are

$$Q_3 = \int_2^\infty \left[\frac{e^{-\kappa_a z\sqrt{t^2-1}}}{k_2^2\sqrt{t^2-1}+k_1^2\sqrt{t^2-\varsigma^2}} - \frac{e^{-\kappa_a zt}}{2}\left(\frac{\alpha_1'}{t}+\frac{\alpha_2'}{t^2}\right)\right]\cos(\kappa_a xt)dt + ASYM_2 \tag{A.25}$$

where $\alpha_1' = 2/(k_1^2+k_2^2)$ and $\alpha_2' = \kappa_a z/(k_1^2+k_2^2)$. Also,

$$ASYM_2 = \sum_{n=1}^{2} \frac{\alpha_n'}{2^n} Re\{E_n[2\kappa_a(z-ix)]\} \tag{A.26}$$

By improving the convergence rate of the Fourier integrals, we have introduced a new function, $E_n(z)$, given by (A.23). From Todd [1954], if $z = x + iy$ (x, y, z are not to be confused with the spatial Cartesian coordinates) then,

$$e^z E_1(z) = R_1 - iR_2 \tag{A.27}$$

where

$$R_1 = \int_0^\infty \frac{(x+p)e^{-p}}{(x+p)^2+y^2}dp \tag{A.28}$$

and

$$R_2 = \int_0^\infty \frac{ye^{-p}}{(x+p)^2+y^2}dp \tag{A.29}$$

These two new integrals can be computed using Laguerre quadrature. That is, from numerical analysis [Abramowitz and Stegun, 1970 §25.4],

$$\int_0^\infty e^{-t}f(t)dt \approx \sum_{i=1}^{k} a_i^{(k)} f(t_i^{(k)}) \tag{A.30}$$

where $t_i^{(k)}$ are the zeros of the Laguerre polynomial, $L_k(t)$, and $a_i^{(k)}$ are the corresponding Christoffel numbers. This approximation is highly accurate for *large* $|z|$ with a maximum error of [Todd, 1954]

$$\begin{aligned} &\frac{(k!)^2}{(|z|^2)^{(k+1/2)}} \qquad for\ x > 0 \\ &\frac{(k!)^2}{(|y|^2)^{(2k+1)}} \qquad for\ x < 0 \end{aligned} \tag{A.31}$$

For smaller values of $|z|$, the series expansion is sufficient [Abramowitz, 1970, §5.1]:

$$E_1(z) = -\gamma - \ln z - \sum_{k=1}^{\infty} \frac{(-1)^k z^k}{k k!} \tag{A.32}$$

where $\gamma = .5772156649\ldots$ is Euler's constant. Higher orders of of E_n may be computed through the recursion relationship [Abramowitz, 1970, §5.1]:

$$E_{n+1}(z) = \frac{1}{n}\left[e^{-z} - zE_n(z)\right] \tag{A.33}$$

where $n = 1, 2, \ldots$.

After examining the error terms of (A.32), and recalling that the maximum value of n is two, we find that if $|z| > 2$ then Todd's [1954] method is superior to the series expansion. For $|z| \leq 2$, the series expansion will suffice.

A.1.2 Method B

The difficulty of the extraction technique in Method A is that ς^2 can be become quite large with respect to the integration variable when $k_y \to k_1$. For this case, the approximation used for u_b becomes invalid for much of the integration range; this will thus induce numerical errors. Second, ς is a function of σ_2 so that for the highly conducting earth, the same difficulties arise. Third, the algebraic steps are involved which could lead to analytical and numerical implementation errors.

To circumvent these difficulty, the results from quasi–static analysis [Wait, 1961] are utilized. Consider the following *whole domain* asymptotic extraction for P:

$$P = \int_0^\infty \left[\frac{e^{-u_a z}}{u_a + u_b} - \frac{e^{-\lambda z}}{\lambda + u_b}\right] \cos \lambda x d\lambda + P_{asym} \qquad (A.34)$$

where

$$P_{asym} = \int_0^\infty \frac{e^{-\lambda z}}{\lambda + u_b} \cos \lambda x d\lambda \qquad (A.35)$$

For $\lambda >> \kappa_a$ but not necessarily $\lambda > |k_2|$, the asymptotic approximation for the integrand of (A.34) is

$$\frac{e^{-u_a z}}{u_a + u_b} - \frac{e^{-\lambda z}}{\lambda + u_b} \sim \frac{\kappa_a^2 e^{-\lambda z}}{2\lambda}\left(\frac{1}{2\lambda^2 + 2\lambda u_b - k_2^2}\right) \qquad (A.36)$$

and for $\lambda >> |k_2|$,

$$\frac{e^{-u_a z}}{u_a + u_b} - \frac{e^{-\lambda z}}{\lambda + u_b} \sim \frac{\kappa_a^2 e^{-\lambda z}}{8\lambda^3} \qquad (A.37)$$

Thus in the interval $[\kappa_a, |k_2|]$, the integrand converges like $1/\lambda$ and in the region $[|k_2|, \infty)$ the convergence is like $1/\lambda^3$, when z is small. Unlike the original integral for P, there is no convergence in the first interval and in the second, the rate is of the order $1/\lambda$. Hence for moderate values of v_b, this method will lead to a rapidly converging integral for *all* values of x and z. Unfortunately, at this time, no similar whole domain technique is found for Q. (Note, in Method A, the convergence rate is also of the order $1/\lambda^3$.)

The integral of (A.35) can be computed in terms of Struve functions, $\mathbf{H}_1$, and Bessel functions of the second kind, Y_1 [Wait, 1961]:

$$P_{asym} = \frac{x^2 - z^2}{v_b^2[z^2 + x^2]^2} + \frac{\pi}{4v_b\tau}\left[\mathbf{H}_1(v_b\tau) - Y_1(v_b\tau)\right] + \frac{\pi}{4v_b\tau^*}\left[\mathbf{H}_1(v_b\tau^*) - Y_1(v_b\tau^*)\right] \tag{A.38}$$

where $\tau = z + ix$ and τ^* is the complex conjugate of τ.

Quadrature is applied to (A.34) in the same way as done for Method A. The resulting expressions for each region can be seen by inspection so that no further discussion will be given.

The numerical computation of the Bessel function, Y_1, has been developed in many of the available numerical software packages [Amos, 1985]. The Struve function can be computed through the series expansion [Abramowitz and Stegun, 1970, §12.1],

$$\mathbf{H}_1(z) = \frac{2}{\pi}\left[\frac{z^2}{1^2 \cdot 3} - \frac{z^4}{1^2 \cdot 3^2 \cdot 5} + \frac{z^6}{1^2 \cdot 3^2 \cdot 5^2 \cdot 7} - \ldots\right] \tag{A.39}$$

Since, our shielding numerical computations involve distances of less than a few wavelengths, the above series is quite efficient for our applications.

APPENDIX B

BOUNDED INTEGRAL OPERATOR PROOF

This section will prove that the integral operators of (4.76) and (4.77) are bounded. Reconsider these two coupled integral equations:

$$I_x^{odd}(\lambda) - \frac{2}{Z_a(\lambda) - Z_{xx}(\lambda)} \int_0^\infty I_y^{odd}(\beta) Z_{xy}(\lambda, \beta) d\beta = \frac{E_x^{odd}(\lambda)}{Z_a(\lambda) - Z_{xx}(\lambda)} \tag{B.1}$$

$$I_y^{odd}(\beta) - \frac{2}{Z_b(\beta) - Z_{yy}(\beta)} \int_0^\infty I_x^{odd}(\lambda) Z_{yx}(\lambda, \beta) d\lambda = \frac{E_y^{odd}(\beta)}{Z_b(\beta) - Z_{yy}(\beta)} \tag{B.2}$$

Now let

$$\begin{aligned} I_x^{odd}(\lambda) &= \frac{G_x(\lambda)}{Z_a(\lambda) - Z_{xx}(\lambda)} \\ I_y^{odd}(\beta) &= \frac{G_y(\beta)}{Z_b(\beta) - Z_{yy}(\beta)} \end{aligned} \tag{B.3}$$

so that (B.1) and (B.2) become,

$$G_x(\lambda) + \int_0^\infty G_y(\beta) K_{xy}(\lambda, \beta) d\lambda = E_x^{odd}(\lambda) \tag{B.4}$$

and

$$G_y(\beta) + \int_0^\infty G_x(\lambda) K_{yx}(\lambda, \beta) d\beta = E_y^{odd}(\beta) \tag{B.5}$$

where

$$\begin{aligned} K_{xy}(\lambda, \beta) &= -2 \frac{Z_{xy}(\lambda, \beta)}{Z_a(\lambda) - Z_{xx}(\lambda)} \\ K_{yx}(\lambda, \beta) &= -2 \frac{Z_{xy}(\lambda, \beta)}{Z_b(\beta) - Z_{yy}(\beta)} \end{aligned} \tag{B.6}$$

Now the integral operators are bounded, provided that [Tricomi, 1985],

$$I_1 = \int_0^\infty \int_0^\infty |K_{xy}|^2 d\lambda d\beta < \infty$$
$$I_2 = \int_0^\infty \int_0^\infty |K_{yx}|^2 d\beta d\lambda < \infty \qquad (B.7)$$

Consider the case where the wires are in an homegeneous medium. Then for idenetical wires, $K_{xy} = K_{yx}$. Hence, only one of the integrals of (B.7), say I_1, need be evaluated. By substituting the impedance expressions of (4.35) and (4.37) into (B.6) we obtain,

$$I_1 = \int_0^\infty \frac{1}{|2\pi i\omega\epsilon_1 Z_b(\beta) + v_1^2 K_0(v_1 a)|^2} \int_0^\infty \beta^2\lambda^2 \left|\frac{e^{-u_1|d|}}{u_1}\right|^2 d\lambda d\beta \qquad (B.8)$$

Since the term $2\pi i\omega\epsilon_1 Z_b(\beta) + v_1^2 K_0(v_1 a)$ does not have any real axis zeros [Hill and Wait, 1977], the estimation

$$I_1 \leq \frac{1}{M_\beta} \int_0^\infty \beta^2\lambda^2 \left|\frac{e^{-u_1|d|}}{u_1}\right|^2 d\lambda d\beta \qquad (B.9)$$

is valid, where

$$M_\beta = \min_{\beta\in[0,\infty)} |2\pi i\omega\epsilon_1 Z_b(\beta) + v_1^2 K_0(v_1 a)| \qquad (B.10)$$

The integral of (B.9) may be evaluated more readily by considering polar coordinates. If $\lambda = R\cos\theta$ and $\beta = R\sin\theta$ then $R^2 = \lambda^2 + \beta^2$ and $d\lambda d\beta = RdRd\theta$. Hence,

$$I_1 \leq \frac{1}{M_\beta} \int_0^{\frac{\pi}{2}} \int_0^\infty R^5 \sin^2\theta\cos^2\theta \left|\frac{e^{-|d|\sqrt{R^2-k_1^2}}}{\sqrt{R^2-k_1^2}}\right| dRd\theta \qquad (B.11)$$

The θ–dependency may be evaluated in close form:

$$I_1 \leq \frac{\pi}{16M_\beta}\int_0^\infty R^5 \left|\frac{e^{-|d|\sqrt{R^2-k_1^2}}}{\sqrt{R^2-k_1^2}}\right|^2 dR \qquad (B.12)$$

Since $\mathrm{Im}[k_1] < 0$, the above integral has no real axis singularities. Also, since $\mathrm{Re}\sqrt{R^2-k_1^2} > 0$, (B.12) converges like $R^3e^{-|d|R}$ for large R. Hence with these two facts, we conclude that I_1 is bounded.

Mathematically, the integral operator is bounded, provided that the surrounding medium contains an infinitesimal amount of loss and that the axial impedance is non–zero. However, such statements do not suffice for numerical applications. If σ_1 was an arbitrarily small number, and the wires were highly conducting (which is the usual case) then $M_\beta \to 0$ as $\sigma_1 \to 0$ and $\sigma_w \to \infty$; consequently, $I_1 \to \infty$. Such *large* numerical singularities will ill–condition the **R** matrix. Thus for dynamic applications, sufficiently lossy media or highly lossy wires are needed.

For the static case (i.e. $k_1 = 0$) and lossy media, (B.12) can be evaluated in close form:

$$I_1 \leq \frac{3\pi}{8M_\beta d^4} \qquad (B.13)$$

where

$$M_\beta = \min_{\beta\in[0,\infty)} |2\pi\sigma_1 Z_b(\beta) + \beta^2 K_0(\beta a)| \qquad (B.14)$$

However, from static theory, $Z_b(\beta) = 1/(\pi a\sigma_w)$. Hence, $M_\beta = (2/a)(\sigma_1/\sigma_w)$ and consequently,

$$I_1 \leq \frac{3\pi}{16}\left(\frac{a}{d^4}\right)\left(\frac{\sigma_w}{\sigma_1}\right) \qquad (B.15)$$

Thus, for the static case, an upper bound for the operator's norm is a function of the square root of the contrasting conductivities and the distance squared between wires.

APPENDIX C

GLOSSARY OF SYMBOLS

This appendix will list and identify many of the symbols and variables peculiar to this dissertation.

Electrical Parameters:

$$k_x = k_1 \sin\theta_0 \cos\phi_0 \qquad k_y = k_1 \sin\theta_0 \sin\phi_0$$

$$k_1 = \sqrt{-i\omega\mu_1(\sigma_1 + i\epsilon_1\omega)} \qquad k_2 = \sqrt{-i\omega\mu_2(\sigma_2 + i\epsilon_2\omega)}$$

$$\gamma_w = \sqrt{i\omega\mu_w(\sigma_w + i\epsilon_w\omega)}$$

Doubled–Valued Functions:

$$v_1 = \sqrt{\beta^2 - k_1^2} \qquad v_2 = \sqrt{\beta^2 - k_2^2}$$

$$v_a = \sqrt{k_y^2 - k_1^2} \qquad v_b = \sqrt{k_y^2 - k_2^2}$$

$$w_1 = \sqrt{\lambda^2 - k_1^2} \qquad w_2 = \sqrt{\lambda^2 - k_2^2}$$

$$w_a = \sqrt{k_x^2 - k_1^2} \qquad w_b = \sqrt{k_x^2 - k_2^2}$$

$$w_w = \sqrt{\lambda^2 + \gamma_w^2} \qquad v_w = \sqrt{\beta^2 + \gamma_w^2}$$

$$p_w = \sqrt{k_x^2 + \gamma_w^2} \qquad q_w = \sqrt{k_y^2 + \gamma_w^2}$$

$$\varsigma_a = \sqrt{k_1^2 - k_y^2} \qquad \varsigma_b = \sqrt{k_2^2 - k_y^2}$$

$$u_1 = \sqrt{\lambda^2 + \beta^2 - k_1^2} \qquad u_2 = \sqrt{\lambda^2 + \beta^2 - k_2^2}$$

$$u_a = \sqrt{\lambda^2 + k_y^2 - k_1^2} \qquad u_b = \sqrt{\lambda^2 + k_y^2 - k_2^2}$$

$$u_c = \sqrt{k_x^2 + \beta^2 - k_1^2} \qquad u_d = \sqrt{k_x^2 + \beta^2 - k_2^2}$$

Geometrical Definitions:

$$\rho_{xz} = \sqrt{x^2 + z^2} \qquad \rho_{yz} = \sqrt{y^2 + z^2}$$

$$\hat{\rho}_{xz} = \sqrt{x^2 + (z-h)^2} \qquad \hat{\rho}_{yz} = \sqrt{x^2 + (z-h-d)^2}$$

$$r_{xz} = \sqrt{(x-x_d)^2 + (z-z_d)^2} \qquad r_{yz} = \sqrt{(y-y_d)^2 + (z-z_d)^2}$$

$$\hat{r}_{xz} = \sqrt{x_d^2 + (z-z_d)^2} \qquad \hat{r}_{yz} = \sqrt{y_d^2 + (z-z_d)^2}$$

$$\rho_d = \sqrt{(x-x_d)^2 + (y-y_d)^2} \qquad R_d = \sqrt{\rho_d^2 + (z-z_d)^2}$$

REFERENCES

Abramowitz, M., and I.A. Stegun (1970), Handbook of Mathematical Functions, Dover, New York, NY.

Amos, D. E. (1985), A Subroutine Package for Bessel Functions of Complex Argument and Nonnegative order, Sandia Report # 1018, Sandia National Laboratories, NM.

Baertlein, B. A. (1988), Frequency Response of E -Polarized Sources Over a Lossy Earth in the Presence of Two -Dimensional Shielding Structures, PhD dissertation, Department of Electrical and Computer Engineering, University of Arizona, Tucson, Az.

Bannister P. R. (1973), "Image theory results for the mutual impedance of crossing earth return circuits", IEEE Trans. Electromagn. Compat. 15(4), 158–160.

Bremmer, H. (1949), Terrestrial Radio Waves, Elsevier, New York, NY.

Butler, C. M. (1972), "Currents induced on a pair of skew crossed wires", IEEE Trans. Ant. Prop. 20(6), 731–736.

Carson, J. R. (1926), "Wave propagation in overhead wires with ground return", Bell Sys. Tech, J. 5, 539–554.

Casey, K. F. (1988), "Electromagnetic shielding behaviour of wire–mesh screens", IEEE Trans. Electromagn. Compat. 30(3), 298–306.

Chang, D. C., and J. R. Wait (1974), "Extremely low frequency propagation along a horizontal wire located above or buried in the earth", IEEE Trans. Com. 22 (4), 421–427.

Chu, G., D. G. Dudley, and T. W. Bristol (1969), "Interaction between an electromagnetic plane wave and a spherical shell", J. Appl. Phys., 40, 3904–3914.

Churchill, R. V. (1972), Operational Mathematics, McGraw–Hill, New York, NY.

Churchill, R. V. and J. W. Brown (1984), Complex Variables and Applications, McGraw–Hill, New York, NY.

Coleman B. L. (1950), "Propagation of electromagnetic disturbances along a thin wire in a horizontally stratified medium", Phil. Mag. Ser. 7, 41, 276–288.

Collin, R. E. (1960), Field Theory of Guided Waves, McGraw–Hill, New York, NY.

dos Santos, A. F. (1972), "Electromagnetic–wave propagation along a horizontal wire above ground", Proc. IEE 119(8), 1103–1109.

Dudley, D. G. and J. P. Quintenz (1975), "Transient penetration of a spherical shell", J. Appl. Phys. 46, 173–177.

Dudley, D. G. (1985), "Error minimization and convergence in numerical methods", Electromagnetics 5, 89–97.

Dudley, D. G. and K. F. Casey (1989), "Pulse propagation on a horizontal wire above ground: Far–zone radiated fields", Radio Sci. 24(2), 224–234.

Felsen, L.B. and N. Marcuvitz (1973), Radiation and Scattering of Waves, Prentice Hall, Inc., Englewood Cliffs, NJ.

Gans, R. (1920), "Das Verhalten Hertzscher Gitter," Ann. Physik 61, 447–454.

Gradshteyn, I. S. and I. Ryzhik (1980), Table of Integrals, Series and Products, Academic Press, Orlanda, FL.

Giri, D. V., S. Chang and F. M. Tesche (1980), "A coupling model for a pair of skewed transmission lines", IEEE Trans. Electomagn. Compat. 22(1), 20–28.

Harrington, R.F. (1968), Field Computation by Moment Methods, Krieger, FL.

Hill, D. A. and J. R. Wait (1977), "Coupling between a dipole antenna and an infinite cable over an ideal ground plane", Radio Sci. 12(2), 231–237.

Hill, D. A. (1988), "Magnetic dipole excitation of a long conductor in a lossy medium", IEEE Trans. on Geo. and Remote Sensing 26 (6), 720 –725.

Ignatowsky W. (1914), "Zur Theorie Ger Gitter," Ann. Physik, 44, 369–436.

Jackson, J. D. (1975), Classical Electrodynamics, Wiley, NY.

Johnson, W.A. and D.G. Dudley (1983), "Real axis integration of Sommerfeld integrals: Source and observation points in air", Radio Sci., 18, 175-186.

Jordan, E. C. and K. G. Balmain (1968), Electromagnetic Waves and Radiating Systems, Prentice– Hall, Englewood, NJ.

Kami, Y. and R. Sato (1986), "Coupling model of crossing transmission lines", IEEE Trans. Electromagn. Compat. 28(4), 204–210.

Kikuchi H. (1978), "Propagation characteristics along a dielectric coated cylindrical conductor above the ground", Proc. IEEE 66(3), 351–352.

King, R. W. R. and T. T. Wu (1975), "Analysis of crossed wires in a plane–wave field" IEEE Trans. Electromagn. Compat. 17(4), 255–265.

King, R. W. R. (1977), "Currents induced in a wire cross by a plane wave incident at an angle" IEEE Trans. Ant. Prop. 25(6), 775–781.

Krakowski, M (1967), "Mutual impedance of crossing earth–return circuits", Proc. IEE 114 (2), 253–257.

Kuester, E. F., D. C. Chang and R. G. Olsen (1978), "Modal theory of long horizontal wire structures above the earth, 1, Excitation", Radio Sci. 13(4), 605–613.

Larsen, T. (1962a), "Numerical investigation of the equivalent impedance of a wire grid parallel to the interface between two media", J. Res NBS, 66D(1), 7–14.

Larsen, T. (1962b), "Survey of the theory of wire grids", IRE Trans. Microwave Theory Tech. 10, 191– 201.

Lamb, H. (1898), "On the reflection and transmission of electric waves by a metallic grating", Proc. London Math. Soc. 29, 523–544.

MacFarlane, G. G. (1946), "Surface impedance of an infinite parallel-wire grid at oblique angles of incidence", J. IEE 93(III A), 1523–1527.

Marin, L. (1975), "Transient electromagnetic properties of two, infinite, parallel wires", Appl. Phys. 5, 333–345.

Maxwell, J. C. (1891), Treatise on Electricity and Magnetism, 3rd. ed., reprint (1954) by Dover, New York, NY.

Olsen, R. G., and D.C. Chang (1974), "Current induced by a plane wave on a thin infinite wire near the earth", IEEE Trans. Ant. Prop. 22(4), 586–589.

Olsen R. G., E. F. Kuester and D. C. Chang (1978), "Modal theory of long horizontal wire structures above the earth, 2, Properties of discrete modes" Radio Sci. 13(4), 615–623.

Olsen R. G., and A. Aburwein (1980), "Current induced on a pair of wires above eath by a vertical electric dipole for grazing angles of incidence", Radio Sci. 15 (4), 733– 742.

Pogorzelski, R. J., and D.C. Chang (1977), "On the validity of the thin wire approximation in analysis of wave propagation along a thin wire over a ground", Radio Sci. 12(5), 699–707.

Press, W. H., B. P. Flannery, S. A. Teukolsky and W. T. Vetterling (1986), Numerical Recipes, Cambridge Press, Cambridge, UK.

Quintenz, J. P. and D. G. Dudley (1974), "Transmission of a transient electromagnetic plane wave through a grating of circular cylinders", Appl. Phys. 4, 349–355.

Ragheb, H. A. and Hamid, M. (1988), "Scattering of a long dipole field by a parallel cylindrical scatterers", IEE Proc. pt H 135(2), 118–124.

Richmond, J. H. (1965), "Scattering by an arbitrary array of parallel wires", IEEE Trans. Microwave Theory Tech. 13(4), 408–412.

Row, R. V. (1955), "Theoretical and experimental study of electromagnetic scattering by two identical conducting cylinders", J. Appl. Phys., 26(6), 666–675.

Schelkunoff, S. A. (1943), Electromagnetic Waves, D. Van Nostrand, New York, NY.

Stakgold, I. (1979), Green's Functions and Boundary Value Problems, Wiley, New York, NY.

Tamir, T. and A. A. Oliner (1963), "Guided complex waves, Pt. 1: Fields at an interface", Proc. IEE 110(2), 310–324.

Tamir, T. and A. A. Oliner (1963), "Guided complex waves, Pt. 2: Relation to radiation patterns", Proc. IEE 110(2), 325–334.

Taylor, C. D., S. M. Lin and H. V. McAdams (1970), "Scattering from crossed wire antennas", IEEE Trans. Ant. Prop. 18, 133–136.

Todd, J. (1954), "Evaluation of the exponential integral for large complex arguments", J. Res. Nat. Bureau Stand., 52(6), 313-317.

Tricomi, F.G. (1985), Integral Equations, Dover, New York, NY.

Wait, J. R. (1954a), "Reflection from a wire grid parallel to a conducting plane", Can. J. Phys. 32, 571–579.

Wait, J. R. (1954b), "Reflection at arbitrary incidence from a parallel wire grid", Appl. Sci. Res., B4(6), 393–400.

Wait, J. R. (1957), "The impedance of a wire grid parallel to a dielectric interface", IRE Trans. Microwave Theory Tech. 5(2), 99–102.

Wait, J.R. (1959), Electromagnetic Radiation From Cylindrical Structures, Pergamon, New York, NY (corrected reprint edition, Peter Peregrinus Ltd, Stevenage, UK, 1988).

Wait, J.R. (1961), "On the impedance of a long wire suspended over the ground", Proc. IRE, 49(10), 1576.

Wait, J. R. (1962), "Effective impedance of a wire grid parallel to the earth's surface", IRE Trans. Ant. Prop. 10(5), 538–542.

Wait, J. R. (1970), Electromagnetic Waves in Stratified Media (2nd edition), Pergamon, Oxford, England.

Wait, J. R. (1972a), "Theory of wave propagation along a thin wire parallel to an interface", Radio Sci. 7(6), 675–679.

Wait, J. R. (1972b), "Electromagnetic wave propagation along a buried insulated wire", Can. J. Phys. 50(20), 2402–2409.

Wait, J. R. (1977a), "Excitation of a coaxial cable or wire conductor located over the ground by a dipole radiator", AEÜ 31(3), 121–127.

Wait, J. R. (1977b), "Excitation of an ensemble of parallel cables by external dipole over a layered ground", AEÜ 31(12), 489–493.

Wait, J. R. (1978a), "Theories of scattering from wire grids and mesh structures", Electromagnetic Scattering, Edited by P.L.E. Uslenghi, Academic Press, 253–287.

Wait, J. R. (1978b), "Excitation of currents on a buried insulated cable", J. Appl. Phys. 49(2), 876–880.

Wait, J. R. (1985), Electromagnetic Wave Theory, Harper and Row, New York, NY (also Wiley, New York, NY, 1987).

Wait, J. R. (1986a), Introduction to Antennas and Propagation, Peregrinus Ltd., London, UK.

Wait, J. R. (1986b), "Impedance conditions for a coated cylindrical conductor", Radio Sci. 21(4), 623–626.

Wessel, W. (1939), "Über Den Durchgang Elektrischer Wellen Durch Drahtgitter", Hochfrequenztech. Elekt. Akust. 54, 62–70.

Wheelon, A. D. (1968), Tables of Summable Series and Integrals Involving Bessel Functions, Holden– Day, San Fransico, CA.

Wilson, L. O. (1974), "The shielding of a plane wave by a cylindrical array of infintely long thin wires", IEEE Trans. Ant. Prop. 22(5), 689–696.

Wise, W. H. (1934), "Propagation of high–frequency currents in ground return circuits", Proc. IRE 22(4), 522–527.

Wise, W. H. (1948), "Potential Coefficients for ground return circuits", Bell Sys. Tech J. 27 (2), 365– 371.

Wu, T. T. (1961), "Theory of the dipole antenna and the two–wire transmission line", J. Math. Phys. 2(4), 550–574.

Yatom, H. and R. Ruppin (1983), "Current induced by a plane wave on a thin infinite coated wire above the ground", IEEE Trans. Ants. Prop. 31(1), 172–174.

Young, J. L. and J. R. Wait (1989a), "Note on the impedance of a wire grid parallel to a homogeneous interface", IEEE Trans. Microwave Theory Tech. 37(7), 1136–1138.

Young, J. L. and J. R. Wait (1989b), "Shielding properties of an ensemble of thin, infinitely long, parallel wires over a lossy half space", IEEE Trans. Electro–magn. Compat. 31(3), 238–244.

Young, J. L. and J. R. Wait (1989c), "Comparison of shielding by infinite and finite planar grids over a lossy half space", IEEE Trans. Electromagn. Compat. (Accepted).